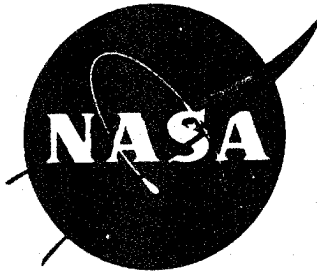


SK1

NASA CR-134555



**THIN-METAL LINED PRD 49-III COMPOSITE
VESSELS**

**BY
J.T. HOGGATT**

**THE BOEING AEROSPACE COMPANY
RESEARCH AND ENGINEERING DIVISION
SEATTLE, WASHINGTON**

JANUARY 1974

**PREPARED FOR
NATIONAL AERONAUTICS AND SPACE ADMINISTRATION**

**NASA-LEWIS RESEARCH CENTER
CONTRACT NAS3-15840
R.F. LARK, PROJECT MANAGER**

19960223 028

DTIC QUALITY INSPECTED 1

DISTRIBUTION STATEMENT A
Approved for public release;
Distribution Unlimited

PLSNO 20787

DTIC DOES NOT HAVE THIS ITEM

- 1 - AD NUMBER: D404863
- 3 - ENTRY CLASSIFICATION: UNCLASSIFIED
- 5 - CORPORATE AUTHOR: BOEING AEROSPACE CO SEATTLE WASH
- 6 - UNCLASSIFIED TITLE: THIN-METAL LINED PRD 49-III COMPOSITE
VESSELS.
- 8 - TITLE CLASSIFICATION: UNCLASSIFIED
- 9 - DESCRIPTIVE NOTE: FINAL REPT., 1 JUN 72 - 1 SEP 73,
- 10 - PERSONAL AUTHORS: HOGGATT, J.T. ;
- 11 - REPORT DATE: JAN , 1974
- 12 - PAGINATION: XXXXXX MEDIA COST: \$ 6.00
- 14 - REPORT NUMBER: ASG 2-5540
- 15 - CONTRACT NUMBER: NAS 3-15840
- 18 - MONITOR ACRONYM: NASA
- 19 - MONITOR SERIES: CR-134555
- 20 - REPORT CLASSIFICATION: UNCLASSIFIED
-
- 28 - ABSTRACT CLASSIFICATION: UNCLASSIFIED
- 30 - ANNOTATION: THIN-METAL LINED PRD 49-III COMPOSITE VESSELS.
- 33 - LIMITATION CODES: 1
- 34 - SOURCE SERIES: F
-

1. Report No. NASA CR-134555	2. Government Accession No.	3. Recipient's Catalog No.	
4. Title and Subtitle Thin-Metal Lined PRD 49-III Composite Vessels		5. Report Date January 1974	
		6. Performing Organization Code ASG 2-5540	
7. Author(s) J. T. Hoggatt		8. Performing Organization Report No.	
		10. Work Unit No.	
9. Performing Organization Name and Address The Boeing Aerospace Company P. O. Box 3999 Seattle, Washington 98124		11. Contract or Grant No. NAS 3-15840	
		13. Type of Report and Period Covered Contractor Report-Final	
12. Sponsoring Agency Name and Address National Aeronautics and Space Administration Washington, D.C. 20546		14. Sponsoring Agency Code	
15. Supplementary Notes Project Manager, R. F. Lark Materials and Structures Division NASA-Lewis Research Center Cleveland, Ohio 44135			
16. Abstract In this program a total of 22 -8" diameter PRD-49-III filament wound vessels were evaluated for burst strength and fatigue performance. Eighteen vessels contained a .003" (.0762 mm) thick 321 stainless steel liner for fluid containment while the remaining four had elastomeric liners. Six of the metal-lined tanks were burst tested at +70°F (+21°C). The final vessel design with a metallic liner gave an average burst pressure of 2560 psi (17.7×10^6 N/m ²) and an average performance factor (PV/W) of 1.75×10^6 inch (4.45×10^6 cm). Twelve metal-lined vessels were cycled at strain levels equivalent to 50% and 75% of ultimate at +70°F (+21°C). All these vessels leaked in a relatively few cycles (20-60 cycles) with failure occurring in all cases in the metallic liner. The thin liner would de-bond from the composite and buckle during depressurization. No composite failures or indications of impending composite failures were obtained in the metal-lined vessels. An elastomeric lined vessel was successfully cycled for 2493 pressure excursions at 75% of ultimate strain prior to composite failure in the dome. The tests concluded that the filament wound composite vessels have excellent fatigue capabilities however significant improvements are required in thin-metal liner technology.			
17. Key Words (Suggested by Author(s)) PRD 49-III fiber Filament Winding Pressure Vessels Advanced Composites Metallic Liners		18. Distribution Statement Unclassified-Unlimited	
19. Security Classif. (of this report) Unclassified	20. Security Classif. (of this page) Unclassified	21. No. of Pages 134	22. Price* \$3.00

* For sale by the National Technical Information Service, Springfield, Virginia 22151

FOREWORD

This report presents the work accomplished by The Boeing Aerospace Company during the period of June 1, 1972 to Sept. 1, 1973 on NASA Contract NAS 3-15840, "Cryogenic Thin-Metal Lined PRD 49-3 Composite Vessels." The work was administered by the National Aeronautics and Space Administration, Lewis Research Center, Materials and Structures Division, Cleveland, Ohio, with Mr. R. F. Lark, Project Manager.

Performance of this contract was under the direction of the Development Programs Organization, The Boeing Aerospace Company, Dr. R. G. Cheatham, Group Supervisor. Mr. J. T. Hoggatt was program Technical Manager. Major contributors to the program include:

A. D. VonVolkli	Materials & Processes
J. H. Laakso	Vessel Design
D. E. Giesecking	Vessel Fabrication
P. D. Smith	
H. M. Olden	Vessel Testing
G. E. Vermilion	
D. W. Nelson	Acoustic Emission

Liner design was performed by Structural Composites Industries, Inc., Azusa, California, by Messrs. E. E. Morris and R. E. Landes.

TABLE OF CONTENTS

		<u>PAGE</u>
1.0	INTRODUCTION	1
2.0	SUMMARY	3
3.0	TEST PROGRAM	4
3.1	VESSEL DESIGN	4
3.1.1	DESIGN CRITERIA	4
3.1.2	COMPOSITE DESIGN	4
3.1.3	STAINLESS STEEL LINER DESIGN	5
3.2	FABRICATION	13
3.2.1	LINER FABRICATION	13
3.2.2	VESSEL FABRICATION	14
3.3	TEST EQUIPMENT AND PROCEDURES	18
3.3.1	INSTRUMENTATION	18
3.3.2	TEST EQUIPMENT	20
3.3.3	TEST PROCEDURES	20
3.4	TEST RESULTS	21
3.4.1	BURST TESTS	21
3.4.2	CYCLIC FATIGUE RESULTS	24
3.4.3	ACOUSTIC EMISSION STUDIES	28
4.0	CONCLUSIONS	31
5.0	REFERENCES	33
6.0	APPENDIX	123
7.0	DISTRIBUTION LIST	126

LIST OF FIGURES

		<u>PAGE</u>
1	Schematic of 8 in. Diameter (20.3 cm) Pressure Vessel	44
2	Ambient Stress-Strain Relationships, Longitudinal Direction of Cylinder (N=Cycle No.)	45
3	Ambient Stress-Strain Relationships, Hoop Direction of Cylinder (N=Cycle No.)	46
4	Metallic Liner Drawing	47
5	Metallic Liner Assembly Drawing	48
6	Liner Boss Details	49
7	Metallic Liner Assembly	50
8	Cross-Section of Tank Boss	51
9	Liner Boss and Weld Zone on Dome	52
10	Dome-to-Body Weld and Longitudinal Body Weld	53
11	Metallic Liner-321 Stainless Steel	54
12	Liner Stabilization Mold	55
13	Filament Winding Equipment	56
14	8" Diameter PRD-49-III Filament Wound Tank - Metal Liner	57
15	Instrumentation for Circumferential Strain Measurements	58
16	Instrumentation for Longitudinal Strain Measurements	59
17	Test System (70°F)	60
18	Vessel in Test Chamber	61
19	Vessel No. 1 after Burst Test	62
20	Pressure vs. Strain Relationship - Vessel No. 1	63

LIST OF FIGURES (CONTINUED)

		<u>PAGE</u>
21	Vessel No. 2 After Burst Test	64
22	Pressure vs. Strain Relationship - Vessel No. 2	65
23	Pressure vs. Strain Relationship - Vessel No. 3	66
24	Vessel No. 3 After Burst Test	67
25	Vessel No. 4 After Burst Test	68
26	Vessel No. 5 After Burst Test	69
27	Vessel No. 6 After Burst Test	70
28	Pressure vs. Strain Relationship - Vessel No. 4	71
29	Pressure vs. Strain Relationship - Vessel No. 5	72
30	Pressure vs. Strain Relationship - Vessel No. 6	73
31	Pressure vs. Strain Relationship of Vessel No. 7 in Cyclic Fatigue	74
32	Pressure vs. Strain Relationship of Vessel No. 7 in Cyclic Fatigue	75
33	Pressure vs. Strain Relationship of Vessel No. 8 in Cyclic Fatigue	76
34	Pressure vs. Strain Relationship of Vessel No. 8 in Cyclic Fatigue	77
35	Pressure vs. Strain Relationship of Vessel No. 9 in Cyclic Fatigue	78
36	Pressure vs. Strain Relationship of Vessel No. 9 in Cyclic Fatigue	79
37	Pressure vs. Strain Relationship of Vessel No. 10 in Cyclic Fatigue	80
38	Pressure vs. Strain Relationship of Vessel No. 10 in Cyclic Fatigue	81
39	Pressure vs. Strain Relationship of Vessel No. 11 in Cyclic Fatigue	82

LIST OF FIGURES (CONTINUED)

		<u>PAGE</u>
40	Pressure vs. Strain Relationship of Vessel No. 11 in Cyclic Fatigue	83
41	Pressure vs. Strain Relationship of Vessel No. 12 in Cyclic Fatigue	84
42	Pressure vs. Strain Relationship of Vessel No. 12 in Cyclic Fatigue	85
43	Pressure vs. Strain Relationship of Vessel No. 13 in Cyclic Fatigue	86
44	Pressure vs. Strain Relationship of Vessel No. 13 in Cyclic Fatigue	87
45	Pressure vs. Strain Relationship of Vessel No. 14 in Cyclic Fatigue	88
46	Pressure vs. Strain Relationship of Vessel No. 14 in Cyclic Fatigue	89
47	Pressure vs. Strain Relationship of Vessel No. 15 in Cyclic Fatigue	90
48	Pressure vs. Strain Relationship of Vessel No. 15 in Cyclic Fatigue	91
49	Pressure vs. Strain Relationship of Vessel No. 16 in Cyclic Fatigue	92
50	Pressure vs. Strain Relationship of Vessel No. 16 in Cyclic Fatigue	93
51	Pressure vs. Strain Relationship of Vessel No. 17 in Cyclic Fatigue	94
52	Pressure vs. Strain Relationship of Vessel No. 17 in Cyclic Fatigue	95
53	Pressure vs. Strain Relationship of Vessel No. 18 in Cyclic Fatigue	96
54	Pressure vs. Strain Relationship of Vessel No. 18 in Cyclic Fatigue	97
55	Pressure vs. Strain Relationship of Vessel No. 19 in Cyclic Fatigue	98
56	Pressure vs. Strain Relationship of Vessel No. 19 in Cyclic Fatigue	99

LIST OF FIGURES (CONTINUED)

		<u>PAGE</u>
57	Pressure vs. Strain Relationship of Vessel No. 20 in Cyclic Fatigue	100
58	Pressure vs. Strain Relationship of Vessel No. 20 in Cyclic Fatigue	101
59	Pressure vs. Strain Relationship of Vessel No. 21 in Cyclic Fatigue	102
60	Pressure vs. Strain Relationship of Vessel No. 21 in Cyclic Fatigue	103
61	Pressure vs. Strain Relationship of Vessel No. 22 in Cyclic Fatigue	104
62	Pressure vs. Strain Relationship of Vessel No. 22 in Cyclic Fatigue	105
63	Vessel No. 22 After Cyclic Testing	106
64	Vessel No. 14 After Cyclic Testing	107
65	Vessel No. 14 After Cyclic Testing	108
66	Pressure vs. Strain Relationship - Vessel No. 19	109
67	Pressure vs. Strain Relationship - Vessel No. 20	110
68	Pressure vs. Strain Relationship - Vessel No. 21	111
69	Vessel No. 7 After Burst Test	112
70	Vessel No. 8 After Burst Test	113
71	Vessel No. 9 After Burst Test	114
72	Vessel No. 10 After Burst Test	115
73	Vessel No. 11 After Burst Test	116
74	Vessel No. 12 After Burst Test	117
75	Vessel No. 19 After Burst Test	118
76	Vessel No. 20 After Burst Test	119
77	Vessel No. 21 After Burst Test	120

LIST OF FIGURES (CONTINUED)

		<u>PAGE</u>
78	Acoustic Emission Data from Vessel Burst Tests	121
79	Acoustic Emission Counts Data from Vessel No. 13	122

LIST OF TABLES

		<u>PAGE</u>
I	Design Requirements for PRD 49-3 Filament Wound Pressure Vessel	34
II	Material Properties Type 321 Stainless Steel (Annealed)	35
III	Vessel Fabrication Parameters	36
IV	Material Selection	37
V	Vessel Weight Summary - Metal-Lined Vessels	38
VI	Vessel Weight Summary - Elastomeric Lined Vessels	39
VII	Vessel Test Results - Burst Test at +70°F	40
VIII	PRD 49-III Yarn Tensile Properties	41
IX	Vessel Test Results - Cyclic Fatigue (+70°F)	42
X	Vessel Test Results - Burst Strength After Fatigue Cycling (+70°F)	43

1.0 INTRODUCTION

Under a previous NASA Contract, NAS3-13330 (Ref.1), it was demonstrated that PRD49-1 and PRD49-3 fiber reinforcements offered significant performance improvements over S-glass and graphite reinforcements in filament wound pressure vessel applications. The improvements were in higher performance factors (PV/W) and better cyclic fatigue life.

This evaluation of PRD fibers was done using an elastomeric lined vessel. Many of the potential system applications defined by NASA requiring a high performance vessel were for the containment of cryogenics or storable propellants. Both are application areas requiring a metallic liner. Under NASA sponsorship, several liner development programs were conducted on filament wound fiberglass vessels (Ref. 2-4). These programs evaluated 6-mil (.152 mm) aluminum and stainless steel liners and various boss designs. It was the intent of this program to evaluate the compatibility of the PRD49-3 composite vessel with a thin, non-load bearing metallic liner by combining the technology gained under those previous programs.

Structural Composite Industries furnished the liner and boss designs. Their design was based on work performed under NASA Contract NAS3-10289 (Ref. 3 & 4). The composite vessel technology was based on work by Boeing under NASA Contract NAS3-13330 (Ref. 1). The adhesive system and liner material selections were from work under Contracts NAS3-6293 (Ref. 2) and NAS3-12047 (Ref. 5) respectively. No material development or evaluations were conducted under this program.

The original scope of this program consisted of testing a series of filament wound vessels for the determination of either ultimate burst strength or cyclic fatigue performance

1.0 (Continued)

at temperatures ranging from +70°F (+21°C) to -423°F (-252°C) (LH₂). The basic liner and vessel design and the material selections were based on those defined operating temperatures. During the course of the program, NASA reviewed their priorities and systems needs, and subsequently redirected the program. The revised program concentrated on obtaining cyclic fatigue performance at +70°F (+21°C). Twelve of the eighteen vessels were cycle tested at either 50% or 75% of ultimate strength with a goal of 4000 pressure cycles.

2.0 SUMMARY

In this program a total of 22 - 8" diameter PRD-49-3 filament wound vessels were evaluated for burst strength and fatigue performance. Eighteen vessels contained a .003" (.0762 mm) thick 321 stainless steel liner for fluid containment while the remaining four had elastomeric liners. Six of the metal-lined tanks were burst tested at +70°F (+21°C). The final vessel design with a metallic liner gave an average burst pressure of 2560 psi (17.7×10^6 N/m²) and an average performance factor (PV/W) of 1.75×10^6 inch (4.45×10^6 cm).

Twelve metal-lined vessels were cycled at strain levels equivalent to 50% and 75% of ultimate at +70°F (+21°C). All these vessels leaked in a relatively few cycles (20-60 cycles) with failure occurring in all cases in the metallic liner. The thin liner would de-bond from the composite and buckle during depressurization. No composite failures or indications of impending composite failures were obtained in the metal-lined vessels.

An elastomeric lined vessel was successfully cycled for 2493 pressure excursions at 75% of ultimate strain prior to composite failure in the dome. The tests concluded that the filament wound composite vessels have excellent fatigue capabilities however significant improvements are required in thin-metal liner technology.

3.0 TEST PROGRAM

3.1 VESSEL DESIGN

3.1.1 DESIGN CRITERIA

The criteria shown below and in Table I were used to arrive at the design details for the liners and the composite vessel evaluated in this program.

Fiber/Matrix - PRD 49-3 continuous filaments impregnated with epoxy resin (See Table I)

Tape Width - Eight strands of roving forming a 0.20 in. (0.508 cm) wide tape.

Winding Pattern - In plane, complemented by a circumferential wrap in the cylinder section

Filament-Winding Tension Prestress - 1000 psi (6.9×10^6 N/m²)

Liner - Stainless Steel, Type 321 (annealed), of 0.003 in. (.0762 mm) thickness

Weld Requirements - Longitudinal seam weld in cylinder plus two girth welds joining domes to cylinder; roll seam welded

Boss Diameter - 1.25 inches (3.175 cm)

Service Temperature - +70°F, -320°F, -423°F (+21°C, -195°C, -252°C)

Burst Pressure - 2000 psi (1.38×10^6 N/m²)

Operating Pressure - 1500 psi (10.34×10^6 N/m²)

3.1.2 COMPOSITE DESIGN

The test vessel was a filament wound PRD49-3 fiber reinforced epoxy composite tank approximately 8.00 inches (20.32 cm) in diameter and 12 inches (30.48 cm) long. A drawing of the vessel is shown in Figure 1.

The vessel was designed to achieve a longitudinal-to-circumferential strain ratio of 1. This was adjusted slightly to initiate failure in circumferential windings. The net result was a ratio of 1.9 circumferential windings to polar windings

3.1.2 (Continued)

rather than a value of 2.0. The criteria for the vessel design are given in Section 3.1.1 and Table I. A NASA supplied computer program, CR-72124 (Ref. 6) was used to generate the dome profile and composite thicknesses. The resulting design is shown in Figure 1. The computer program uses a netting analysis that assumes constant stresses along the path of the filament and a negligible structural contribution of the resin matrix. The computer program accounts for contributions of a liner and the required inputs for a 3 mil (.0762 mm) 321 stainless steel liner were made.

The vessel was designed for a operating temperature of +70°F to -423°F (+21°C to -252°C).

3.1.3 STAINLESS STEEL LINER DESIGN

The design and analysis of an 8 in. (20.32 cm) diameter by 12 in. (30.48 cm) long closed end stainless steel cylinder to be used as a metal liner for the PRD 49-3/epoxy filament-wound pressure vessels designed in Section 3.1 is presented in this section.

3.1.3.1 Membrane Design

Dimensional coordinates of the stainless steel head contours and other geometric characteristics of the .003 in (.0762 mm) thick metal shell were established by a previously developed computer program for analysis of metal-lined filament-wound pressure vessels (Ref. 6). Computer program input variables were based on the design criteria of Section 3.1.1 and the material properties of the metal shell listed in Table II.

Computer output was also used to construct typical single cycle burst stress-strain curves for the longitudinal and hoop direction of the cylinder as shown in Figures 2 and

3.1.3.1 (Continued)

3, respectively. Since the plastic portion of the metal shell compressive stress-strain curve is not considered in the Reference 6 computer program, the zero to operating pressure cyclic curves ($N \geq 1$), shown in Figures 2 and 3, are results of hand calculations. The hand calculations were based on the assumption that compressive properties of the metal shell can be approximated by the established values for the tensile properties. Equations for load equilibrium and strain compatibility between the filament and metal shells were then used to determine the cyclic relations depicted in the figures. It should be noted from the figures that the large plastic compressive strains in the metal induced by each operating cycle leads to the requirement for a reliable and strong bond between metal and filament shells to prevent general instability of the metal shell, or localized liner buckling during fatigue cycling. Without such a bond, buckling and subsequent liner failure during pressure cycling would be anticipated.

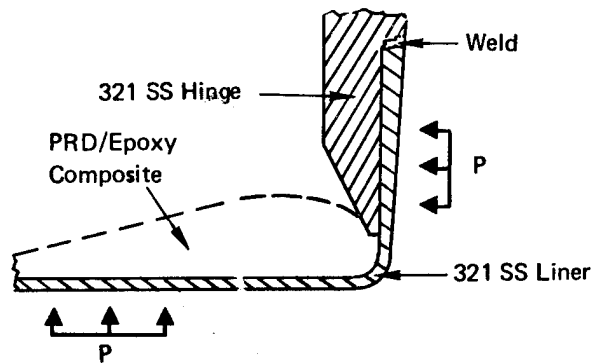
3.1.3.2 Boss Design Analysis

The concept and special features of the "Hinge Boss" selected for this liner design are described in Reference 3, and a demonstration of its use in metal-lined filament-wound pressure vessels is reported in Reference 4. The boss is constructed from annealed type 321 stainless steel; significant dimensions used for this analysis were taken from Figures 4-6. As noted in Figure 5, the 0.003-in. (.0762 mm) metal membrane thickness was gradually increased to 0.006 in. (0.152 mm) as the region of the port is approached. This increase in liner thickness was selected as a fabrication aid to reduce liner fragility during assembly of mating boss components.

3.1.3.2 (Continued)

A. Hinge Design

An idealized model of the boss is shown in the following schematic.



Referring to the schematic, pressure is applied over the entire internal surface of the stainless steel liner (including the neck section) forcing the liner to strain with the filament wound composite. Pressure vent holes are provided in the boss body (not shown in schematic) to allow for this action. Computer output indicated the biaxial strain in this region of the membrane induced by the burst pressure was 0.021 in/in (0.021 cm/cm) resulting in a metal membrane stress of 53.5 ksi. ($3.67 \times 10^8 \text{ N/m}^2$).

In the region where the composite "build-up" no longer provides backing for, or strain control of the liner, a structural hinge (short cylinder) is incorporated.

3.1.3.2 (Continued)

The combined thickness of the hinge/liner at this point was selected to insure hoop stress continuity in the metal, [i.e., for a pressure of 2000 psi (13.79×10^6 N/m²)] and a combined hinge/liner thickness of approximately 0.023-in. (.058 cm), the hoop stress in the metal is 53.5 ksi (3.67×10^6 N/m²). The axial location of this specific hinge/liner thickness was fixed by the expected composite build-up at the neck of the boss. It was estimated the composite build-up would be twice the thickness of the total cylinder composite - or approximately 0.10 in. (.254 cm).

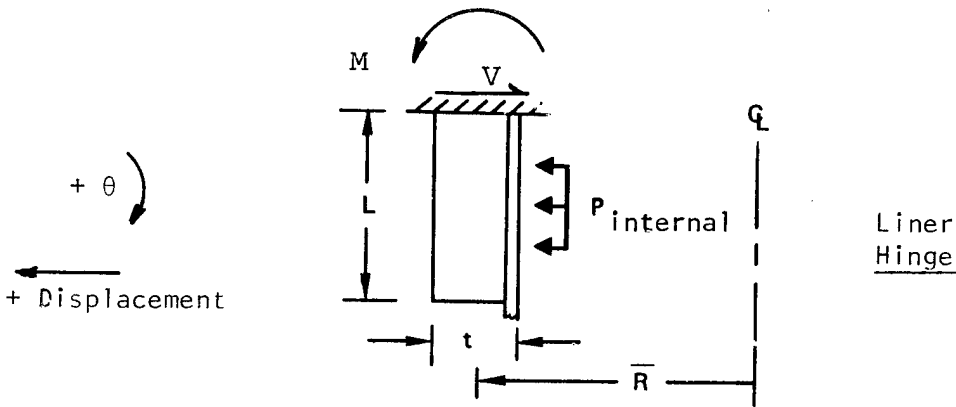
At the upper rigid end of the hinge, the liner must be welded to the short cylinder section to complete the required seal of the liner. The liner was thickened gradually from 0.006 in. (0.152 mm) to 0.015 in. (0.38 mm) at this point to simplify the welding procedure. The total thickness of the metal hinge/liner at the rigidly fixed upper end is dictated by the maximum combined meridional stress (membrane plus bending) induced by the burst pressure. The meridional membrane stress in the liner decreases as the liner thickness increases, and the value at the weld is

$$\sigma_{\phi} = 53.5 (0.006)/0.015$$

$$\sigma_{\phi} = 21.4 \text{ ksi} (1.48 \times 10^8 \text{ N/m}^2)$$

A short cylinder discontinuity analysis (outlined in Reference 3) was used to establish the meridional bending stress. The required geometry used in the analysis are defined in the following idealized schematic.

3.1.3.2 (Continued)



The induced bending moment at the burst pressure is

$$M = \frac{p\bar{R}t}{6C_7} \left[\frac{3}{1 - \mu^2} \right]^{1/2}$$

where

$$p = 2000 \text{ psi} \quad (13.79 \times 10^6 \text{ N/m}^2)$$

$$t = 0.160 \text{ in} \quad (.406 \text{ cm})$$

$$L = 0.411 \text{ in} \quad (1.04 \text{ cm})$$

$$\bar{R} = 0.685 \text{ in} \quad (1.74 \text{ cm})$$

$$\mu = 0.3$$

$$C_7 = \frac{2C_3C_6 - C_4C_5}{C_4}$$

3.1.3.2 (Continued)

The short cylinder coefficients, C_i , are a function of the effective cylinder length (λL), which is found from the expression

$$\lambda L = \left[\frac{3(1 - \mu^2)}{\bar{R} t^2} \right]^{1/4} L$$

$$\lambda L = \left[\frac{3(1 - .3^2)}{(0.685)^2 (.16)^2} \right]^{1/4} \quad (0.411)$$

$$\lambda L = 1.596$$

and, from page 297 of Reference 7

$$C_3 = 1.339$$

$$C_4 = C_5 = 1.467$$

$$C_6 = 1.355$$

Thus,

$$C_7 = \frac{2(1.339) - (1.467)^2}{1.467} = 1.007$$

$$M = \frac{2000(.685) (.16)}{6(1.007)} \left[\frac{3}{1 - (.3)^2} \right]^{1/2}$$

$$M = 65.9 \text{ in.lb./in} \quad (29.9 \text{ Kg-m/m})$$

The maximum meridional bending stress located at the inside surface of the liner is

$$\sigma_b = \frac{6M}{t^2} = \frac{6(65.9)}{(.16)^2}$$

$$\sigma_b = 15.5 \text{ ksi} \quad (1.07 \times 10^8 \text{ N/m}^2)$$

3.1.3.2 (Continued)

and the maximum combined meridional stress is

$$\sigma_{\max} = 21.4 + 15.5 = 36.9 \text{ ksi} \quad (2.54 \times 10^8 \text{ N/m}^2)$$

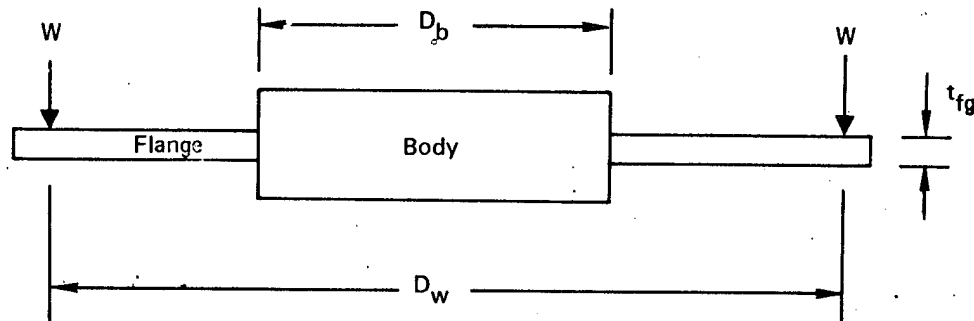
Based on a 75.0 ksi ($5.17 \times 10^8 \text{ N/m}^2$) ultimate strength for annealed 321 stainless steel, the margin of safety is

$$\text{M.S.} = \frac{75.0}{36.9} - 1 = \underline{\underline{+1.03}}$$

At the operating pressure of 1500 psi ($1.03 \times 10^8 \text{ N/m}^2$) the maximum meridional stress is 75% of the burst value - or 27.7 ksi ($1.91 \times 10^8 \text{ N/m}^2$). Thus, during operation the weld is not stressed beyond the yield point.

B. Flange Design

The second critical section of the boss is the flange, which is designed to react against the axial port load. Stresses there were determined by using the conservative assumption that the flange is a flat plate with a concentrated annular load and a fixed inner edge (the body).



3.1.3.2 (Continued)

The end-for-end wrap pattern of the longitudinal filaments produces a rigid band around the boss that supports the flange. The load applied (W) is the reaction of the boss flange bearing against the composite structure (liner + filament-wound composite). The total load is, therefore, equivalent to the pressure acting over the area within the reaction circle. The diameter (D_w) at which the load is assumed to act is

$$D_w = (1 + \epsilon_{f,l})D_b + 2.0w_l$$

Where,

$$\epsilon_{f,l} = \text{longitudinal filament strain at failure} \\ - 0.021 \text{ in/in (0.021 cm/cm)}$$

$$w_l = \text{filament winding tape width} = 0.20 \text{ in} \\ (.508 \text{ cm})$$

$$D_b = \text{boss diameter} \sim 1.24 \text{ in. (3.15 cm)}$$

The bending stress (σ_b) at the juncture of the flange and boss is calculated in accordance with formulas for loading on a flat plate (Reference 7, Case 22, Page 242):

$$\sigma_b = \beta_{22}W/t_{fg}^2$$

Where,

$$\beta_{22} \approx \frac{D_w}{D_b} - 1$$

$$W = \left[\pi p_b D_w^2 \right] / 4$$

$$t_{fg} = \text{flange thickness} = 0.194 \text{ in (0.493 cm)}$$

3.1.3.2 (Continued)

Solving the relationships

$$\begin{aligned}D_w &= (1 + 0.021) 1.24 + 2.0 (0.2) \\ &= 1.67 \text{ in} \quad (4.24 \text{ cm})\end{aligned}$$

$$\beta_{22} = \frac{1.67}{1.24} - 1 = 0.35$$

$$W = \pi(2000)(1.67)^2/4 = 4380 \text{ lbs} (1989 \text{ Kg})$$

The bending stress is

$$\sigma_b = 0.35(4380)/(0.194)^2 = 40.8 \text{ ksi} (2.8 \times 10^8 \text{ N/m}^2)$$

and the margin of safety is

$$\text{M.S.} = \frac{75.0}{40.8} - 1 = \underline{\underline{+0.84}}$$

3.2 FABRICATION

3.2.1 LINER FABRICATION

The liner was fabricated from 321 stainless steel per the drawings shown in Figures 4 through 6. The liner shell consisted of five individual pieces as illustrated in the schematic (Figure 7). The domes were hydroformed to contour and the center body section roll-formed.

The first step of the liner assembly process was to assemble the bosses. The two pieces of the boss and the liner close-out section were assembled and electron beam welded. A cross-section of an assembled boss is shown in Figure 8. This assembly was then roll-seam welded to the domes as shown in Figure 9. Next the center body section was roll formed and the longitudinal weld made. This section was then joined to the domes for the final closeout (See Figure 10). All joints, with the exception of the electron beam weld in the bosses, were lapped and roll-seam welded. The entire liner was then annealed to relieve the stresses.

3.2.1 (Continued)

The liner was subjected to X-ray inspection and helium leak checks and then weighed and labeled. A completed liner is shown in Figure 11.

There were no major problems encountered in the liner fabrication and all tolerances were held. The liner was very fragile and extreme care had to be taken to prevent denting or buckling the shell. To facilitate handling and to maintain alignment of the bosses, a wood dowel was inserted through the boss opening of one end and extended over the length of the tank.

3.2.2 VESSEL FABRICATION

In preparation for winding the vessels, the stainless steel mandrel was sized by placing it into a fiberglass mold. This mold, shown in Figure 12, was made to the exact outside contour of the liner. Since the liner was very unstable the sizing mold was used to obtain the correct vessel length and boss alignment. While the liner was in the mold the winding support shaft was installed and secured to the bosses. An internal pressure of 5 psi (3.45×10^4 N/m²) was applied to the liner to insure contact with the mold and then final adjustments were made.

On the initial vessels (Nos. 1 through 4), water-soluble plaster was sloshed inside the liner to provide additional support. The plaster was sloshed with the liner in the sizing mold and allowed to dry in the mold for a minimum of 36 hours at +160°F (+71°C). The mandrel was then removed from the sizing mold and permitted to dry an additional 36 hours at +160°F (+71°C) prior to winding the vessel. During the entire drying cycle, moisture was free to escape through the open bosses.

3.2.2 (Continued)

The shaft was installed in the mandrel just prior to winding. Concurrently with the fabrication of the initial five vessels, tests were conducted to determine whether or not the plaster support was really required. These tests showed that all tolerances could be held by merely pressurizing the mandrel to 10 psi ($6.9 \times 10^4 \text{ N/m}^2$). The plaster was subsequently deleted.

The prepared mandrel, whether or not it contained plaster, was installed in the winding machine and pressurized to 10 psi ($6.9 \times 10^4 \text{ N/m}^2$). That level of pressure brought the liner to contour without distortion. Next the liner was solvent cleaned with MEK, lightly abraded with "Scotchbrite" and then solvent cleaned again. The adhesive and scrim cloth were then applied. The adhesive used for each vessel is noted in Table III. The scrim cloth in all cases was style A-18752 nylon scrim purchased from Stein and Stein Textiles.

The polar windings were applied over the uncured adhesive while the mandrel was under internal pressurization. All polar windings were applied at 504 indexes per mandrel revolution. The band density was varied to obtain the desired fiber count. For vessels No. 1 and 2, the polar windings were applied at 402 yarns per inch (158 yarns/cm) using a band consisting of five yarns. The remaining vessels (No. 3 through 22) were wound using four yarns per band and a final yarn count of 321 yarns per inch (126 yarns/cm). The windings were applied under a tension of 0.5 lbs. per yarn (227 grams/yarn). Figure 13 shows the initial polar windings being applied on the metal liner.

The circumferential windings were applied after the polar winds and not interspersed. The first layer of circs were applied with a pressure of 10 psi ($6.9 \times 10^4 \text{ N/m}^2$) in the mandrel. The pressure was then increased 4 psi ($2.76 \times 10^4 \text{ N/m}^2$)

3.2.2 (Continued)

for each additional 2 layers of circs to a maximum of 20 psi ($13.79 \times 10^4 \text{ N/m}^2$). For example, the 2nd and 3rd layers were applied with a 14 psi ($9.66 \times 10^4 \text{ N/m}^2$), mandrel pressure; the 4th and 5th applied with 18 psi ($12.4 \times 10^4 \text{ N/m}^2$), and layers 6 through 8 with 20 psi ($13.79 \times 10^4 \text{ N/m}^2$). The purpose for the gradual increase was to prevent mandrel distortion and buckling of the previous circumferential windings.

The instrumentation clips and the thermocouple were wound into the vessels with the last layer of circumferential windings.

The vessels were cured in an air circulating oven per the prescribed cure schedule for the resin system used. Internal mandrel pressurization was maintained during the entire cure by means of a 2-way regulator. A 2-way regulator is required to maintain a constant pressure in the mandrel during heat-up and cool-down of the vessel.

Upon completion of the cure, the plaster support mandrel was washed from the vessel. The vessel was then leaked checked with a helium leak detector to insure liner integrity after fabrication and subjected to a general inspection. Weight, dimensions and internal volume were recorded on all vessels. Figure 14 shows a completed vessel. Weight summaries on each vessel are given in Tables V and VI.

Although no problems were encountered in the basic vessel fabrication, one serious problem did arise during the curing of the vessels. Due to the high negative coefficient of thermal expansion of the PRD-49 circumferential windings and the positive expansion of the stainless steel liner, buckles occurred in the liner during the curing operation. The buckles formed in the cylindrical section and at the tangent point of the domes. Approximately three wrinkles, equally

3.2.2 (Continued)

spaced, would form in the cylinder and run the length of the vessel. From the uniform pattern and the type of wrinkle it was evident that the liners were intact after the winding process and the vessel dimensions were within tolerance. The buckling occurred in the oven at temperatures above +200°F (+93°C). As the vessel temperature increased, the composite contracted and the liner attempted to expand. The adhesive constrained the liner to a great extent but at the elevated temperatures (>200°F) (>93°C) the thermal stresses in the liner were of sufficient magnitude that the adhesive could no longer constrain the metal and buckling occurred.

In an attempt to alleviate the wrinkles by minimizing the thermal stresses the cure cycle for vessel No. 5 was altered. Vessel No. 5 was fabricated with the same resin system, but instead of curing the vessel 4 hours at +300°F (+149°C), the vessel was cured 4 hours at +200°F (+93°C). The completed vessel had no evidence of wrinkles, thereby substantiating the conclusions of the previous study. Unfortunately, resin system No. 2, having an anhydride hardner, required a temperature of +250°F (+121°C) to fully cure. The resin system was completely jelled but not cured after the abbreviated cure cycle. The vessel was tested and performed satisfactorily (See section 3.4). This vessel confirmed the cause of the liner buckling and a lower temperature resin system was sought. Vessel No. 6 was fabricated with an epoxy/polyamide resin system; Epon 828/Versamide 140 (36 phr). The system was cured 7 days at room temperatures. The resulting vessel had no evidence of liner wrinkles and the composite was of good structural quality. The vessel was burst tested and exhibited excellent composite strength and modulus values. The disadvantages of the resin system were its short pot life and high initial viscosity. In winding

3.2.2 (Continued)

the vessel it was required to mix several small resin batches to maintain a suitable working life and acceptable winding viscosity. Because of this limitation an alternate room temperature system was sought.

Work performed by Lawrence Radiation Laboratory (Ref. 8) showed good success and PRD 49-3 fiber/resin compatibility with a room temperature curing system consisting of 100 parts DER 332* / 36 part T-403 hardener**.

Samples of this resin system were obtained and used to fabricate vessel No. 7. This vessel also came out in excellent condition and performed very well. Based on these findings, it was decided to use this resin system for the remaining vessels.

Consideration was given to filling the liner with a fluid and pressurizing the composite during winding to compensate for the thermal stresses during cure. An analysis of this approach revealed that pressurization levels of 300-500 psi ($2.06 - 3.45 \times 10^6 \text{ N/m}^2$) were required. Such a high level of pressurization impose unnecessary hazards during winding and would have an adverse effect upon the PRD-49 filament composite so it was not pursued.

3.3 TEST EQUIPMENT AND PROCEDURES

3.3.1 INSTRUMENTATION

Each vessel was instrumented to recorded vessel temperature, longitudinal strain, circumferential strain, internal pressure, and acoustic emission response (count rate and total count).

* Dow Chemical epoxy resin

** Jefferson Chemical

3.3.1 (Continued)

Vessel temperatures were measured with a chromel-Alumel thermocouple embedded in the final layer of circumferential windings.

The circumferential and longitudinal strains were measured with the aid of two transducers as shown in Figure 15 and 16 respectively. The strain transducers were connected to strain gaged beryllium copper blades such that the output of the resultant bridge circuit was proportional to the deflection of the blade tips. The electrical deflection indicators (EDI) were calibrated in the test environment prior to each test.

For the circumferential strain, a 0.012 inch (.305 mm) diameter wire was wrapped 360° around the circumference of the test vessel at its mid-point and attached to each tip of the EDI. Thus, the circumferential strain could be calculated from the measured EDI deflection and the known vessel circumference. (The vessel diameter given in Table V is based on the mean circumference as measured on an optical comparator. The circumferential gage length is the circumference at the exact location of the wire). For the first tests the circumferential elongation and internal tank pressure were recorded on a two-axis recorder giving a continuous plot of elongation versus pressure. For the cyclic test this data was recorded on a 14-channel Sangamo Model 3500 magnetic tape recorder and then re-plotted as desired.

For the longitudinal strain measurement, the tips of the EDI arms were attached to two studs embedded (installed during vessel fabrication) in the vessel wall as shown in Figure 16. The longitudinal strain was calculated from the measured longitudinal elongation (EDI output) and the known gage

3.3.1 (Continued)

length between the two studs. The longitudinal elongation versus pressure data was obtained in the same manner as that stated for the circumferential strains.

Internal Pressure measurements were obtained from pressure transducers located at the exit end of the pressure vessel.

Acoustic emission phenomena was monitored with Endevco type 2272 accelerometers which were connected to Dynamics 6987 charge amplifiers and a 1 KHz "hi-pass" filter. This data was then recorded on 2-channels of the Sangamc recorder. Equipment was available to record count rate and total acoustical count.

3.3.2 TEST EQUIPMENT

Testing was performed with a hydraulic pump unit with a capacity of 55 gpm (208 lpm) at 3000 psig (20.7×10^6 N/m²). Pressure and pressurization rate was controlled through a closed loop servo valve system. A Data-trak programmer provided accurate and controlled pressurization rates and pressure cycle profiles. The test vessels were installed in a heavy steel chamber for safety precautions and to provide temperature control. A forced draft hot air heating system was used to maintain a temperature of 70°F \pm 5°F (21°C \pm 2°C) test temperature condition in the chamber.

A schematic of the test system is shown in Figure 17. A picture of an installed vessel is shown in Figure 18.

3.3.3 TEST PROCEDURE

Burst Test - For the burst tests, the vessels were pressurized to failure at a constant rate of 1000 psi/minute (6.89×10^6 N/m² per minute). All instrumentation data was recorded continuously.

3.3.3 (Continued)

Fatigue Tests - Vessels 7-18 were cycled fatigue tested at a pressurization rate of 1000 psi (6.89×10^6 N/m²)/minute to the desired percentage of ultimate strength and then decreased at the same rate to approximately 40 psi (27.6×10^4 N/m²). There was no hold period at either the peak or the low point of the cycle.

Vessels 19-22 were cycled in the same manner except the pressurization and depressurization rates were increased to 3000 psi (20.7×10^6 N/m²)/minute.

In all cases, data was recorded continuously.

3.4 TEST RESULTS

In this program a total of 22 vessels were tested. Six vessels were subject to single cycle burst and 16 vessels were cyclic fatigue tested using the equipment and procedures described in Section 3.3. All tests were conducted at +70°F (+21°C).

3.4.1 BURST TESTS

Vessels No. 1-6 were burst tested and the results of these tests are shown in Table VII . An explanation of how the values in Table VII are calculated is given in Appendix A.

Vessel No. 1 burst at a pressure of 2440 psi (16.8×10^6 N/m²) with failure occurring in the dome (See Figure 19). The circumferential strain was significantly lower than the longitudinal strain, as shown in Figure 20 , which is undesirable for maximum fiber efficiency. This poor efficiency was reflected in a low performance factor for the vessel. To force the burst into the cylindrical section of the vessel, the number of circumferential windings were reduced from 800 to 760 yarns/inch (315 to 300 yarns/cm) for Vessel No. 2.

3.4.1 (Continued)

Vessel No. 2 did fail in the circumferential windings as desired (Figure 21) at a pressure of 2750 psi ($19.0 \times 10^6 \text{ N/m}^2$). This provided a very good performance gain; however, after reviewing the stress-strain behavior of the tank (Figure 22) it was evident that further optimization could be obtained by lowering the burst pressure. In Vessel No. 3, to lower the burst pressure, the longitudinal fiber count was reduced from 402 to 321 yarns/inch (158 to 126 yarns/cm) and the circumferential count reduced from 760 to 608 yarns/inch (299 to 239 yarns/cm).

Vessel No. 3 failed at a burst pressure of 2400 psi ($16.6 \times 10^6 \text{ N/m}^2$) with a performance factor of 1.73×10^6 inches ($4.39 \times 10^6 \text{ cm}$). The pressure vs strain relationships are shown in Figure 23 . The vessel gave the desired strain behavior and it was decided to use the design of this particular vessel for the remaining tanks and concentrate efforts towards solving the liner buckling problem that was occurring during fabrication (see Section 3.2.2). Vessel (No.3) is shown in Figure 24.

Vessels No. 4, 5 and 6 failed at values of 2640 psi ($18.2 \times 10^6 \text{ N/m}^2$), 2520 psi ($17.4 \times 10^6 \text{ N/m}^2$), and 2680 psi ($18.5 \times 10^6 \text{ N/m}^2$) respectively. These vessels are shown in Figures 25 26 and 27 with the corresponding stress strain curves shown in Figures 28 , 29 and 30 . The vessels, although fabricated from different resin systems or exposed to different cures, showed no significant differences in burst strength (Table VII) and gave very good performance factors [$(>1.75 \times 10^6 \text{ in.})$ ($>4.45 \times 10^6 \text{ cm}$)].

The PRD 49-3 filament wound tanks in general, gave very good results in terms of translating fiber properties to the composite vessel properties. Table VIII shows the tensile strengths and modulus of the fibers used in the vessel fabrication. The

3.4.1 (Continued)

vessels exhibited nominal fiber stresses of 360 - 380,000 psi ($24.8 - 26.2 \times 10^8 \text{ N/m}^2$) and composite modulus values in the $14-16 \times 10^6$ psi ($9.7 - 11 \times 10^{10} \text{ N/m}^2$) range as shown in Table VII. (The composite modulus values for axial windings shown in Table VII are higher than calculated by the rule of mixtures because of contributions of both the liner and the hoop windings. Similarly, this applies to the hoop winding modulus values shown. The total wall modulus values shown considers the total wall thickness in the calculation of modulus. (See Appendix A). For Vessels No. 3-6 the average total wall modulus in the axial and hoop direction were 4.94 and 9.72×10^6 psi (3.4 and $6.7 \times 10^{10} \text{ N/m}^2$) respectively. These values are approximately a factor of 2 higher than that obtainable with S-glass filament wound vessels.

The performance factors for the vessels were very good, especially considering the strength of the fiber used. An average performance factor, based on composite weight, of 1.77×10^6 inches (4.5×10^6 cm) was achieved with Vessels No. 3-6. (The performance factor of a similar S-glass vessel based on composite weight, is $1.0 - 1.2 \times 10^6$ inches or $2.5 - 3.0 \times 10^6$ cm). If the weight of the metal liner is included, this reduces to a value of 1.1×10^6 inches (2.79×10^6 cm). The performance factor of the entire tank was $\approx .56 \times 10^6$ inches (1.42×10^6 cm). When considering this latter value one must take into account that the metallic fittings on these particular tanks were larger than structurally required for a vessel in the 2500 psi ($17.2 \times 10^6 \text{ N.m}^2$) operating range and weighted ≈ 294 gram each. Both fittings combined constituted approximately 49% of the total vessel weight and reflects a fictitiously low performance factor for design purposes. The fittings were refined and reduced to a weight of 100 grams each in vessels 19-22. With further refinements it's feasible to reduce the fitting weight

3.4.1 (Continued)

to 10% of the total vessel weight resulting in a total vessel performance factor (including liner and composite) in the range of 0.9×10^6 inches (2.3×10^6 cm).

3.4.2 CYCLIC FATIGUE RESULTS

Vessels 7-22 were subjected to cyclic fatigue loading at either 50 or 75% of ultimate strength. Vessels No. 7-18, contained stainless steel liners while Vessels 19-22, fabricated under a program modification, contained slosh-type elastomeric liners. All 16 vessels had the same composite construction and configuration, although a few adhesive changes were made in some vessels as shown in Table III .

The results of the cyclic fatigue testing are summarized in Table IX. Vessels 7-10, 15, 16 and 19-22 were cycled at 75% of ultimate strain, and vessels 11-14, 17 and 18 were tested at 50% of ultimate strain.

The pressure levels for cycling were established from the maximum strains from vessels No. 3-6.

Vessel No.	Max. Strain, %	Max. Pressure, psi (10^6 N/m ²)
3	1.57	2400 (16.6)
4	1.61	2640 (18.2)
5	1.63	2520 (17.4)
6	<u>1.82</u>	<u>2680</u> (<u>18.5</u>)
Average	1.66	2560 (17.7)

From these values, 50% and 75% of ultimate strain were 0.83% and 1.24% respectively or nominal pressure levels of 1270 (8.76×10^6 N/m²) and 1900 (13.1×10^6 N/m²) psig. Consequently vessels No. 7-10, 15 and 16 were cycled at 1900 psi (13.1×10^6 N/m²) and vessels 11-14, 17 and 18 were cycled at 1270 psi (8.76×10^6 N/m²). Vessels 19-22 were also cycled at 75% of

3.4.2 (Continued)

ultimate strain or 1.24%. Since these vessels did not contain a metallic liner, a strain level of 1.24% was reached at 1500 psi ($10.3 \times 10^6 \text{ N/m}^2$). (These latter vessels were made under a program modification and a different lot of PRD 49-3 fiber was used in their fabrication. Strain was the only common factor that could be applied).

Figures 31 through 62 show the stress-strain curves for each vessel in both the longitudinal and circumferential directions. In reviewing the curves, it should be noted that the first cycle and in some cases the second cycle were not pressurized to the peak cyclic pressure since the instrumentation used required one or two cycles to obtain an accurate pressure setting.

All the vessels, whether cycled at 50% or 75% of ultimate, reached a state of equilibrium after about the third pressure cycle. Thereafter, very little change occurred in either the vessel modulus or the hysteresis loop. However, the stress-strain curve of the metal-lined composite vessel in this equilibrium condition was not as linear as an uncycled vessel. This is evident by comparing the stress-strain curves of vessels 7-18 to those of vessels 1-6. On the other hand the modulus of the vessels did increase by a value of $\approx 1-2 \times 10^6$ psi ($0.7 - 1.4 \times 10^{10} \text{ N/m}^2$) as a result of cycling.

There were distinct differences in the stress-strain behavior of the metallic-lined vessels (No. 7-18) and the elastomeric lined vessels (No. 19-22) during cyclic testing. The latter vessels experienced only a minor change in composite modulus, showed very little hysteresis and maintained essentially linear stress-strain behavior throughout their cyclic loading. In contrast, the metallic lined vessels did increase in modulus,

3.4.2 (Continued)

had considerable hysteresis and did not maintain a linear stress-strain behavior. The stress-strain curves for vessels 19-22 during cycling compare favorably to the uncycled metal-lined tanks (No. 1-6). In fact the stress-strain relationship for vessel No. 22 did not change over 2493 pressure cycles. No indication of impending failure could be detected from either the longitudinal or circumferential strains in that vessel.

The total number of pressure cycles which each vessel withstood is given in Table IX. All the vessels with the exception of No. 22, failed in the liner. Vessel No. 22 withstood 2493 cycles and failed in the dome as shown in Figure 63.

The metallic-lined vessels during cycling would buckle away from the composite wall and within relatively few cycles (usually less than 10) the liner would pin-hole and leak. Leakage would generally occur at the liner seams since these were the points of peak stress. Liner de-bonding and buckling could be readily detected with the acoustic emission sensors so a fairly accurate assessment was made at which point these events occurred.

The polyurethane adhesive developed under a previous NASA program (Ref. 2) and specified for use in this program did not provide adequate adhesion to the stainless steel. Several attempts were made to obtain better adhesion to the liner and prevent or delay the buckling.

A epoxy-polyamide adhesive was used on vessels No. 9 and 10, and a slight improvement resulted. Still the performance of these vessels was substantially below the goal of 4000 cycles or composite failure. On vessel No. 15 a more flexible adhesive with higher peel strength was tried unsuccessfully. Vessel No. 16 used EA934 epoxy adhesive and again no significant improvement

3.4.2 (Continued)

was noted and the mode of failure remained the same. The adhesion to the stainless steel was good but the liner would separate in localized areas and immediately liner failure would occur. With relatively high consistency the initial leakage would occur in the dome-to-body weld area. On vessels 17 and 18 the weld area was reinforced with PRD 49-3 style 120 fabric to reduce the strain. Vessel No. 17 had one layer and vessel No. 18 had two layers of fabric reinforcement in the tangent region. Both vessels used EA934 adhesive with primer. These vessels reached 125 and 230 cycles respectively. The composite portion of all the cycled tanks was in excellent condition after test as evidenced by viewing tank No. 14 in Figures 64 and 65, (except where locally damaged by release of the hydraulic fluid).

It is obvious from the data that greater cyclic life would have been obtained if increased liner-to-composite adhesion could have been obtained. A heat cured adhesive system could have been incorporated had not the initial thermal-stress problem been encountered during fabrication (see Section 3.2.2). This may have given a slight improvement but not actually solved the problem. The welded seams in the liner are stress risers and if possible, future designs should eliminate as many welds as possible, even at the sacrifice of adding weight by fabricating a thicker liner. Using a 3-mil (.076 mm) liner imposes many limitations on material selection, fabrication and assembly techniques. By increasing the thickness to about 10 mils (.254 mm) the liner could possibly be constructed with only one central weld.

Vessels No. 9-12 after their initial testing were slosch-coated with an elastomeric sealant PR 1440 from Products Research and recycled.

These vessels went an additional 50; 1, 230 and 900 cycles respectively before detectable leakage again occurred. The vessels themselves did not fail.

3.4.2 (Continued)

Vessels 19-22, each containing an elastomeric liner, were cycled 473, 115, 607, and 2493 cycles respectively before leakage or failure occurred. Liner leakage occurred in vessels 19-21 and the tests had to be terminated. Vessel No. 22 failed in the composite as a result of fatigue.

After completing the fatigue tests, vessels No. 7-12 and 19-21 were burst tested to determine the effects of cycling on their ultimate performance. The results of these tests are shown in Table X. All nine tanks had the same basic composite construction and failed at an average pressure of 2,005 psi ($13.8 \times 10^6 \text{ N/M}^2$) with a deviation of ± 250 psi ($\pm 1.72 \times 10^6 \text{ N/M}^2$). The stress-strain curves for each of these vessels are shown in Figures 31-42 and 66-68. The broken tanks are shown in Figures 69 through 77. All nine tanks from the fatigue tests were leaking at the time they were taken to burst and that leakage may have precipitated failure. This is apparently the case in vessels No. 7 and 10 which failed near or below the cyclic pressure. The values shown in Table X may therefore be conservative, although by comparing the ultimate strains they are not unrealistically low. For example, vessels No. 19-21 had ultimate strains of the same magnitude as vessels 3-6 even though the pressures were lower. This seems to indicate that the metallic liners in the latter vessels (No. 3-6) contributed to the vessels performance. There is no evidence that cycling the vessels enhanced the performance of the vessel as was the case with PRD 49-I vessels tested under a previous program (Ref. 1).

3.4.3 ACOUSTIC EMISSION STUDIES

The purpose of the acoustic emission studies was to determine if the technique could be used as a quality assurance or safety procedure that would predict or detect impending vessel failure. Vessels were instrumented to record count rate and total count of acoustic emissions transmitted from the vessels.

3.4.3 (Continued)

Vessels No. 1-6 were burst tested and the acoustic emission curve for each is shown in Figure 78. Each of the vessels contained a stainless steel liner which proved to be a detriment to the acoustic studies. The emissions from the liner were of such high magnitude when compared to those emitted by the composite that the latter emissions were lost in the background noise. This was unfortunate since it was the emissions from the composite that was of primary concern. In reviewing Figure 78 it can be noted that the curves contain no severe spikes indicative of filament breakage, resin crazing or other high energy releases typical of composite fracture, until immediately prior to burst. In a previous program, Reference 1, it was shown that PRD-49 composites show relatively little acoustic activity until relatively high stress levels are attained (>80% of ultimate). Excluding the noise of the liner, similar results were obtained in this program but because of the high background noise, impending composite failure could not be detected prior to reaching approximately 98% of ultimate strength. At that level of sensitivity the technique is not satisfactory as a non-destructive quality assurance test technique.

During the fatigue testing of the composite vessels, where the pressure excursions were a fraction of the ultimate burst values the background noise of the liner made it virtually impossible to record the low level acoustic emission signals associated with the fatigue type degradation of the tanks. The metallic liner gave strong emission signals during each pressurization and depressurization cycle and these emissions increased with time. Initially the liner emissions were due merely to elastic and plastic strain. Eventually the liner would debond from the composite wall (a gradual process over several pressure cycles) and these signals were detected. Once debonding occurred liner buckling would occur, followed in a relatively few cycles by liner tearing (metal fatigue) and leakage. All this activity

3.4.3 (Continued)

would mask any small signal emitted by the composite. A typical curve for a metal-lined tank under cyclic fatigue is shown in Figure 79.

One major event that was monitored effectively by the acoustic sensors was that of liner buckling. Once buckling did occur it could be detected on both the pressurization and depressurization cycles. Upon pressurization the liner buckles would relieve themselves at approximately 500 psi and then on depressurization the liner buckles would again form at about the same pressure level.

In summary, monitoring the acoustic emission signals of a thin metal lined composite vessel during pressurization, using the techniques employed in this program, does not appear to be a feasible way of evaluating performances and/or integrity of the filamentary composite portion of the vessel. Signals from the metal liner make it impossible to pick up the low-level but structurally significant signals from the composite. Without the isolation of those signals no correlation or predictions on the composite can be made. Major revisions in the instrumentation, sensors, or monitoring technique may produce more qualitative data. The existing technique can detect major events associated with the tank as a whole, such as liner debonding or leakage and could be a valuable tool in that capacity.

4.0 CONCLUSIONS

- A. It was demonstrated that a 3-mil (.0762 mm) stainless steel closed-end liner could be fabricated and used as a mandrel for filament-wound case construction without buckling or distortion. The liner concept appears acceptable for the long term storage of gases or corrosive fluids requiring only single cycle operation. The concept evaluated in this program is not practical at this stage for multi-cycle usage, with the deficiency lying in the metallic liner. The composite portion of the vessel has demonstrated excellent cyclic performance both in this and a previous program (Ref. 1.).

Because of the good performance gains possible with the PRS-49-III composite vessels, it is recommended that alternate liner approaches be taken to achieve a reliable system. Namely, reduce the number of welds in the liner. To accomplish this, it may require using a thicker liner to permit other modes of fabrication and assembly.

- B. PRD-49-III fiber performed well as a reinforcement for filament wound tanks and pressure vessels. Performance factors in excess of 1.75×10^6 inch (4.45×10^6 cm) were consistently obtained. Although liner failures prevented the accumulation of several fatigue data points, one vessel withstood 2493 pressure cycles at 75% of ultimate strain.

Metal-lined vessels, taken to burst after varying degrees of fatigue cycling, had performance factors ranging from 1.31 to 1.44×10^6 inches (3.33 to 3.66×10^6 cm). (The metal liners were not leak-free on the cycled vessels at the time of burst evaluation.) There appears to be no difference in the performance factors between vessels

4.0 (Continued)

cycles at 50% and 75% of ultimate or in the number of pressure cycles the vessels had previously been subjected prior to burst.

- c. Acoustic emission studies performed on the thin metal lined composite vessels evaluated in this program did not prove to be an acceptable method of detecting or predicting composite or filamentary failure. The acoustic emission signals from the metallic liner were of such high magnitude that the low-level signals from the composite were completely masked. The test technique could detect gross events such as liner debonding or liner buckling.

5.0 REFERENCES

1. Hoggatt, J. T.; "Development of Cryogenic PRD 49-1 Filament-Wound Tanks," NASA CR-120835, The Boeing Company, Seattle, Washington, December 1971
2. Toth, J. M., Jr.; and Soltysiak, D. J.; "Investigation of Smooth-Bonded Metal Liners for Glass Fiber Filament-Wound Pressure Vessels," NASA CR-72165, Douglas Aircraft Co., Inc., Santa Monica, Calif., May 1967
3. Landes, R. E. and Morris, E. E.; "Analysis of Filament-Wound Dome and Polar Boss of Metal-Lined Glass-Filament-Wound Pressure Vessels," NASA CR 72599, Aerojet-General Corporation, January 1970
4. Morris, E. E. and Landes, R. E.; "Cryogenic Glass-Filament-Wound Tank Evaluation," NASA CR 72948, Structural Composites Industries, July 1971
5. Hall, C.A., et al; "Low Thermal Flux Glass-Fiber Tubing for Cryogenic Service," NASA CR-72797, Martin Marietta Corp., Denver, Colorado, March 1971
6. Darms, F. J. and Landes, R. E.; "Computer Program for the Analysis of Filament-Reinforced Metal-Shell Pressure Vessels," NASA CR 72124, Aerojet-General Corporation, Rev. May 1972
7. Roark, R. J.; "Formulas for Stress and Strain," 4th Edition, McGraw-Hill Book Company, 1965
8. Chiao, T. T., Moore, R.L.; "A Room-Temperature-Curable Epoxy for Advanced Fiber Composites," UCRL-74751, Lawrence Livermore Laboratory, Livermore, Calif., September 1973

Table I : Design Requirements for PRD 49-3 Filament Wound Pressure Vessel

FIBER

Type	PRD 49-3	--
Specific Gravity	0.052 lb/in ³	1.44 g/cc
Tensile Strength	375,000 psi	25.86 x 10 ⁸ N/m ²
Modulus	18 x 10 ⁶ psi	12.4 x 10 ¹⁰ N/m ²

RESIN

Type; Epoxy	Epon 828/Empol 1040/MNA/BDMA	--
Tensile Strength (R.T.)	4,000 psi	27.6 x 10 ⁶ N/m ²
Modulus	0.5 x 10 ⁶ psi	0.3 x 10 ¹⁰ N/m ²
Coefficient of Thermal Expansion	32.11 x 10 ⁻⁶ in/in/°F	57.86 x 10 ⁻⁶ cm/cm/°C
Specific Gravity	.040 lb/in ³	1.11 g/cc

COMPOSITE

Fiber Volume	68 ± 2%	68 ± 2%
Per Ply Thickness	0.004 inches	0.010 cm
Poissons Ratio	0.3	0.3
Coefficient of Thermal Expansion	-2.75 x 10 ⁻⁶ in/in/°F	-4.95 x 10 ⁻⁶ cm/cm/°C

LINER

Material	Series 300 Stainless Steel	--
Thickness (Nominal)	0.003 Inches	0.076 mm
Boss Diameter-O.D. (Nominal)	1.25 Inches	3.18 cm
Boss Design	"Hinge" Concept	--

GENERAL REQUIREMENTS

Design Temperature	+70°F	+21°C
Operational Temperature	-423°F to +70°F	-252°C to +21°C
Inside Vessel Diameter	8.0 Inches	20.32 cm
L/D Ratio	1.5	1.5
Longitudinal-to-Circumferential Strain Ratio	1.0	1.0
Burst Pressure-Nominal	2000 psi	1.38 x 10 ⁶ N/m ²

Table II: Material Properties Type 321 Stainless Steel (Annealed)

Property	Fortran Symbol	Value	
Density	RHOL	0.289 lb/in ³	8.0 g/cc
Coefficient of Thermal Expansion (+75°F to -423°F) (+21°C to -252°C)	ALFL	6.76 × 10 ⁻⁶ in/in/°F	12.2 × 10 ⁻⁶ cm/cm/°C
Tensile-Yield Strength	SYL	38,000 psi	2.62 × 10 ⁸ N/m ²
Derivative of Yield Strength with Respect to Temperature	DSYLDT	-116.0 psi/°F	-1.44 × 10 ⁶ N/m ² /°C
Elastic Modulus	EL	28.0 × 10 ⁶ psi	19.3 × 10 ¹⁰ N/m ²
Derivative of Elastic Modulus with Respect to Temperature	DELDT	-8030. psi/°F	-99.7 × 10 ⁶ N/m ² /°C
Plastic Modulus	EI	384,000 psi	26.5 × 10 ⁸ N/m ²
Derivative of Plastic Modulus with Respect to Temperature	DEIDT	-0.1 psi/°F	-.124 × 10 ⁴ N/m ² /°C
Pisson's Ratio	VL	0.295	0.295
Derivative of Poisson's Ratio with Respect to Temperature	DNULDT	0.0 1/°F	0.0 1/°C
Ultimate Strength		75,000 psi	5.17 × 10 ⁸ N/m ²

Table III Vessel Fabrication Parameters

	Vessel																					
	1	2	3	4	5	6	7	8	9	10	11	12	13	14	15	16	17	18	19	20	21	22
Liner	✓	✓	✓	✓	✓	✓	✓	✓	✓	✓	✓	✓	✓	✓	✓	✓	✓	✓	✓	✓	✓	✓
• 321 Stainless Steel																						
• Elastomeric																						
Scrim - Style A2757/14																						
Adhesive - See Table IV	1	1	1	1	1	1	1	1	2	2	1	1	1	1	3	4	5	5	-	-	-	-
Composite Fiber Count																						
• Polar Windings - Yarns/Inch	402	402	321	→	→	→	→	→	→	→	→	→	→	→	→	→	→	→	→	→	→	321
Yarns/Cm	158	158	126	→	→	→	→	→	→	→	→	→	→	→	→	→	→	→	→	→	→	126
Circumferential Windings - Yarns/Inch	800	760	608	→	→	→	→	→	→	→	→	→	→	→	→	→	→	→	→	→	→	608
Yarns/Cm	315	299	239	→	→	→	→	→	→	→	→	→	→	→	→	→	→	→	→	→	→	239
Winding Tension - Lbs/Yarn	0.5	→	→	→	→	→	→	→	→	→	→	→	→	→	→	→	→	→	→	→	→	0.5
Gm/Yarn	227	→	→	→	→	→	→	→	→	→	→	→	→	→	→	→	→	→	→	→	→	227
Resin System - See Table IV	6	6	6	6	6	6	7	8	→	→	→	→	→	→	→	→	→	→	→	→	→	8
Cure Cycle - See Below	A	A	A	A	B	C	→	→	→	→	→	→	→	→	→	→	→	→	→	→	→	C
Special Notes - See Below															D	D	E	E				

Special Notes: (D) 1 Layer 120 Style PRD 49-3 Fabric, 2.54 cm Wide, Placed as Local Reinforcement in Tangent Region
 (E) Same as (D) Except 2 Layers of Fabric Inserted

Cure Cycle: (A) 2 Hrs @ 150° F (65° C)
 4 Hrs @ 300° F (149° C)
 (B) 4 Hrs @ 200° F (93° C)
 (C) 7 Days @ +77° F (25° C)

TABLE IV MATERIAL SELECTION

ITEM	MATERIAL	FORMU- LATION PARTS BY WT.	SUPPLIER
1	Adiprene L-100 Epirez 510 MOCA	100 20 17	General Electric Celanese Coatings Co. E. I. DuPont
2	Epon 828 Epoxy Resin Epon 812 Epoxy Resin Versamid 115 Versamid 125 Methyl Ethyl Ketone Solvent	50 50 50 50 10	Shell Chemical Co. Shell Chemical Co. General Mills, Inc. General Mills, Inc.
3	PR 1440 A-2 Hardener	100	Products Research Co. Products Research Co.
4	EA 934 Epoxy Adhesive EA 934 Catalyst	100 33	Hysol Co. Hysol Co.
5	Same as Item (4) except surface primed with: Metal Bond 329, type D Primer	-	-
6	Epon 828 Epoxy Resin Empol 1040 Resin Dodecenyl Succinic Anhydride Benzyl dimethylamine	100 20 115.9 1.0	Shell Chemical Co. Emery Industries, Inc. Allied Chemical Corp. Sumner Chemical Co.
7	Same as Item (2) without methyl ethyl ketone solvent	-	-
8	DER 332 Epoxy Resin T-403 Amine Hardener	100 36	Dow Chemical Co. Jefferson Chemical

Table V : Vessel Weight Summary — Metal-Lined Vessels

Vessel No.	1	2	3	4	5	6	7	8	9	10	11	12	13	14	15	16	17	18
Total Length, cm	38.15	39.40	39.68	39.48	39.59	39.08	39.31	39.62	39.75	39.69	39.63	39.66	39.73	39.74	39.68	39.63	39.61	39.71
Outside Diameter, cm	20.78	20.73	20.68	20.65	20.61	20.61	20.61	20.61	20.63	20.62	20.66	20.65	20.63	20.63	20.61	20.63	20.62	20.62
Internal Volume, cc	9,250	9,300	9,330	9,320	9,330	9,310	9,330	9,330	9,330	9,330	9,340	9,340	9,340	9,330	9,330	9,330	9,320	9,330
Circ Gage Length, cm	65.33	65.18	64.77	64.92	64.99	64.92	65.10	64.99	65.02	65.02	65.07	65.13	64.99	64.99	64.92	64.97	65.18	65.10
Long. Gage Length, cm	16.54	16.28	15.09	14.61	15.09	15.47	14.35	14.61	14.88	14.94	15.16	15.14	15.27	14.66	15.59	15.39	14.76	15.14
Total Vessel Weight, gms	1,354	1,280	1,180	1,200	1,184	1,218	1,205	1,198	1,189	1,189	1,207	1,212	1,213	1,217	1,227	1,250	1,282	1,270
Total Liner Weight, gms	764	765	766	769	765	767	766	766	768	770	773	765	774	762	762	761	766	764
Adhesive/Scrim, Weight, gm	56*	56*	56*	56*	56*	56*	56*	56*	40**	40**	56*	56*	56*	56*	60**	80**	80**	80**
Composite Weight, gms	534	459	358	375	363	395	383	376	381	379	378	391	383	399	405	409	436	426



Fittings weight of 293.5 gms each included in Liner weight

* Estimated weight from several trials

** Actual weight of adhesive and scrim applied

Table VI: Vessel Weight Summary – Elastomeric Lined Vessels

Vessel No.	19	20	21	22
Total Length, cm	39.67	39.73	39.61	39.72
Outside Diameter, cm	20.64	20.66	20.60	20.72
Internal Volume, cc	9,375	9,380	9,380	9,390
Circ. Gage Length, cm	64.82	64.87	64.87	65.07
Long Gage Length, cm	15.31	15.11	15.54	15.27
Total Vessel Weight, gms	642	637	635	661
Total Liner Weight, gms	216	216	216	216
Adhesive/Scrim Weight, gm *	56	56	56	56
Composite , Weight, gms	370	365	363	389

* Estimated weight from several trials

Table VII Vessel Test Results - Burst Test at +70°F

	Vessel Number					
	1	2	3	4	5	6
Burst Pressure, psi [10^6 N/m ²]	2440 [16.8]	2750 [19.0]	2400 [16.6]	2640 [18.2]	2520 [17.4]	2680 [18.5]
Failure Location	Boss	CIRCS	CIRCS	CIRCS	CIRCS	CIRCS
Modulus, Composite, 10 ⁶ psi [10^{10} N/m ²]						
Total Wall Axial	4.04 [2.79]	5.25 [3.62]	4.88 [3.37]	5.10 [3.52]	5.17 [3.57]	4.62 [3.19]
Total Wall Hoop	8.15 [5.62]	8.56 [5.90]	9.88 [6.81]	11.30 [7.79]	9.29 [6.41]	8.42 [5.81]
Axial Windings Only	11.99 [8.27]	13.53 [9.33]	14.65 [10.10]	15.32 [10.57]	14.00 [9.66]	13.45 [9.28]
Hoop Windings only	13.39 [9.23]	14.26 [9.83]	14.82 [10.22]	16.90 [11.66]	14.73 [10.16]	13.43 [9.26]
Rupture Strain (%)						
Axial Direction	1.32	1.28	1.57	1.61	1.61	1.59
Hoop Direction	1.28	1.48	1.52	N.A.	1.63	1.82
Fiber Stress, psi [10^8 N/m ²]						
Axial Direction	268,800 [18.54]	302,900 [20.89]	331,200 [22.84]	364,300 [25.12]	347,300 [23.99]	369,800 [25.50]
Hoop Direction	267,400 [18.44]	317,277 [21.88]	346,100 [23.87]	381,200 [26.29]	363,900 [25.10]	387,000 [26.69]
Performance Factor, PV/W, 10 ⁶ in [10^6 cm]						
Composite Only*	1.17 [2.97]	1.55 [3.94]	1.73 [4.39]	1.82 [4.62]	1.79 [4.55]	1.75 [4.45]
Total Wall**	0.86 [2.18]	1.03 [2.62]	1.05 [2.67]	1.11 [2.82]	1.09 [2.77]	1.1 [2.79]
Total Vessel***	0.46 [1.17]	0.56 [1.42]	0.53 [1.35]	0.57 [1.45]	0.55 [1.40]	0.57 [1.45]

* Based on Weight of Composite Only

** Based on Weight of Composite, Adhesive and Liner Less Weight of Bosses

*** Based on Total Tank Weight

TABLE VIII: PRD 49-III YARN TENSILE PROPERTIES

SPECIMEN No.	TENSILE STR		MODULUS	
	KSI	10^8 N/M ²	10^6 PSI	10^{10} N/M ²
1-1	395	27.2	18.6	12.8
1-2	401	27.7	18.8	13.0
1-3	402	27.7	18.6	12.8
2-1	445	30.7	19.1	13.2
2-2	347	23.9	18.9	13.0
2-3	366	25.2	18.9	13.0
3-1	364	25.1	19.0	13.1
3-2	412	28.4	19.2	13.2
3-3	395	27.2	19.0	13.1
4-1	380	26.2	19.1	13.2
4-2	408	28.1	19.4	13.4
4-3	384	26.5	18.7	12.9
5-1	285	19.7	18.6	12.8
5-2	367	25.3	18.5	12.8
5-3	380	26.2	18.8	13.0
6-1	384	26.5	19.0	13.1
6-2	379	26.1	19.0	13.1
6-3	354	24.4	19.1	13.2
7-1	390	26.9	19.4	13.4
7-2	373	25.7	18.6	12.8
7-3	438	30.2	18.7	12.9
7-4	406	28.0	19.0	13.1
8-1	533	36.8	19.1	13.2
8-2	460	31.7	19.1	13.2
8-3	450	31.0	19.4	13.4
8-4	395	27.2	19.2	13.2
AVERAGE	396	27.3	18.9	13.0

YARN AREA = 4.58×10^{-5} in² [29.55×10^{-5} cm²]

Table IX Vessel Test Results - Cyclic Fatigue (+70° F)

	7	8	9	10	11	12	13	14	15	16	17	18	19	20	21	22
Cyclic Pressure, psi [10^6 N/m ²]	1900 [13.1]	1900 [13.1]	1900 [13.1]	1900 [13.1]	1270 [8.76]	1270 [8.76]	1270 [8.76]	1270 [8.76]	1900 [13.1]	1900 [13.1]	1270 [8.76]	1270 [8.76]	1500 [10.3]	1500 [10.3]	1500 [10.3]	1500 [10.3]
% of Ult. Strength	75	75	75	75	50	50	50	50	75	75	50	50	75	75	75	75
Ult. Cyclic Strain, % Longitudinal	1.29	1.34	1.26	1.28	0.77	0.82	0.83	0.81	1.22	1.12	0.72	0.76	1.15	1.16	1.14	1.05
Circumferential	1.36	1.38	1.37	1.29	0.79	0.84	0.82	0.82	1.41	1.33	0.92	0.88	1.36	1.37	1.37	1.33
Composite Modulus, 10^6 psi [10^{10} N/m ²] Longitudinal - Initial	4.80 [3.31]	4.31 [2.97]	4.71 [3.25]	4.55 [3.14]	5.39 [3.72]	4.20 [2.90]	4.77 [3.29]	5.13 [3.54]	5.03 [3.47]	5.13 [3.54]	4.62 [3.19]	5.13 [3.54]	4.41 [3.04]	4.23 [2.92]	4.44 [3.06]	4.55 [3.14]
- Secondary	4.80 [3.31]	5.71 [3.94]	5.03 [3.47]	6.06 [4.18]	5.39 [3.72]	4.90 [3.38]	5.27 [3.63]	6.15 [4.24]	5.03 [3.47]	5.23 [3.61]	5.77 [3.98]	5.23 [3.61]	4.68 [3.23]	3.28 [2.95]	4.97 [3.43]	4.55 [3.14]
Circumferential - Initial	9.01 [6.21]	9.05 [6.24]	8.7 [6.00]	8.08 [5.57]	8.82 [6.08]	8.29 [5.72]	8.21 [5.66]	8.73 [6.02]	7.69 [5.30]	8.21 [5.66]	8.21 [5.66]	8.55 [5.89]	7.29 [5.02]	7.26 [5.0]	7.27 [5.01]	6.73 [4.64]
- Secondary	9.85 [6.79]	9.85 [6.79]	9.85 [6.79]	10.10 [6.97]	9.09 [6.27]	9.41 [6.49]	10.77 [7.43]	11.08 [7.46]	9.23 [6.37]	9.67 [6.67]	10.26 [7.08]	9.85 [6.79]	7.87 [5.43]	7.88 [5.43]	8.55 [5.90]	7.13 [4.92]
No. of Pressure Cycles	22	21	65 [50]*	110 [1]*	27 [230]*	26 [900]*	24	17	12	47	125	230	473	115	607	2493
Type of Failure	Liner Leakage															Composite (Dome)
Type of Liner	Metallic															Elastomeric

* Represents number of cycles placed on vessel after the metallic liner failed. Vessel slosh coated with an elastomeric liner and retested.

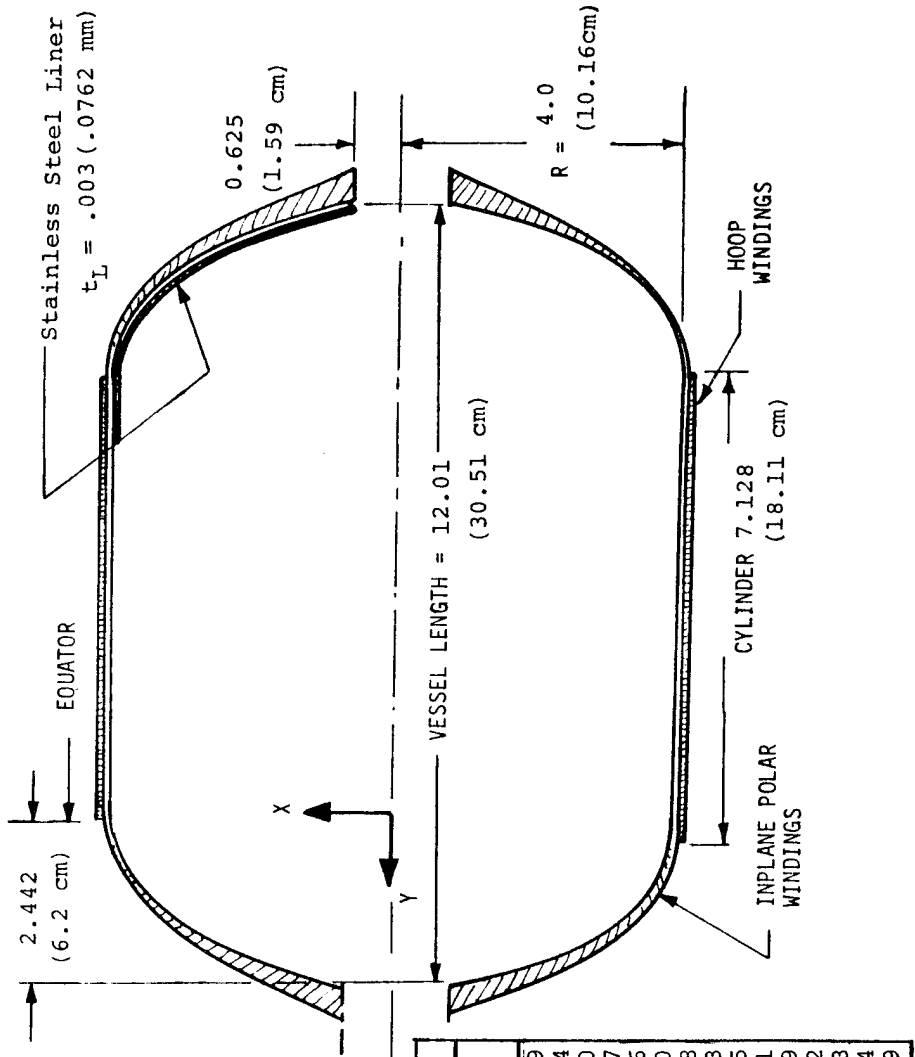
** Initial modulus is based on first pressure cycle. Secondary modulus is at equilibrium (\approx 5th cycle). All modulus values based on total composite wall thickness

Table X Vessel Test Results – Burst Strength After Fatigue Cycling (+70°F)

	Vessel Number										
	No. 7	No. 8	No. 9	No. 10	No. 11	No. 12	No. 19	No. 20	No. 21		
Burst Pressure, psi [10^6 N/m ²]	1750 [12.07]	1990 [13.27]	2040 [14.07]	1920 [13.24]	1870 [12.89]	2170 [14.97]	1940 [13.37]	2240 [15.54]	2130 [14.69]		
Failure Location No. of Pressure Cycles ¹	Dome 22	Dome 21	Dome 115	Dome 111	Dome 257	Dome 926	Dome 473	Dome 115	Dome 607		
Modulus, Composite, 10^6 psi [10^{10} N/m ²]											
Total Wall Axial	4.80 [3.31]	5.71 [3.94]	5.03 [3.47]	6.06 [4.18]	5.39 [3.72]	4.90 [3.38]	4.68 [3.23]	4.28 [2.95]	4.97 [3.42]		
Total Wall Hoop	9.85 [6.79]	9.85 [6.79]	9.85 [6.79]	10.10 [6.97]	9.09 [6.27]	9.41 [6.49]	7.87 [5.43]	7.88 [5.43]	8.55 [5.89]		
Axial Windings Only	14.16 [9.77]	16.16 [11.14]	14.23 [9.81]	18.18 [12.54]	14.23 [9.81]	14.46 [9.97]	11.43 [7.88]	11.24 [7.75]	12.97 [8.94]		
Hoop Windings Only	14.87 [10.26]	15.27 [10.53]	15.62 [10.77]	15.15 [10.45]	13.64 [9.41]	14.01 [9.66]	13.33 [9.19]	13.06 [9.01]	13.86 [9.56]		
Total Strain at Rupture (%)											
Axial Direction	1.09	1.32	1.3	1.25	1.29	1.56	1.46	1.66	1.50		
Hoop Direction	1.23	1.39	1.48	1.26	1.28	1.59	1.59	1.88	1.76		
Fiber Stress, psi [10^8 N/m ²]											
Axial Direction	251,600 [17.53]	286,200 [19.74]	293,400 [20.23]	276,100 [19.04]	268,900 [18.54]	312,100 [21.52]	279,000 [19.24]	322,200 [22.22]	306,300 [21.21]		
Hoop Direction	252,700 [17.43]	287,400 [19.82]	294,600 [20.32]	277,300 [19.12]	270,000 [18.62]	313,400 [21.61]	280,200 [19.32]	323,500 [22.31]	307,600 [21.21]		
Performance Factor, PV/W 10^6 In [10^6 cm] ²	1.18 [2.99]	1.37 [3.48]	1.38 [3.52]	1.31 [3.33]	1.28 [3.25]	1.44 [3.65]	1.36 [3.46]	1.57 [4.00]	1.52 [3.87]		

¹ Total no. of pressure cycles given vessel prior to pressurizing to failure

² Based on weight of composite only



DOME CONTOUR				
	Inches		cm	
	Y	X	Y	X
Equator	0.000	3.992	0.000	10.139
	0.159	3.982	0.404	10.114
	0.359	3.961	0.912	10.060
	0.558	3.916	1.417	9.947
	0.757	3.849	1.923	9.776
	0.956	3.760	2.428	9.550
	1.155	3.645	2.934	9.258
	1.354	3.501	3.439	8.893
	1.553	3.321	3.945	8.435
	1.752	3.095	4.450	7.861
	1.950	2.905	4.953	7.379
	2.147	2.414	5.453	6.132
	2.308	1.962	5.862	4.983
	2.325	1.545	5.906	3.924
	2.436	1.153	6.187	2.929
Boss				

FIGURE 1 SCHEMATIC OF 8 IN. DIAMETER (20.3 cm) PRESSURE VESSEL

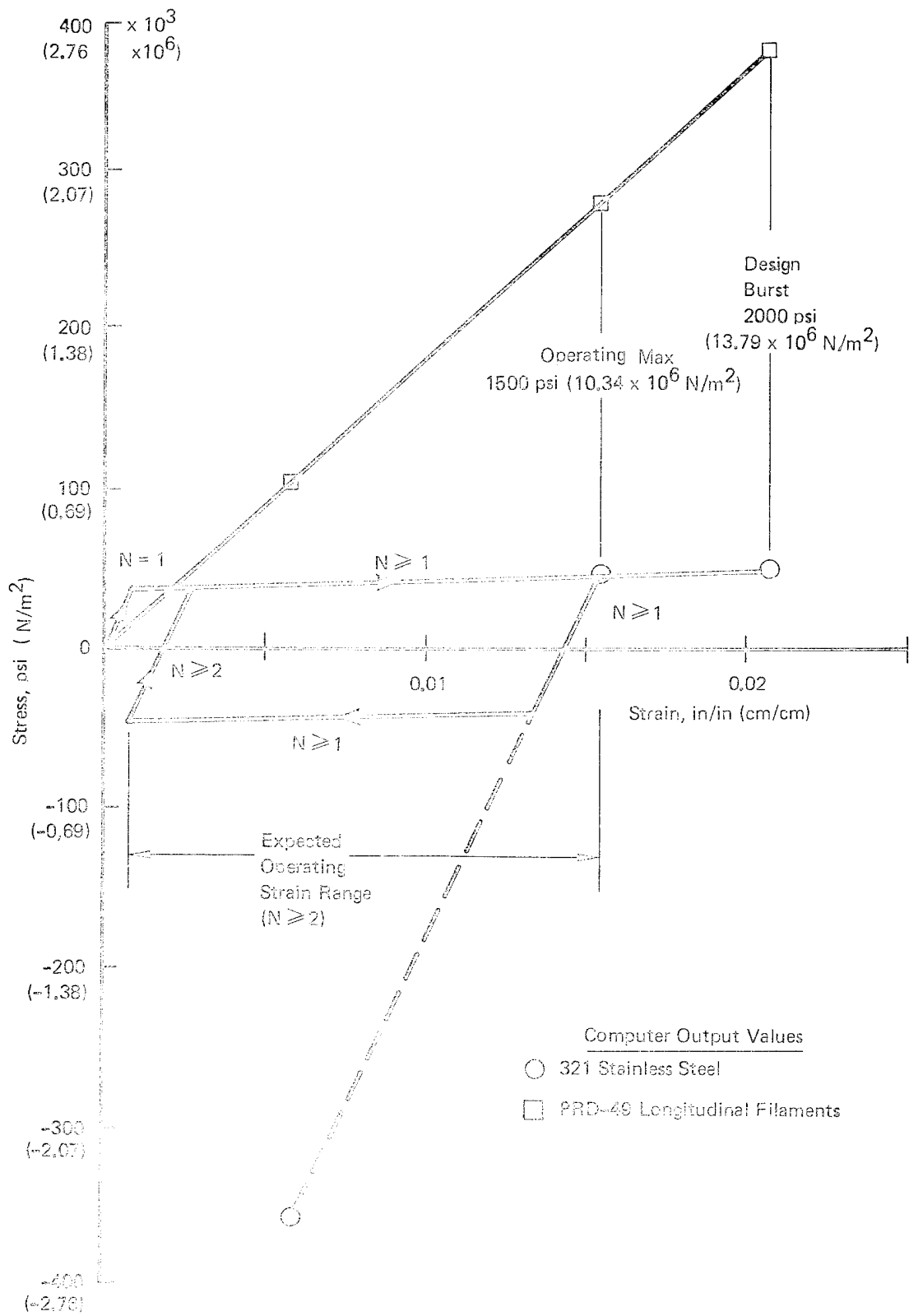


Figure 2: Ambient Stress-Strain Relationships, Longitudinal Direction of Cylinder (N = Cycle No.)

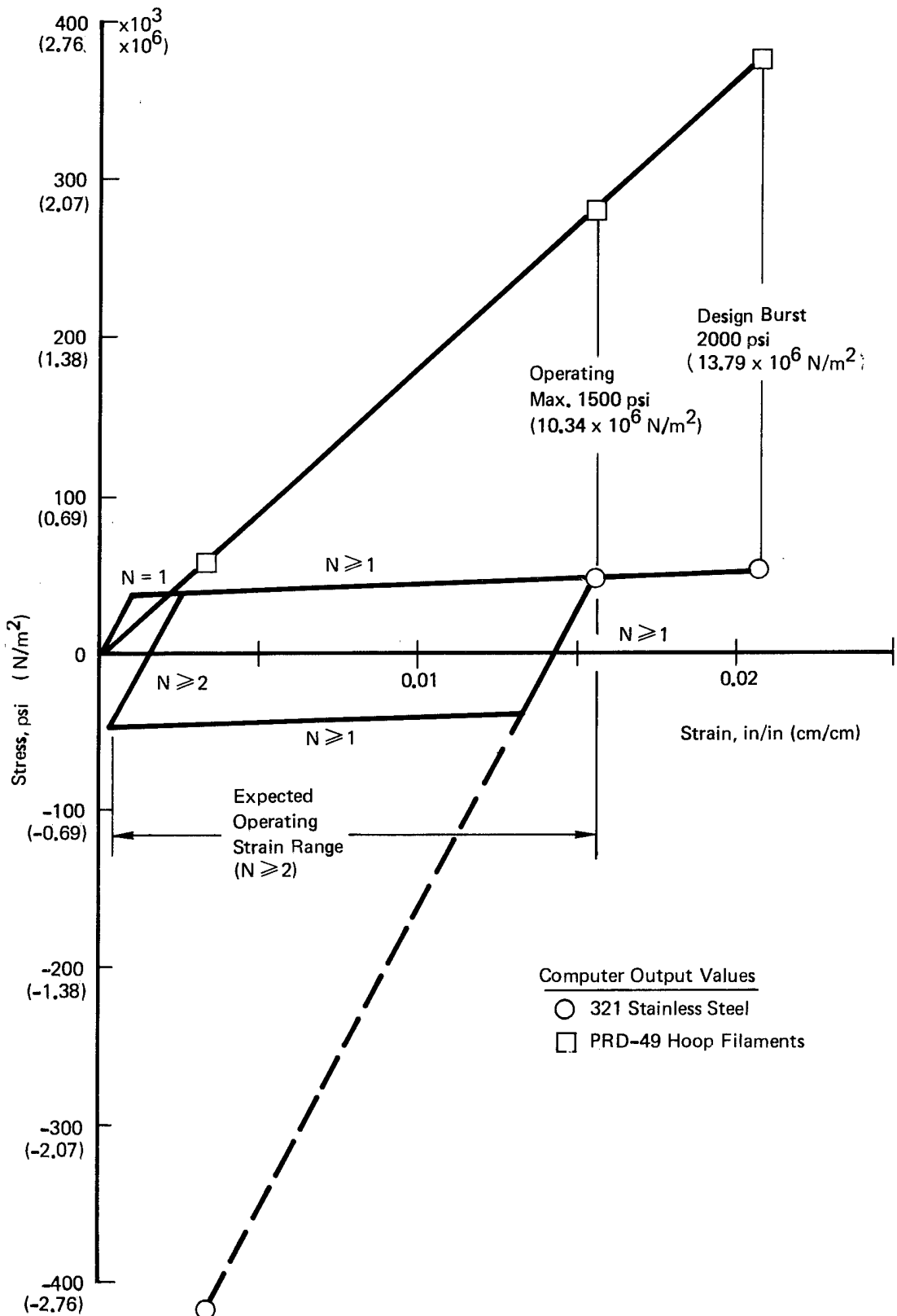
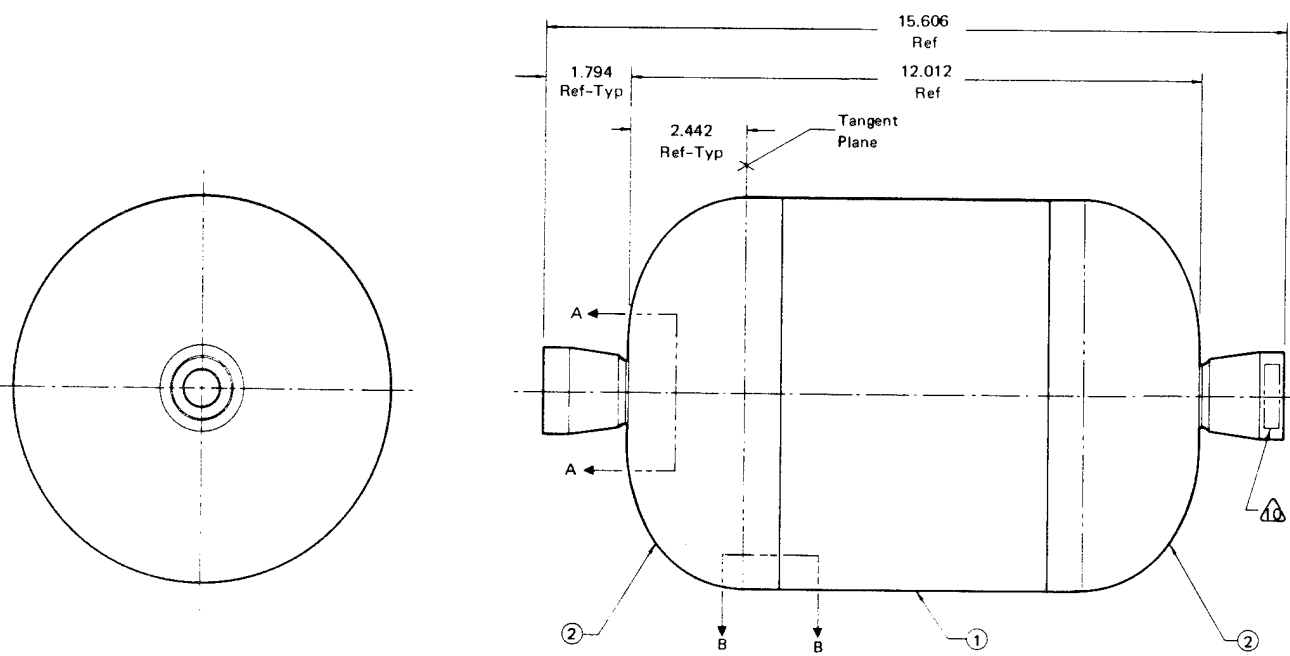
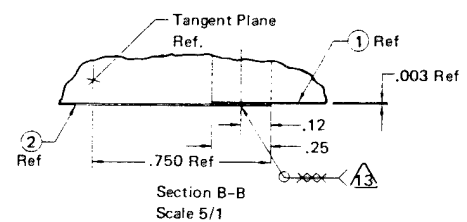
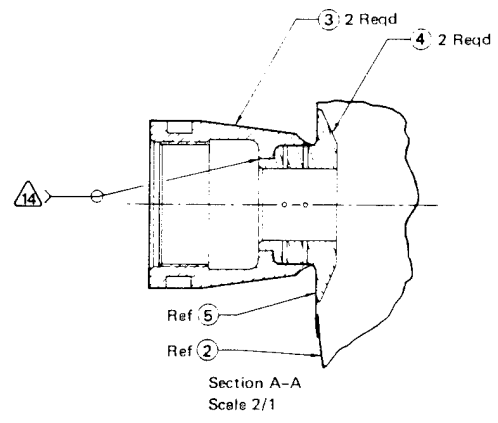


Figure 3 : Ambient Stress-Strain Relationships, Hoop Direction of Cylinder ($N =$ Cycle No.)



- NOTES:
1. Remove all burrs and sharp edges
 2. Interpret drawing per MIL-D-1000
 3. Machined surfaces to be $\sqrt{125}$ unless otherwise specified
 10. Contour shall not deviate more than .010 from true contour
 5. Thickness tolerance for items 1 & 5 shall be $+0.002$ Tolerance for item 2 shall be $+0.000$ be -0.000 .
 11. Surfaces indicated may be match machined, if reqd, to mating part.
 7. Radiograph inspect all welds prior to lead test, per Boeing specification BAC 5915-acceptance level Class A.
 8. Leak test liner assembly by pressurizing with freon gas type F-12 to 7 ± 1 PSIG and examining all welded areas with G.E. Halogen leak detector, model H2. An acceptable alternate test is to apply soap solution over entire exterior surface, holding at 7 ± 1 PSIG for 15 minutes minimum. All leaks will be noted, repaired, and test repeated.
 12. Apply one layer of item 6, teflon, to indicated surface of item 5. Teflon shall be .001 thk per ams 2515 with the following additional requirements:
 - A. Surface preparation-light grit blast.
 - B. Prime with type 850-204 or 851-204 solution
 - C. Topcoat application shall be teflon 851-224, 851-225 or 851-205.
 - D. Mask off surfaces not to be coated.
 - E. Teflon not to extend into filet area.
 13. Mark per ASD5215P with assigned assembly serial no.
 11. Mark container per ASD 5215N with 1269315-1 and assigned serial no.
 12. These dimensions to be coordinated to insure 7.128 length between tangent planes.
 13. Resistance seam weld per MIL-W-6858, Class A.
 14. Electron beam weld per BAC 5959.



QUANTITY REQD -1	NOMENCLATURE OR DESCRIPTION	MATERIAL	SPECIFICATION	ITEM NUMBER
A/R	Teflon	-	AMS 2515	6
2	Cup	Foil, Cres Type 321 Annealed	AMS 5510H	5
2	Boss	Bar, Cres Type 321 Annealed	AMS 5645G	4
2	Collar	Bar, Cres Type 321 Annealed	AMS F645G	3
2	Dome	Foil, Cres Type 321 Annealed	AMS 5510H	2
1	Cylinder	Foil, Cres Type 321, Annealed	AMS 5510H	1

FIGURE 4 - METALLIC LINER DRAWING

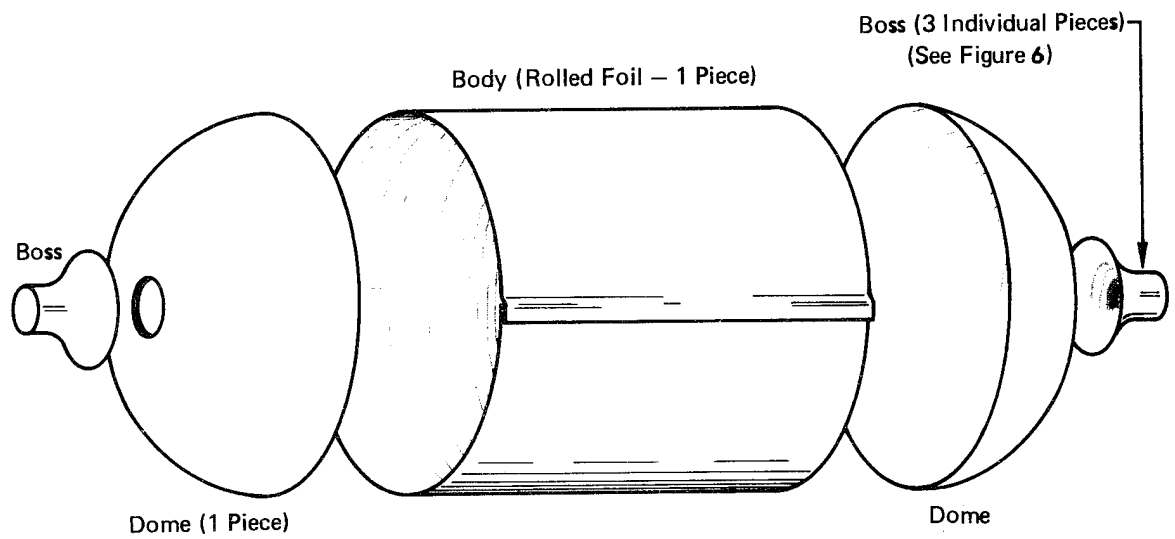


Figure 7 : Metallic Liner Assembly

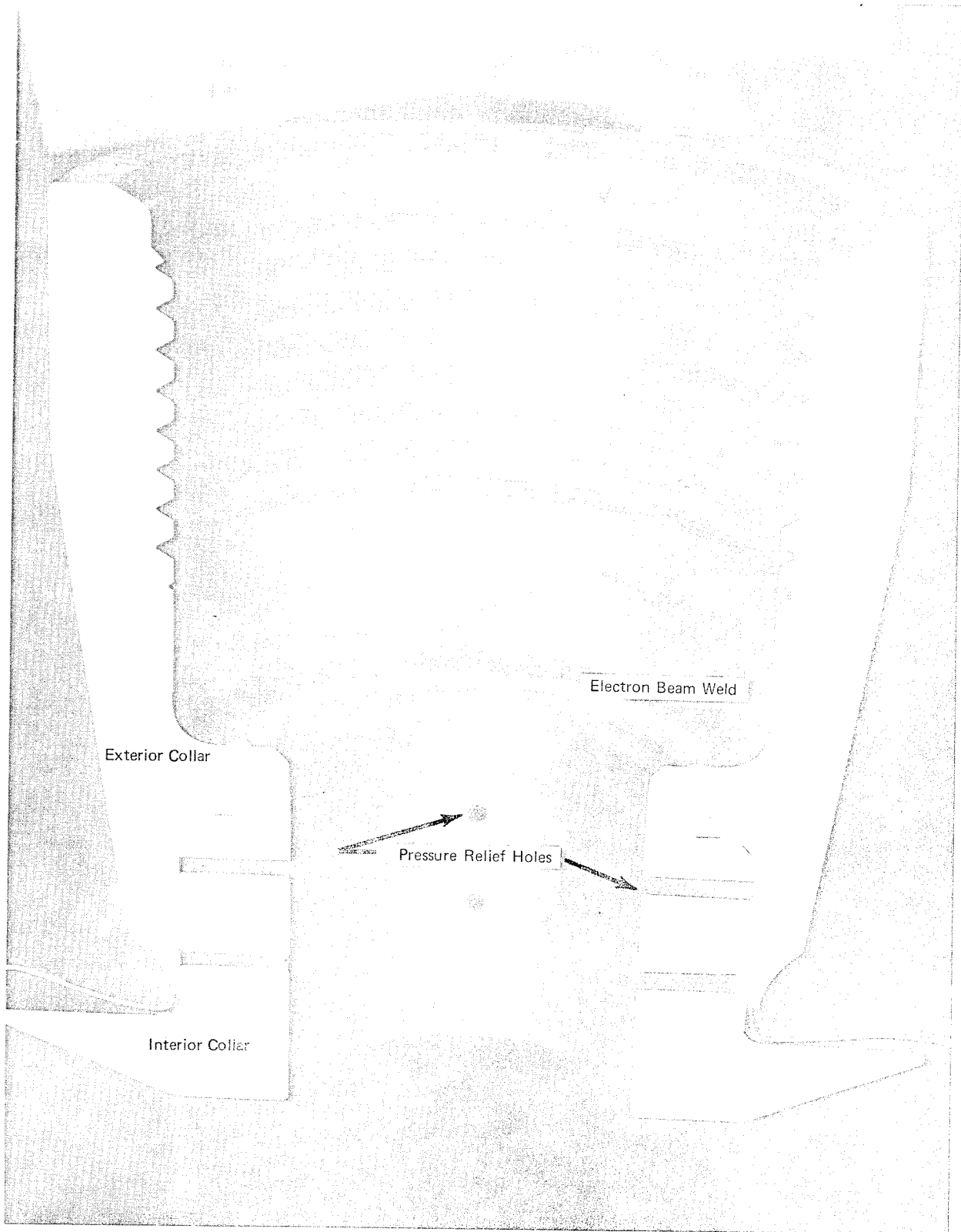


FIGURE 8 – CROSS-SECTION OF TANK BOSS

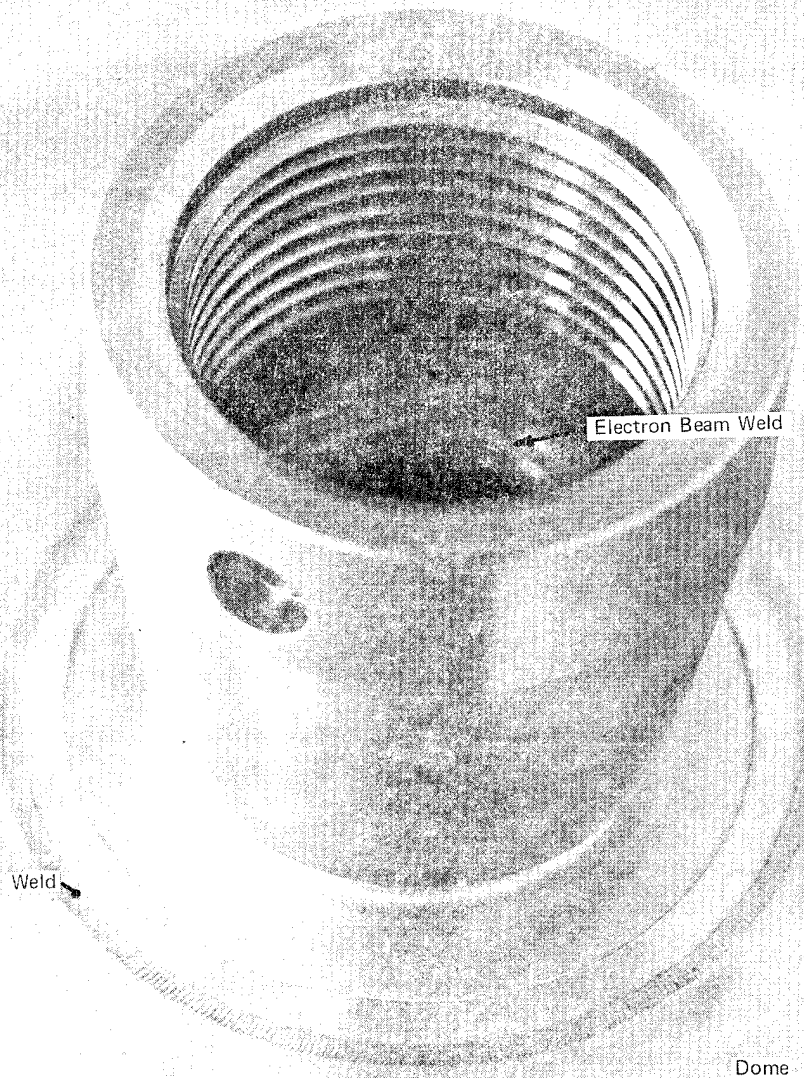


FIGURE 9 – LINER BOSS AND WELD ZONE ON DOME

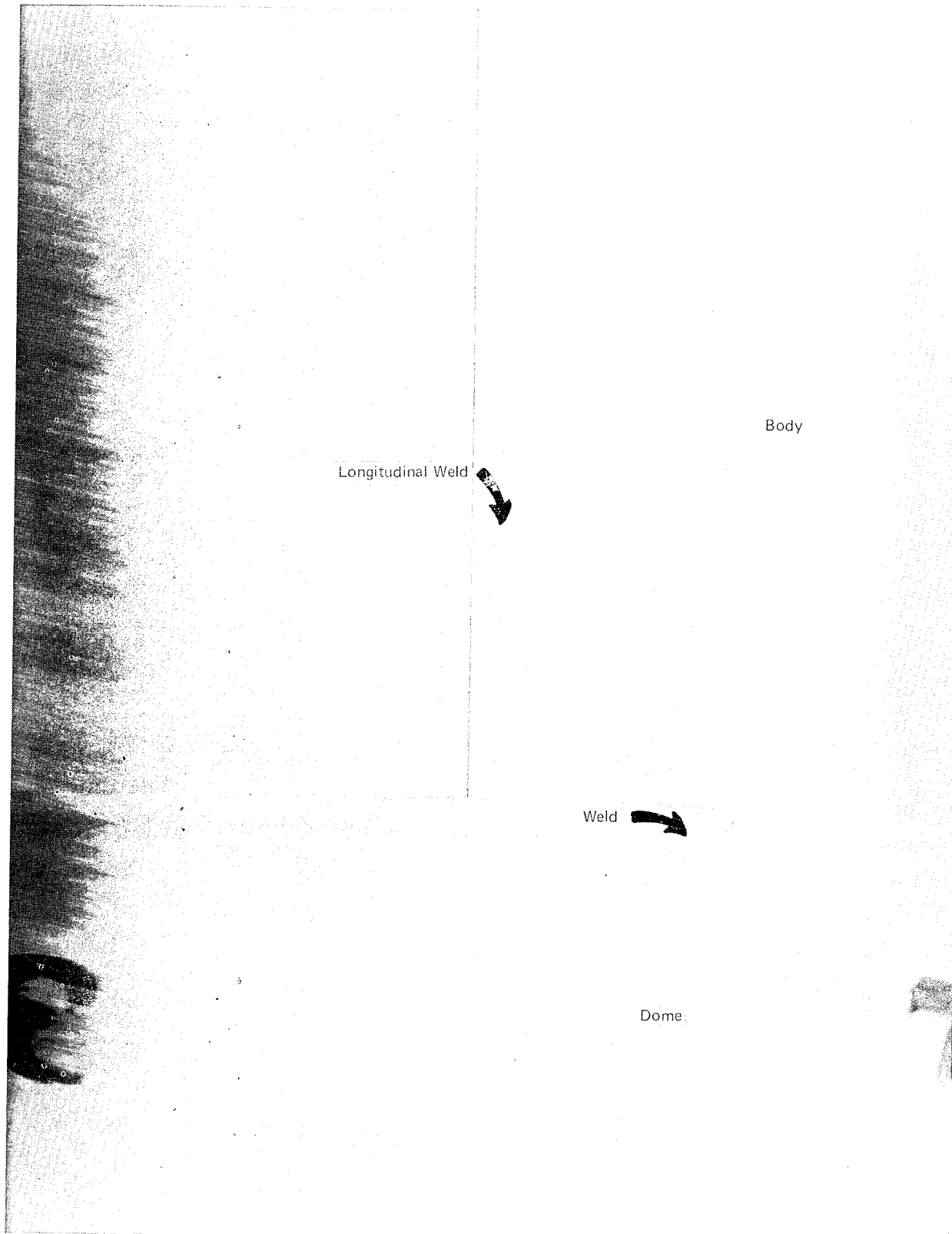


FIGURE 10 DOME -TO-BODY WELD AND LONGITUDINAL BODY WELD

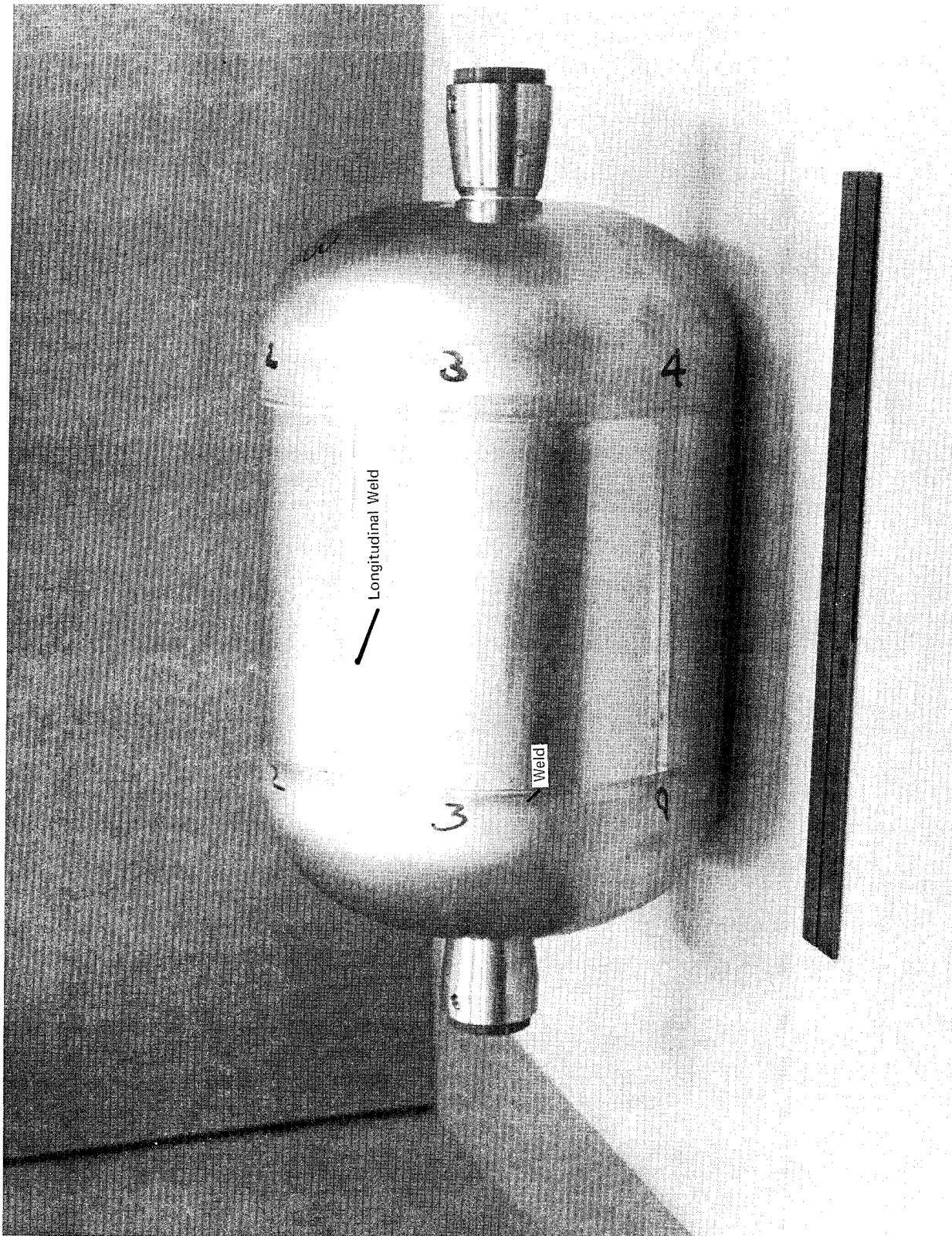


FIGURE 11 — METALLIC LINER—321 STAINLESS STEEL

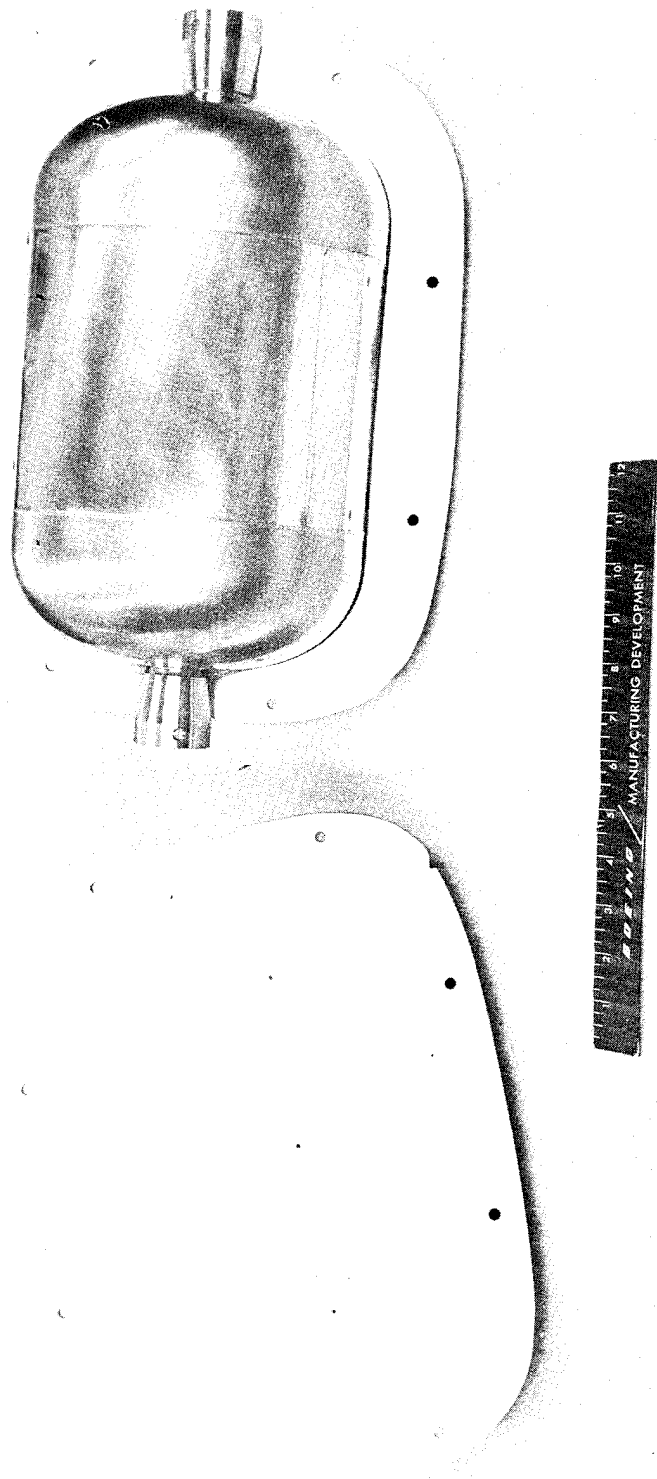
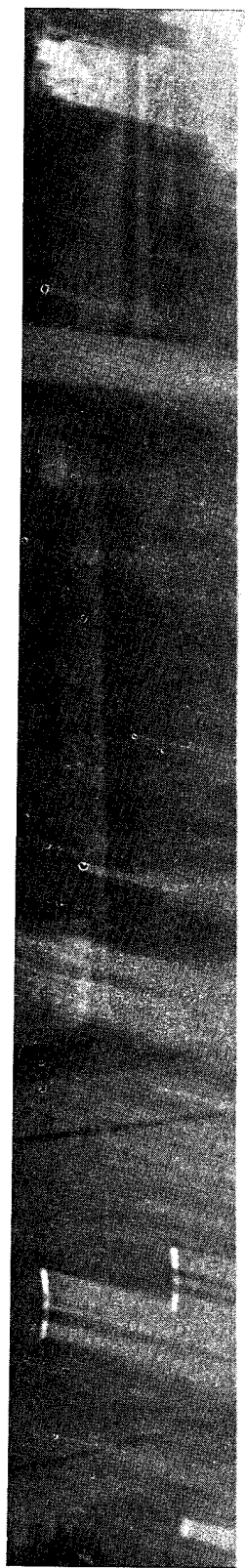


FIGURE 12--LINER STABILIZATION MOLD

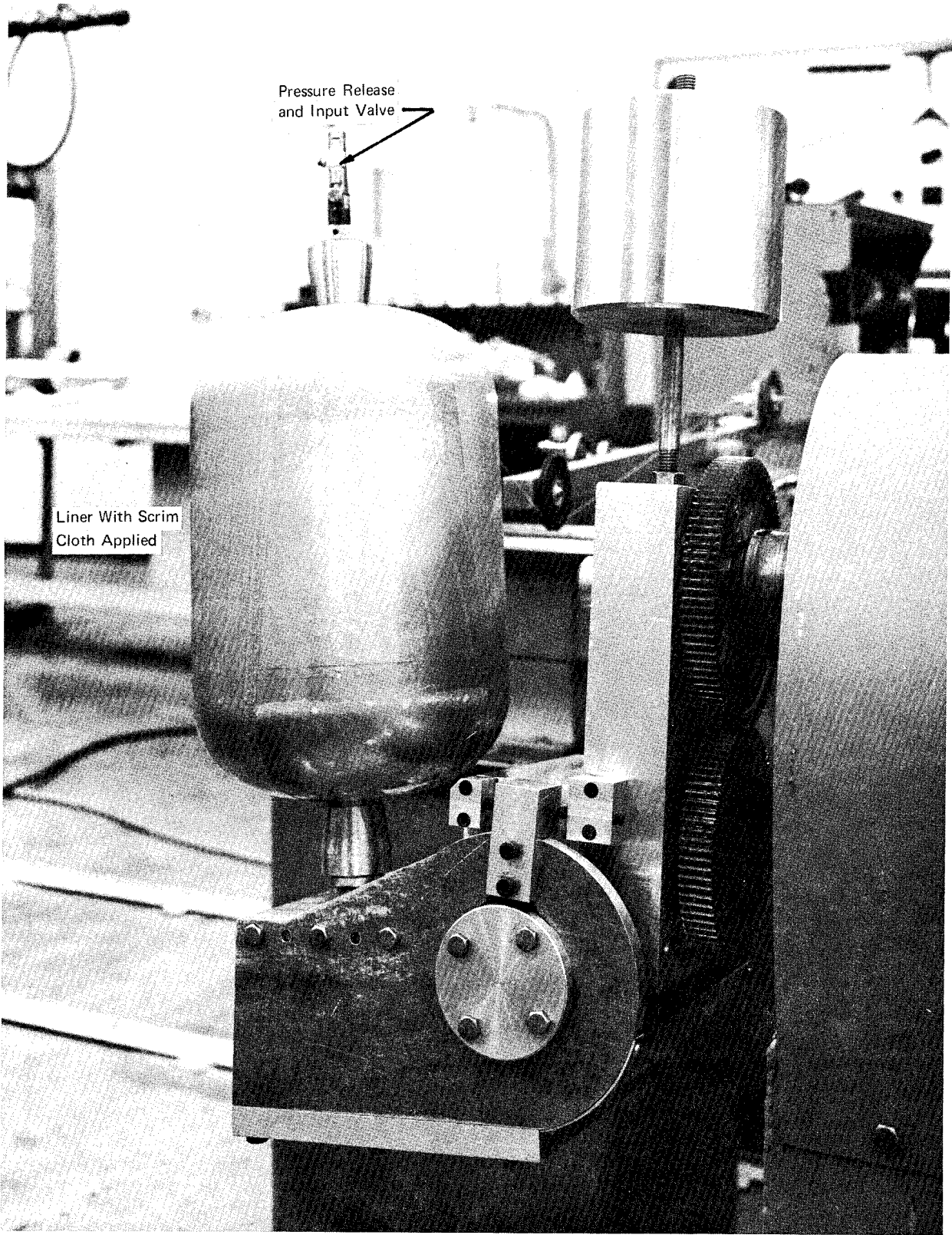


FIGURE 13—FILAMENT WINDING EQUIPMENT



FIGURE 14--8"DIAMETER PRD-49-III FILAMENT WOUND TANK--METAL LINER

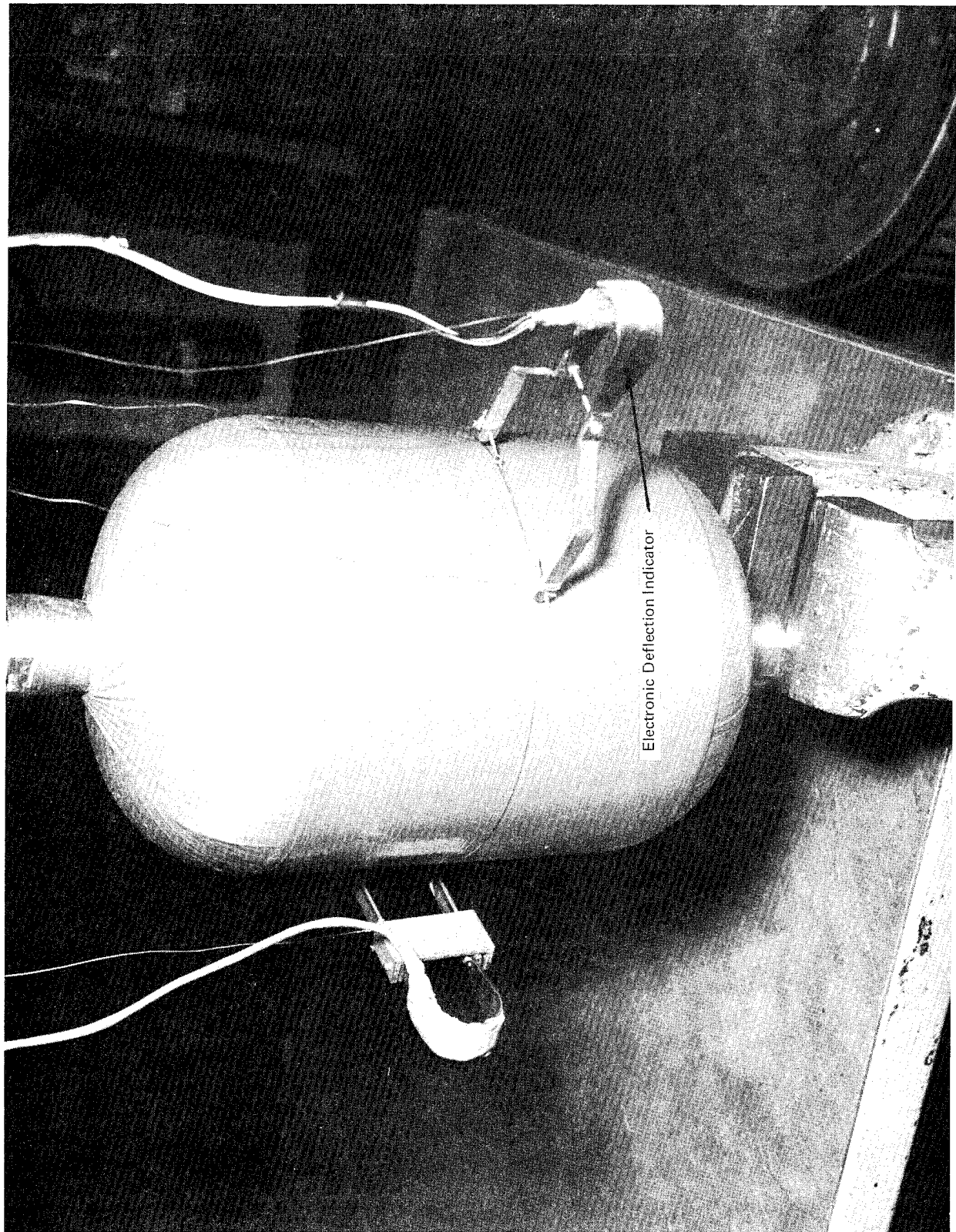


FIGURE 15—INSTRUMENTATION FOR CIRCUMFERENTIAL STRAIN MEASUREMENTS

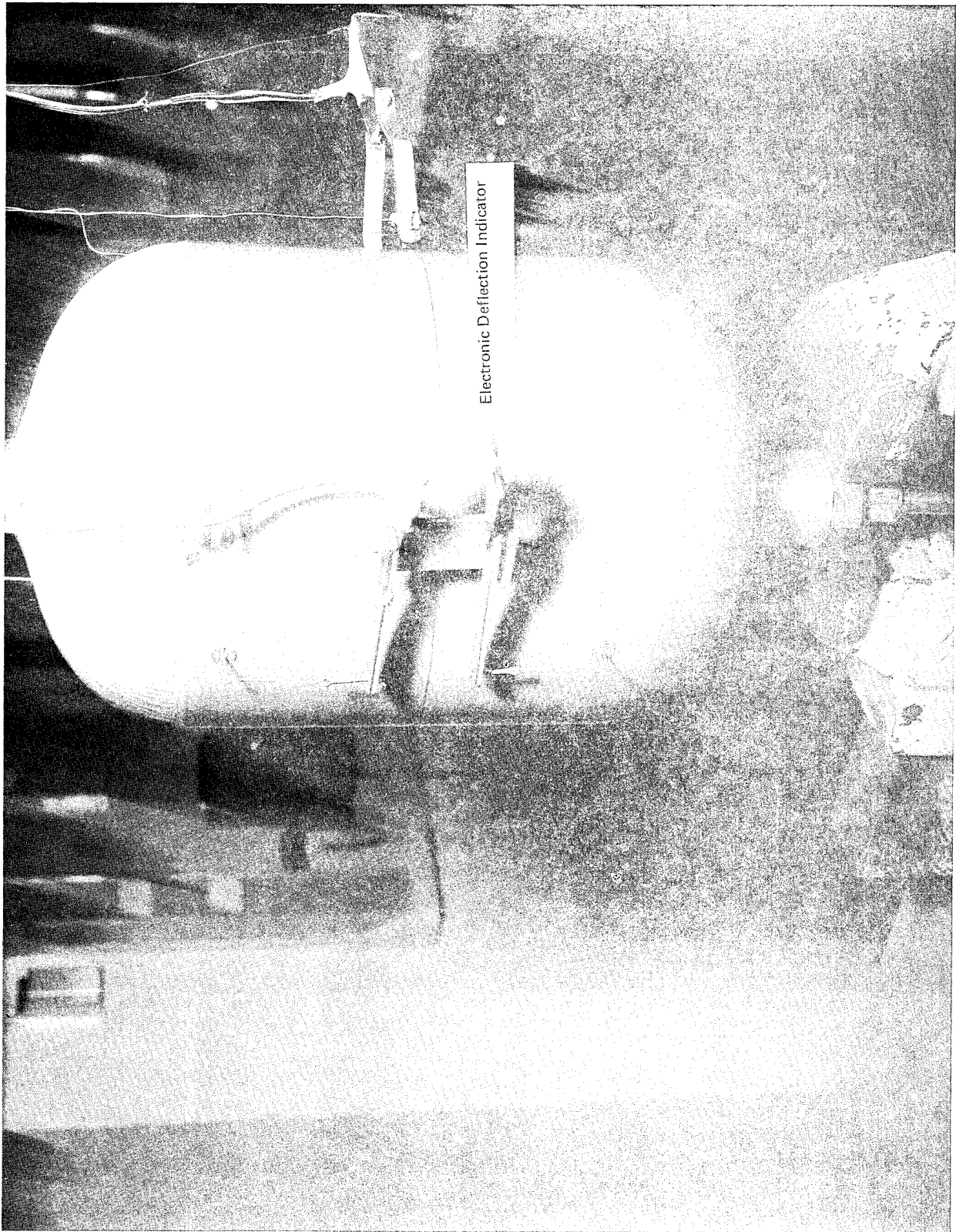


FIGURE 16—INSTRUMENTATION FOR LONGITUDINAL STRAIN MEASUREMENTS

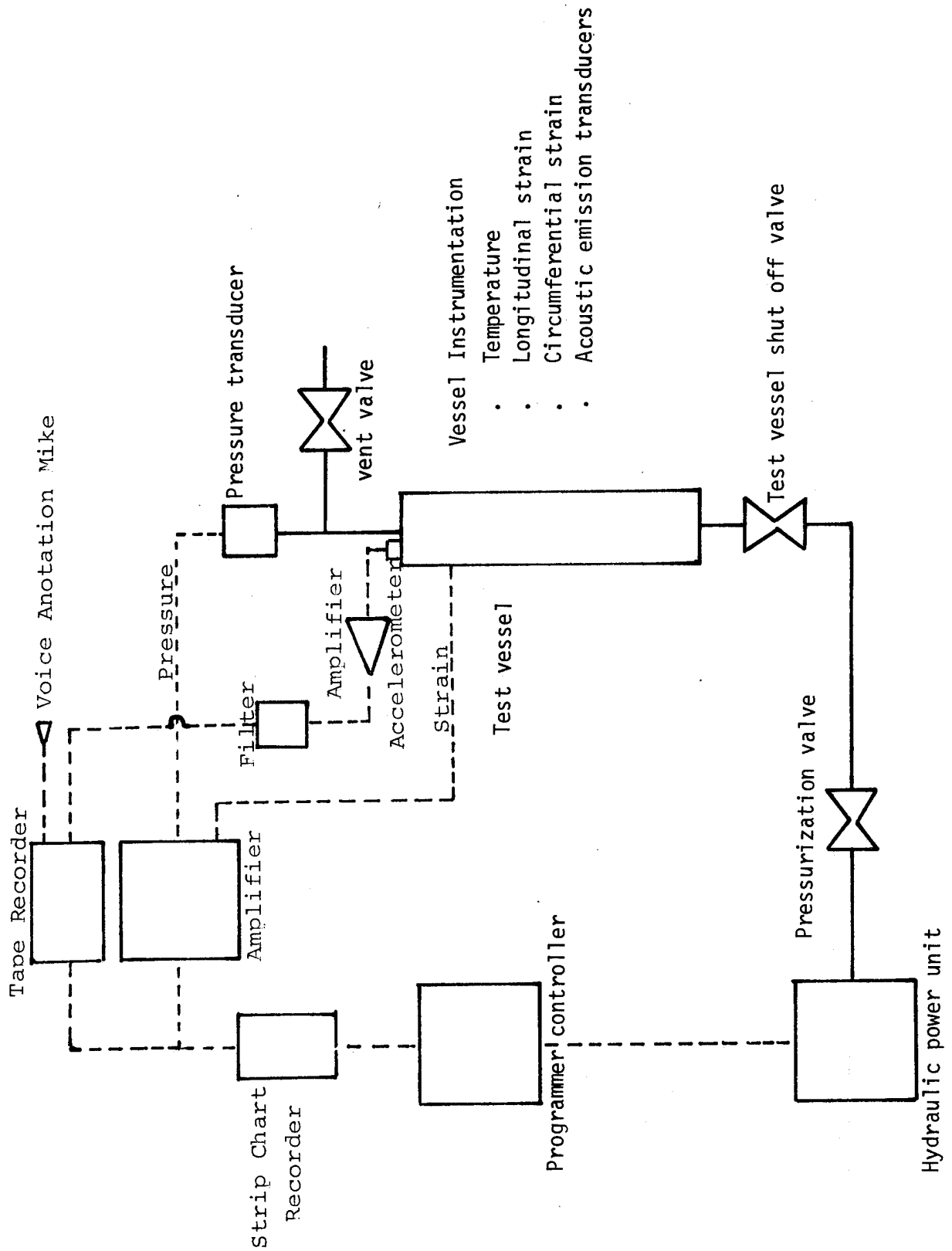


Figure 1.7 TEST SYSTEM (70°F)

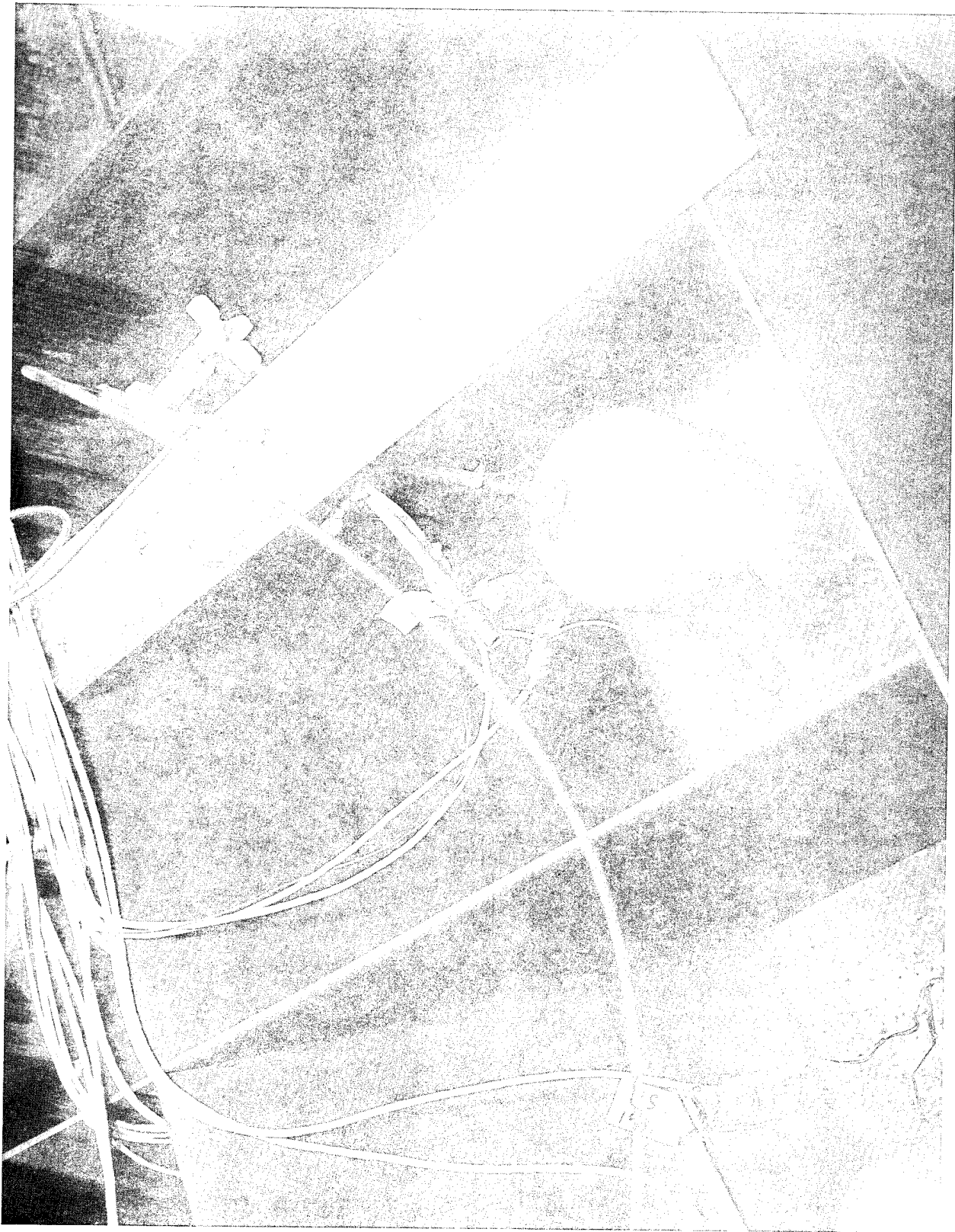


FIGURE 18—VESSEL IN TEST CHAMBER



FIGURE 19—VESSEL NO. 1 AFTER BURST TEST

$P_{ult} = 2440 \text{ psig} [16.6 \times 10^6 \text{ N/m}^2]$

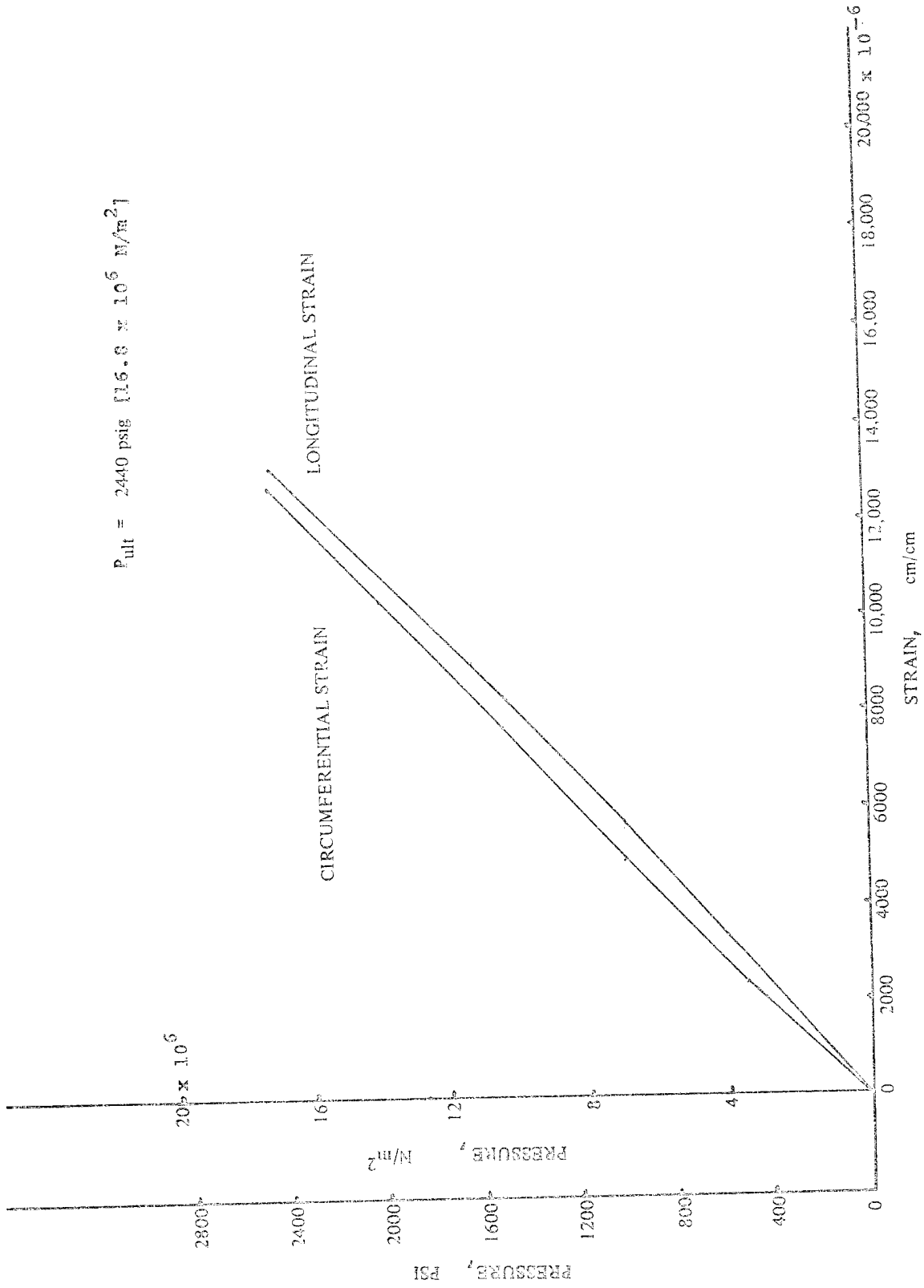


FIGURE 20 PRESSURE VS. STRAIN RELATIONSHIP - VESSEL NO. 1

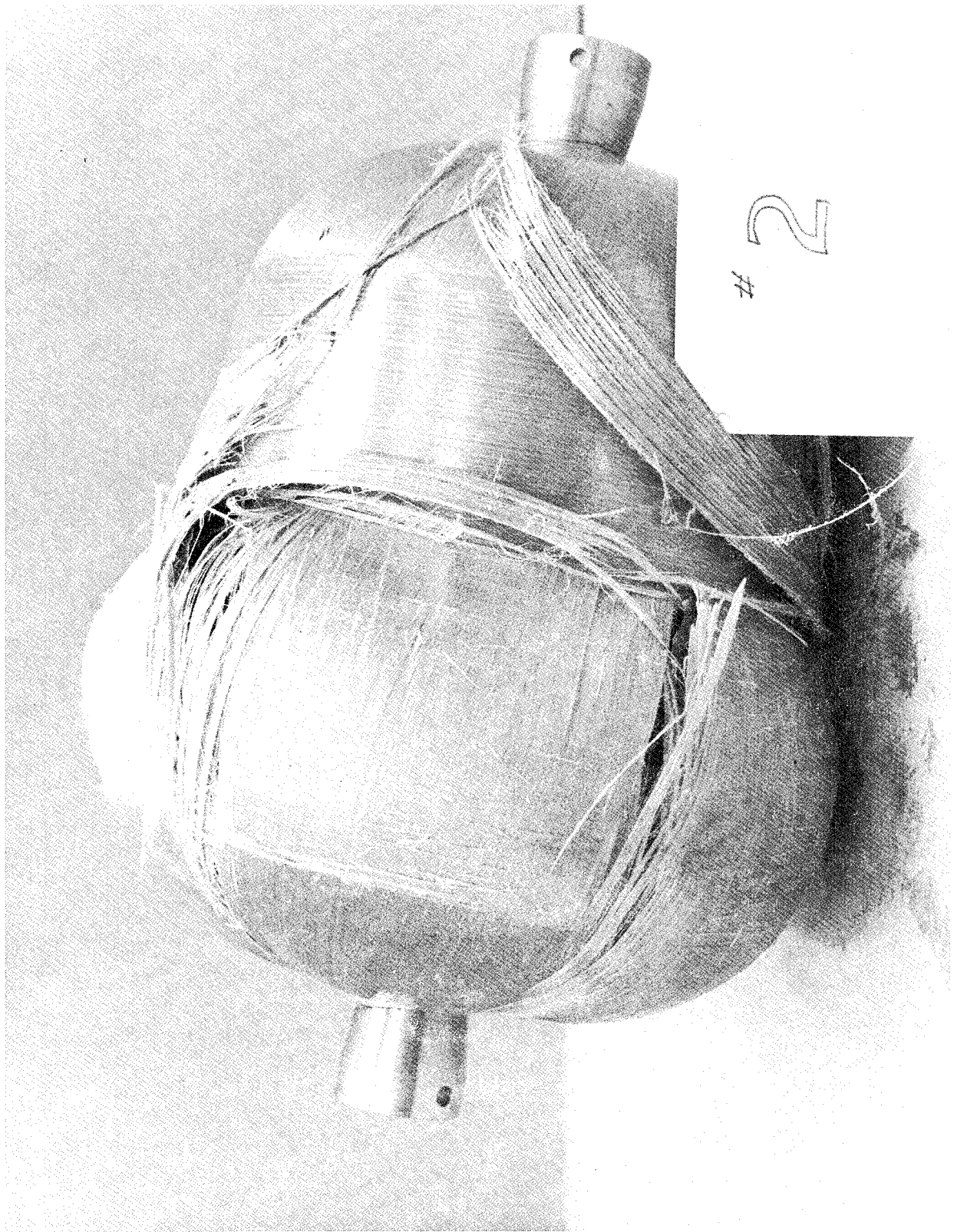


FIGURE 21 - VESSEL NO. 2 AFTER BURST TEST

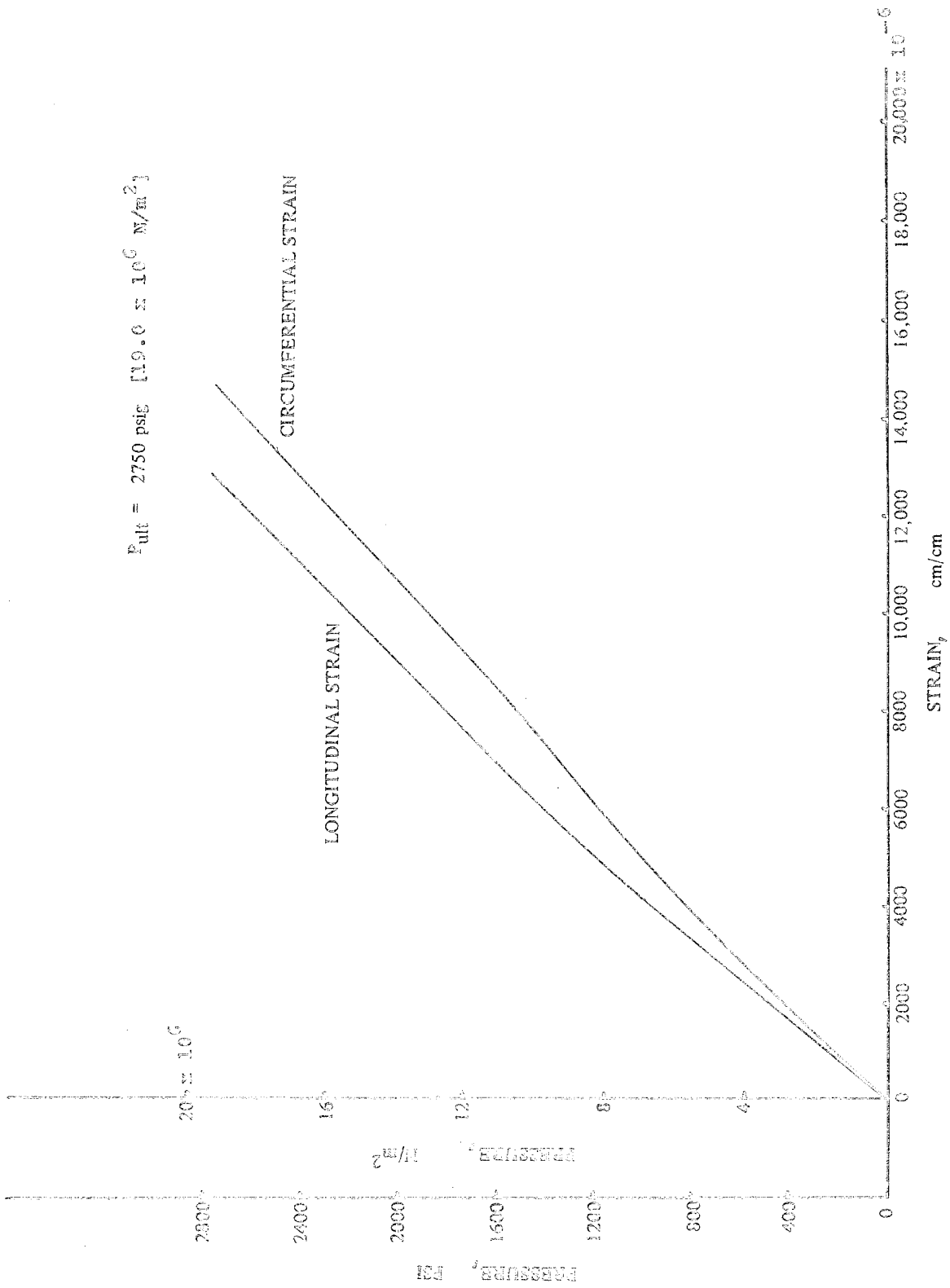


FIGURE 22 PRESSURE VS. STRAIN RELATIONSHIP - VESSEL NO. 2

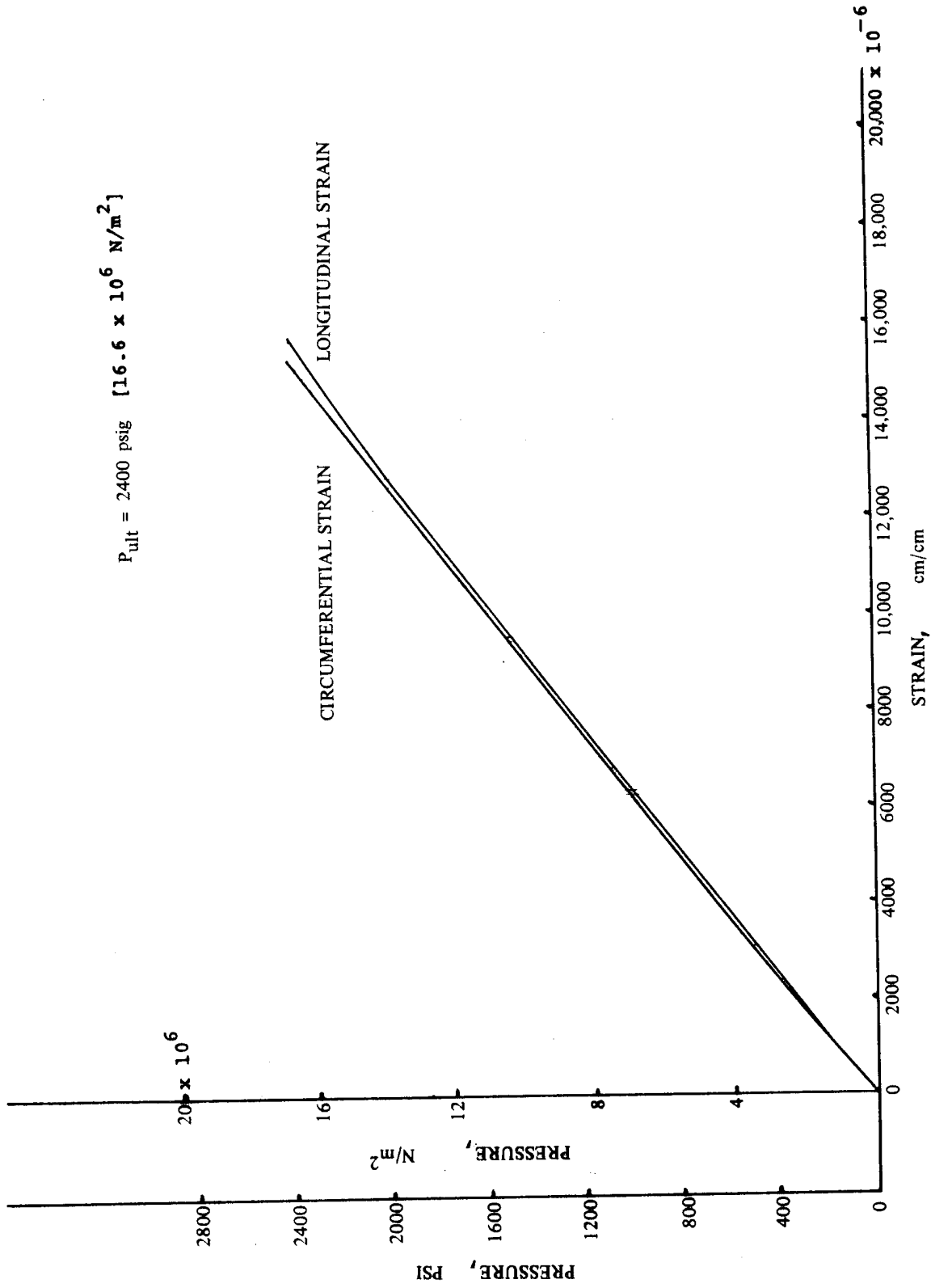


FIGURE 23 PRESSURE VS. STRAIN RELATIONSHIP - VESSEL NO. 3



FIGURE 24—VESSEL NO. 3 AFTER BURST TEST

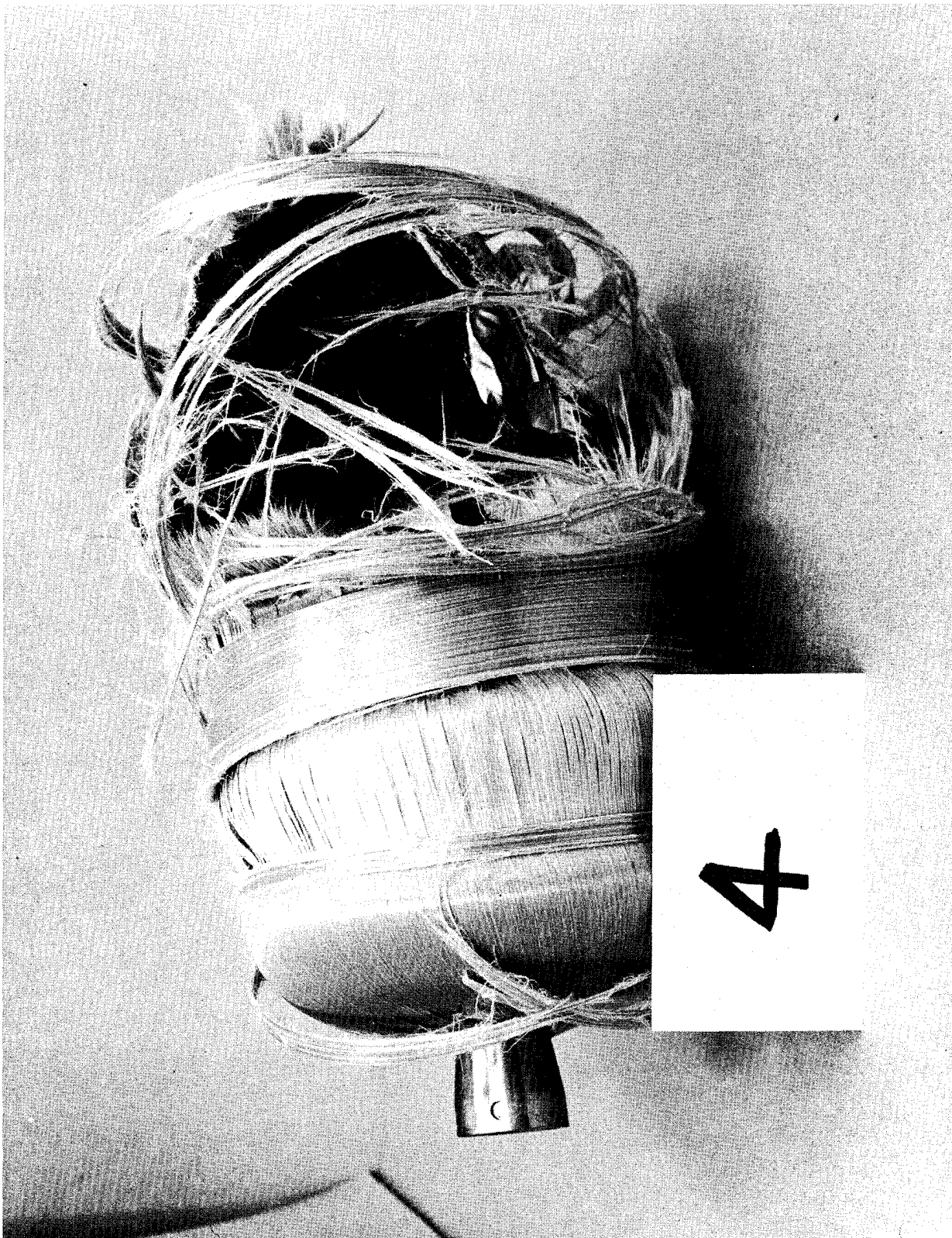


FIGURE 25 - VESSEL NO. 4 AFTER BURST TEST

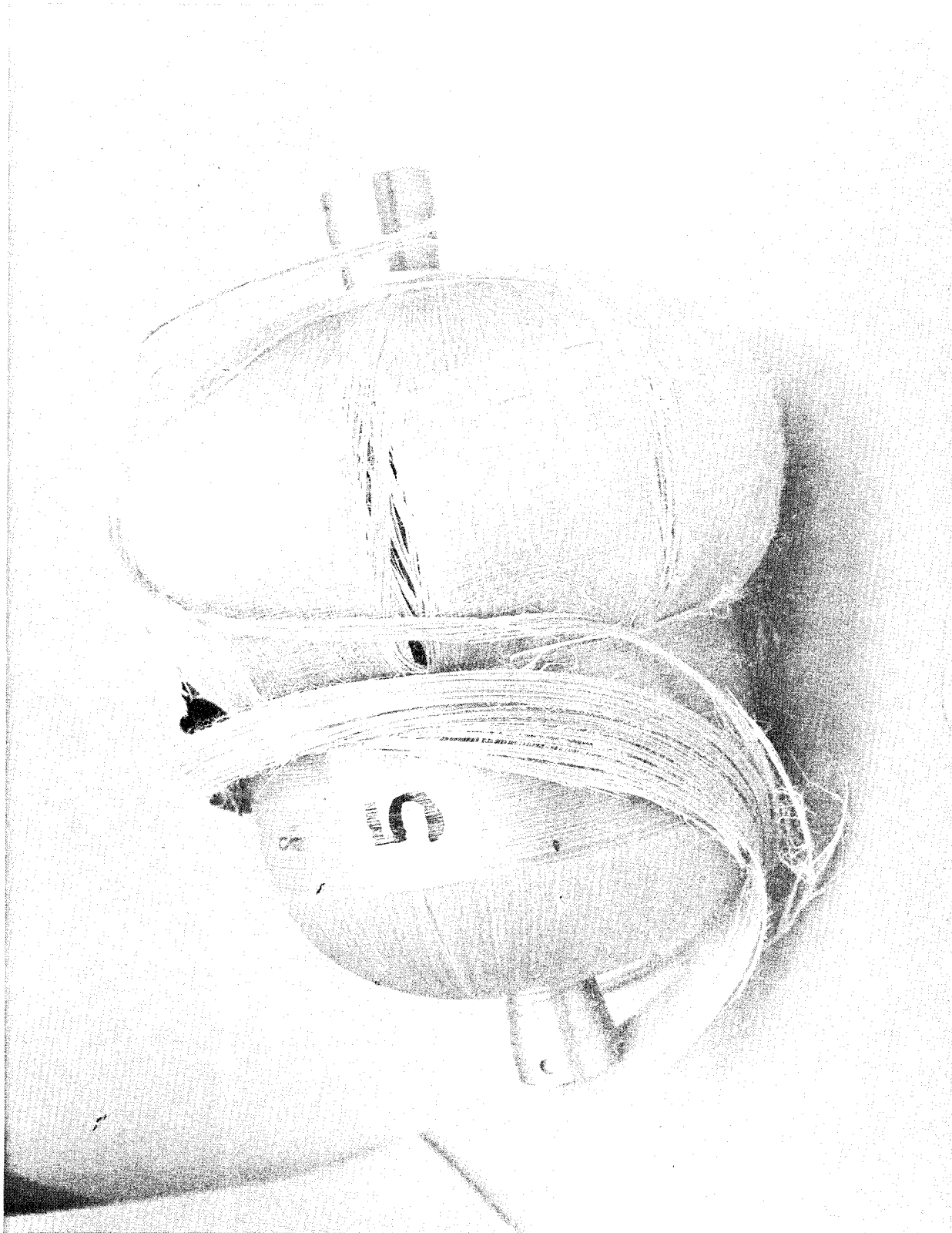


FIGURE 26—VESSEL NO. 5 AFTER BURST TEST

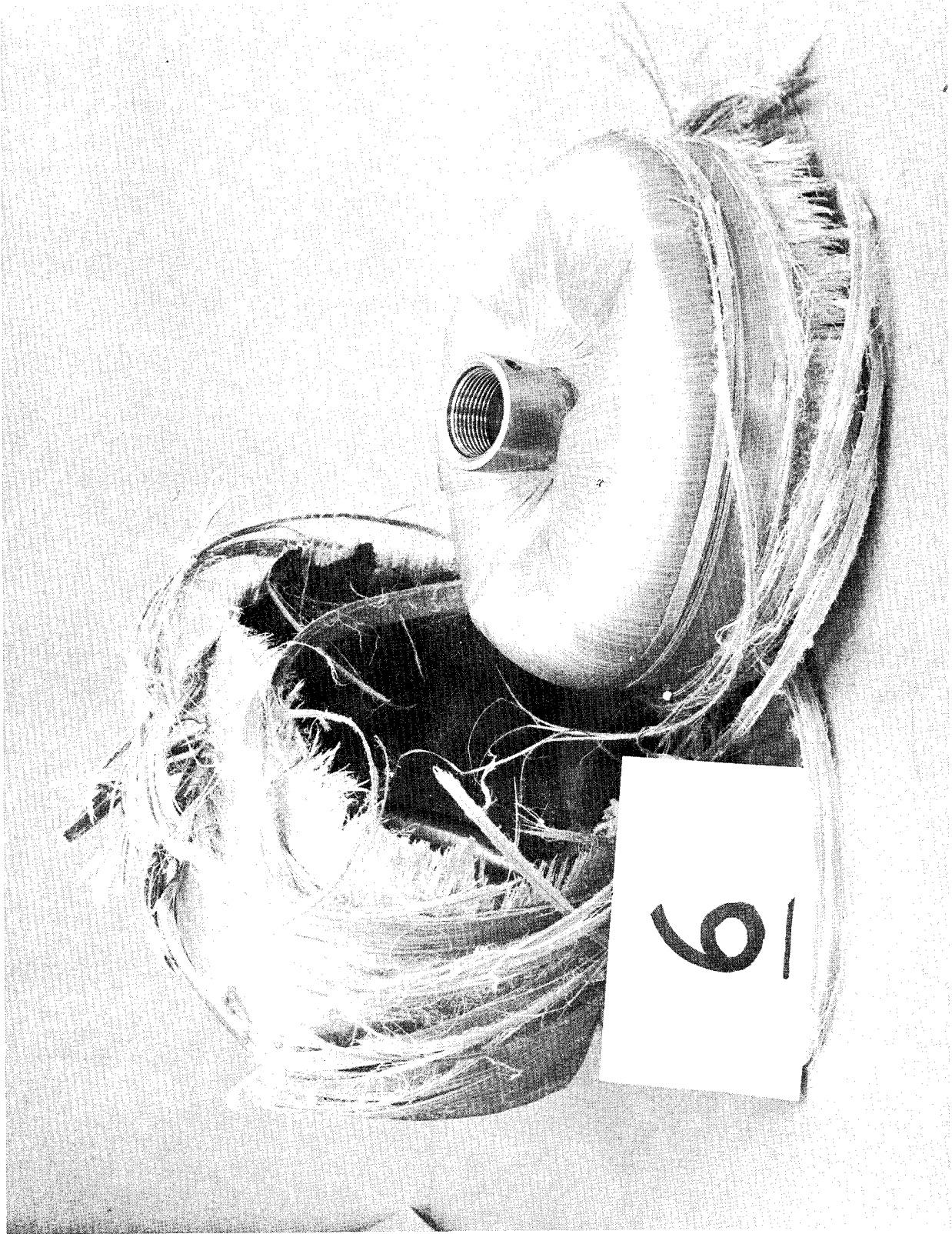


FIGURE 27--VESSEL NO. 6 AFTER BURST TEST

$$P_{ult} = 2640 \text{ psig } [18.2 \times 10^6 \text{ N/m}^2]$$

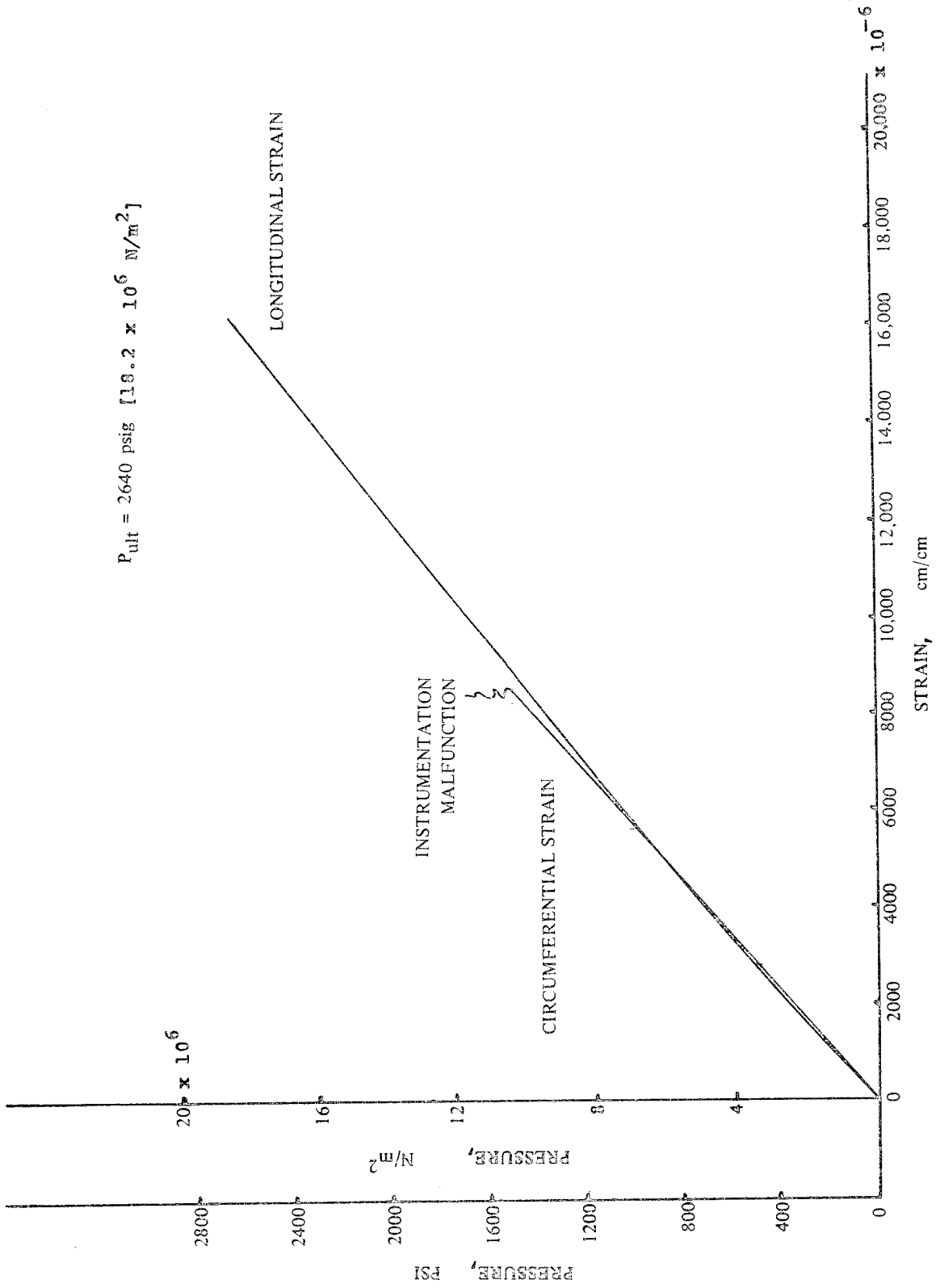


FIGURE 28 PRESSURE VS. STRAIN RELATIONSHIP - VESSEL NO. 4

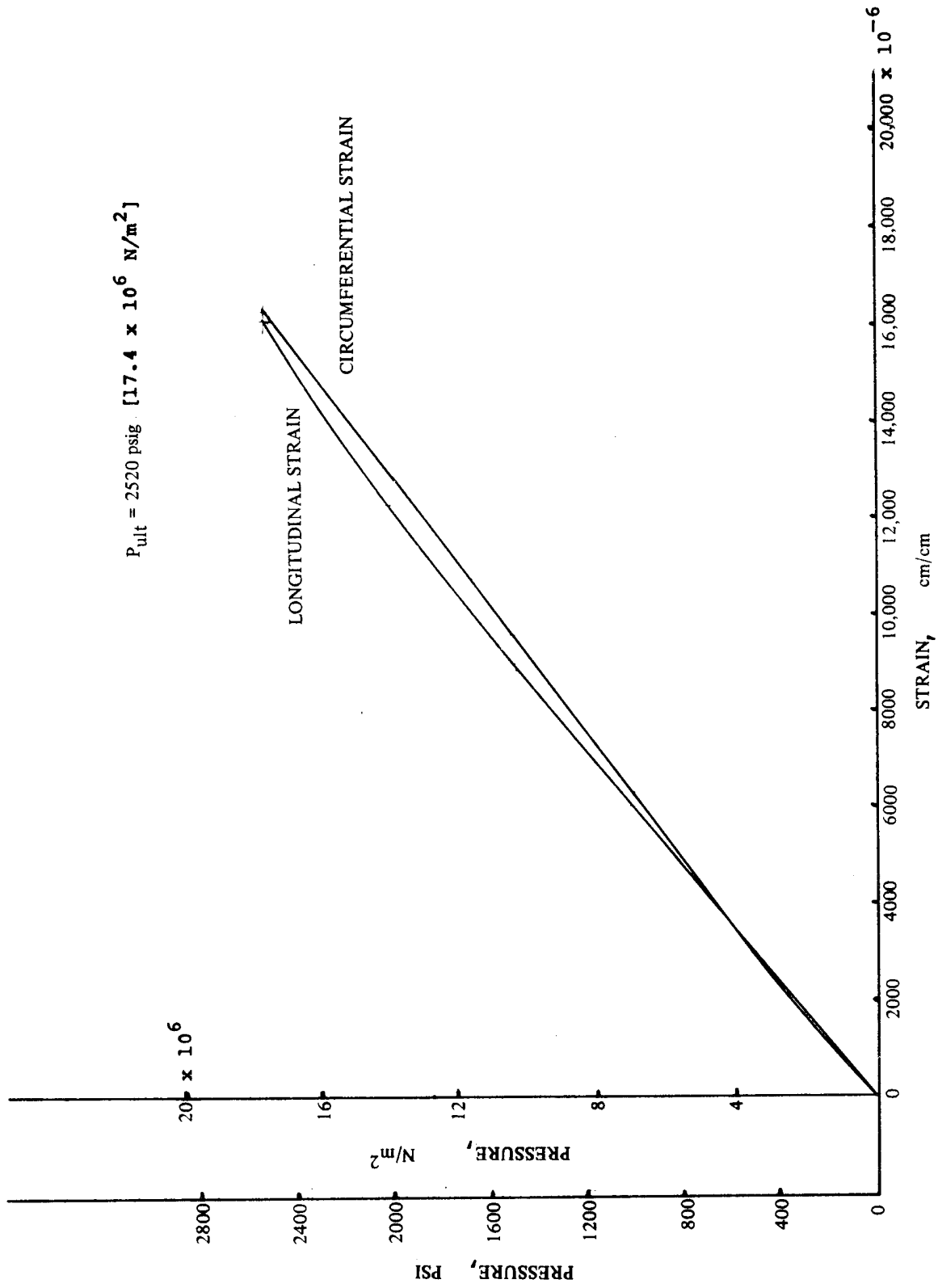


FIGURE 29 PRESSURE VS. STRAIN RELATIONSHIP—VESSEL NO. 5

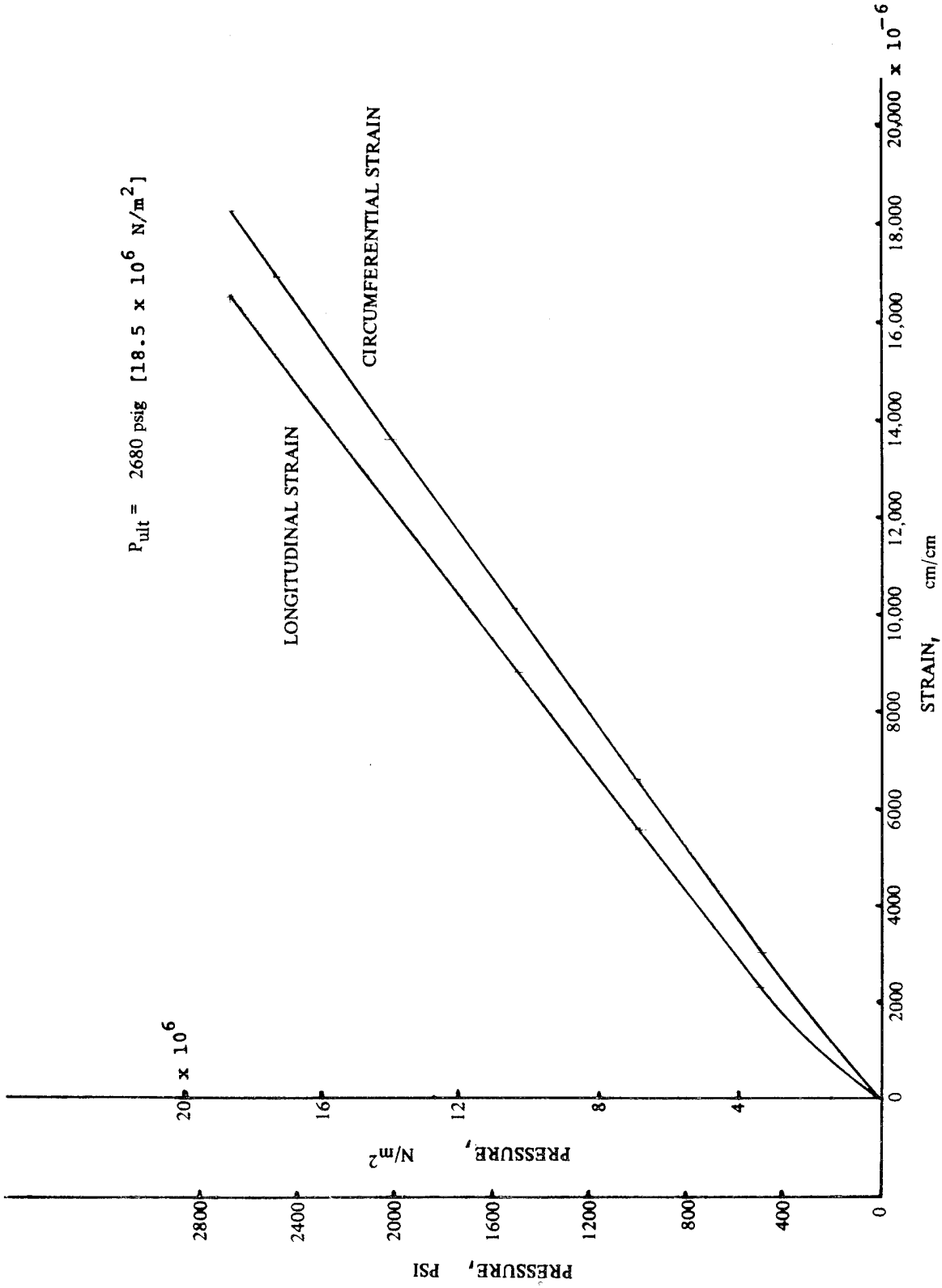


FIGURE 30 PRESSURE VS. STRAIN RELATIONSHIP—VESSEL NO. 6

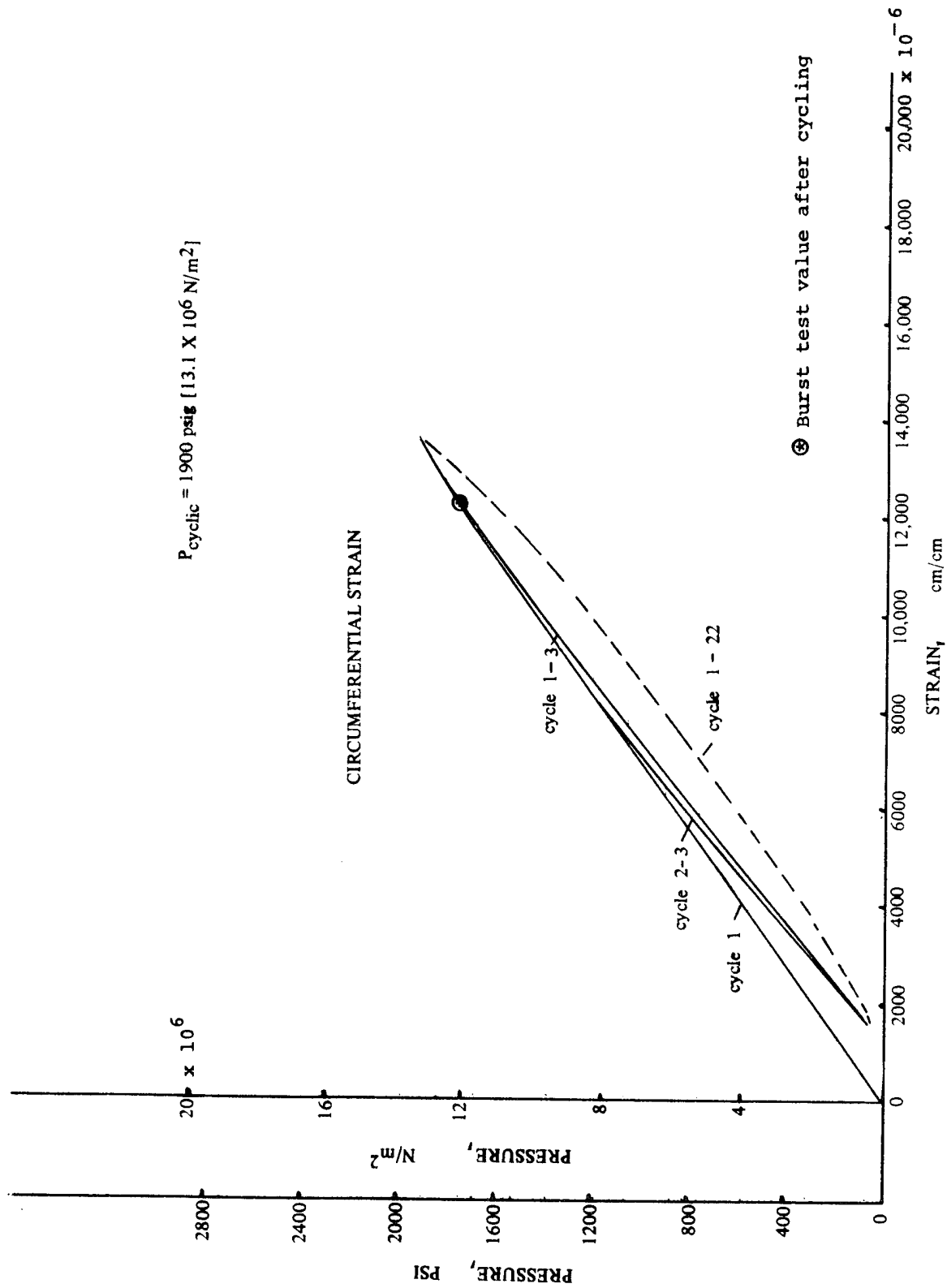


FIGURE 31 PRESSURE VS. STRAIN RELATIONSHIP OF VESSEL NO. 7 IN CYCLIC FATIGUE

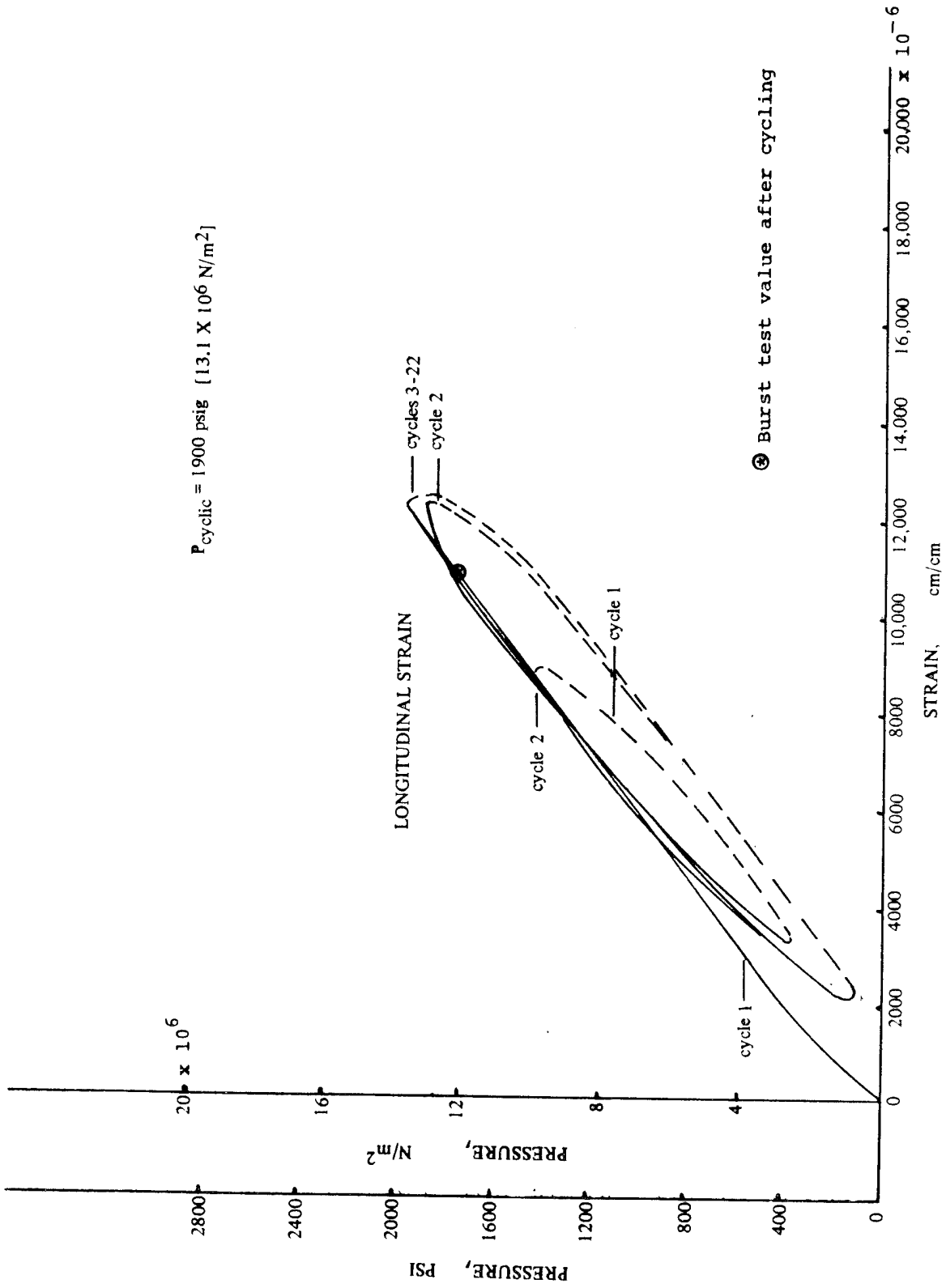


FIGURE 32 PRESSURE VS. STRAIN RELATIONSHIP OF VESSEL NO. 7 IN CYCLIC FATIGUE

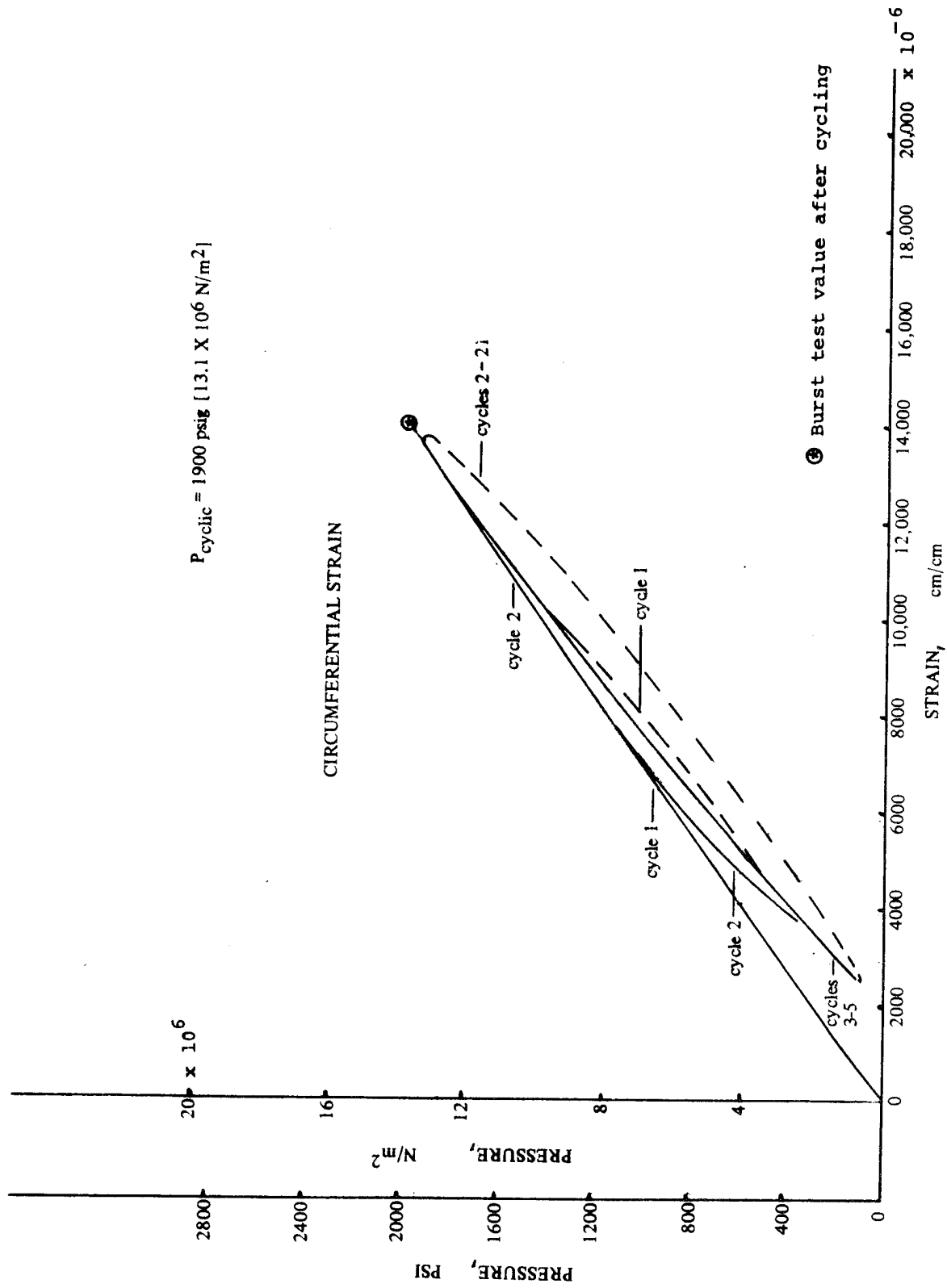


FIGURE 33 PRESSURE VS. STRAIN RELATIONSHIP OF VESSEL NO. 8 IN CYCLIC FATIGUE

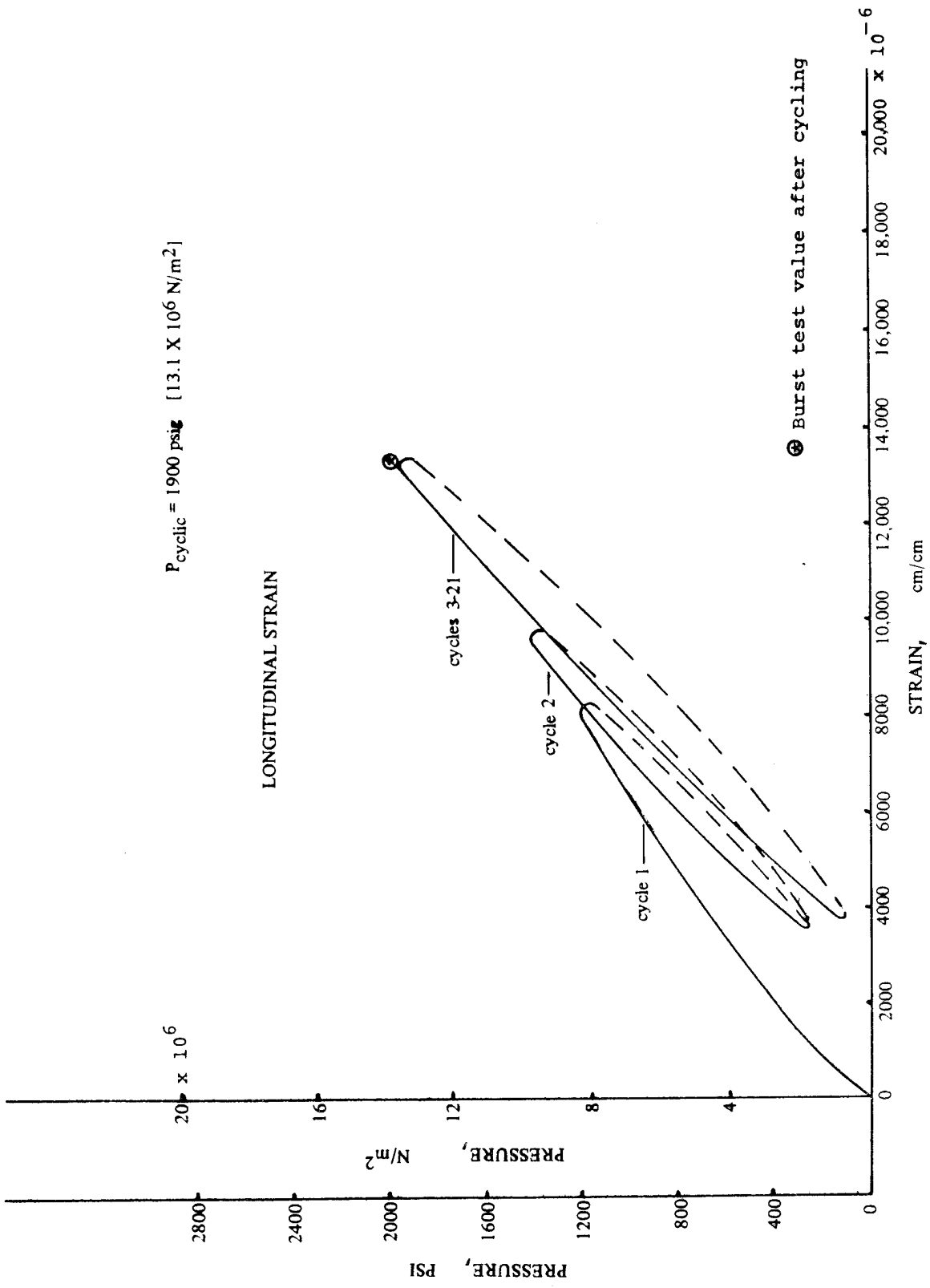


FIGURE 34 PRESSURE VS. STRAIN RELATIONSHIP OF VESSEL NO. 8 IN CYCLIC FATIGUE

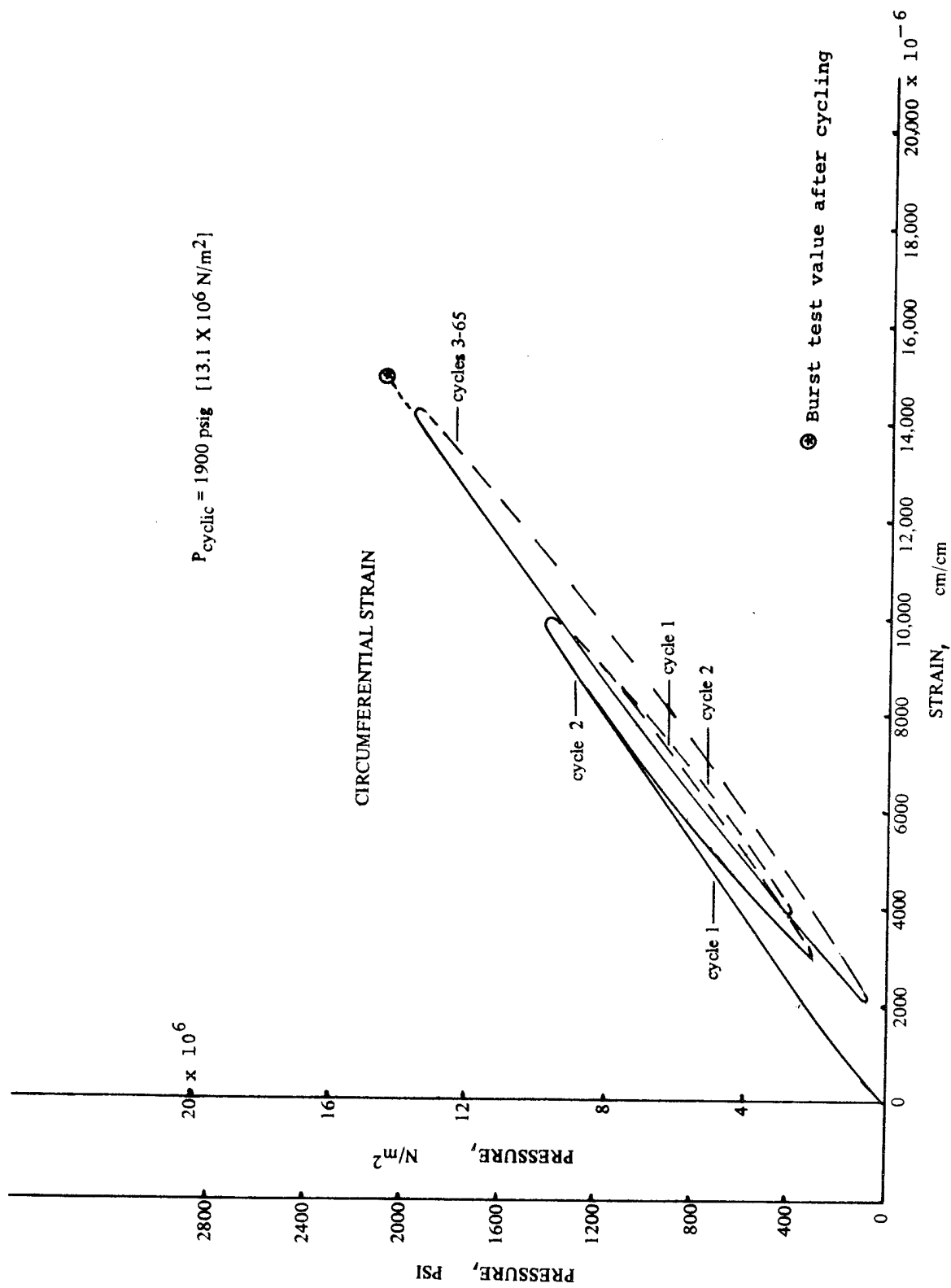


FIGURE 35 PRESSURE VS. STRAIN RELATIONSHIP OF VESSEL NO.9 IN CYCLIC FATIGUE

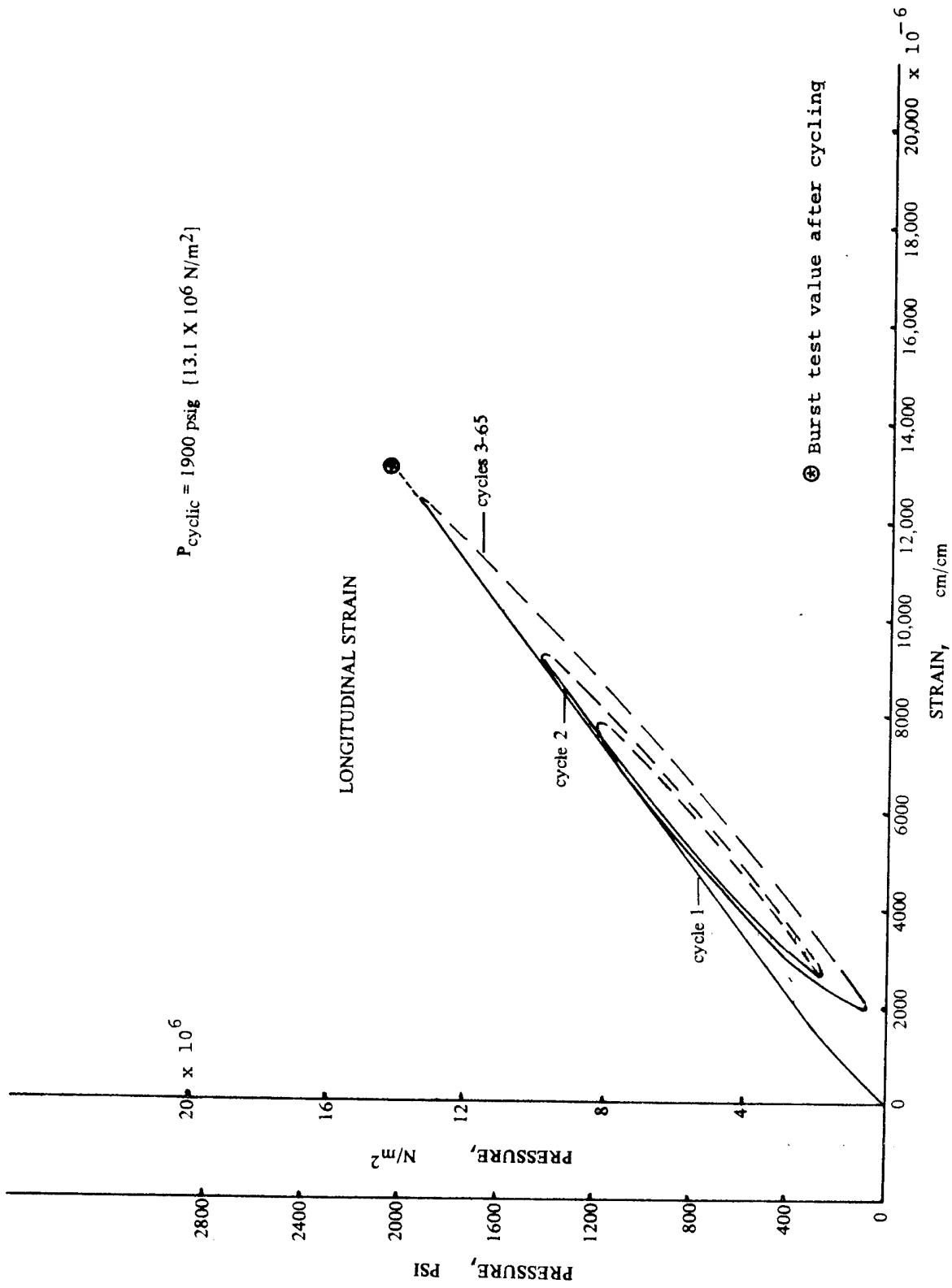


FIGURE 36 PRESSURE VS. STRAIN RELATIONSHIP OF VESSEL NO. 9 IN CYCLIC FATIGUE

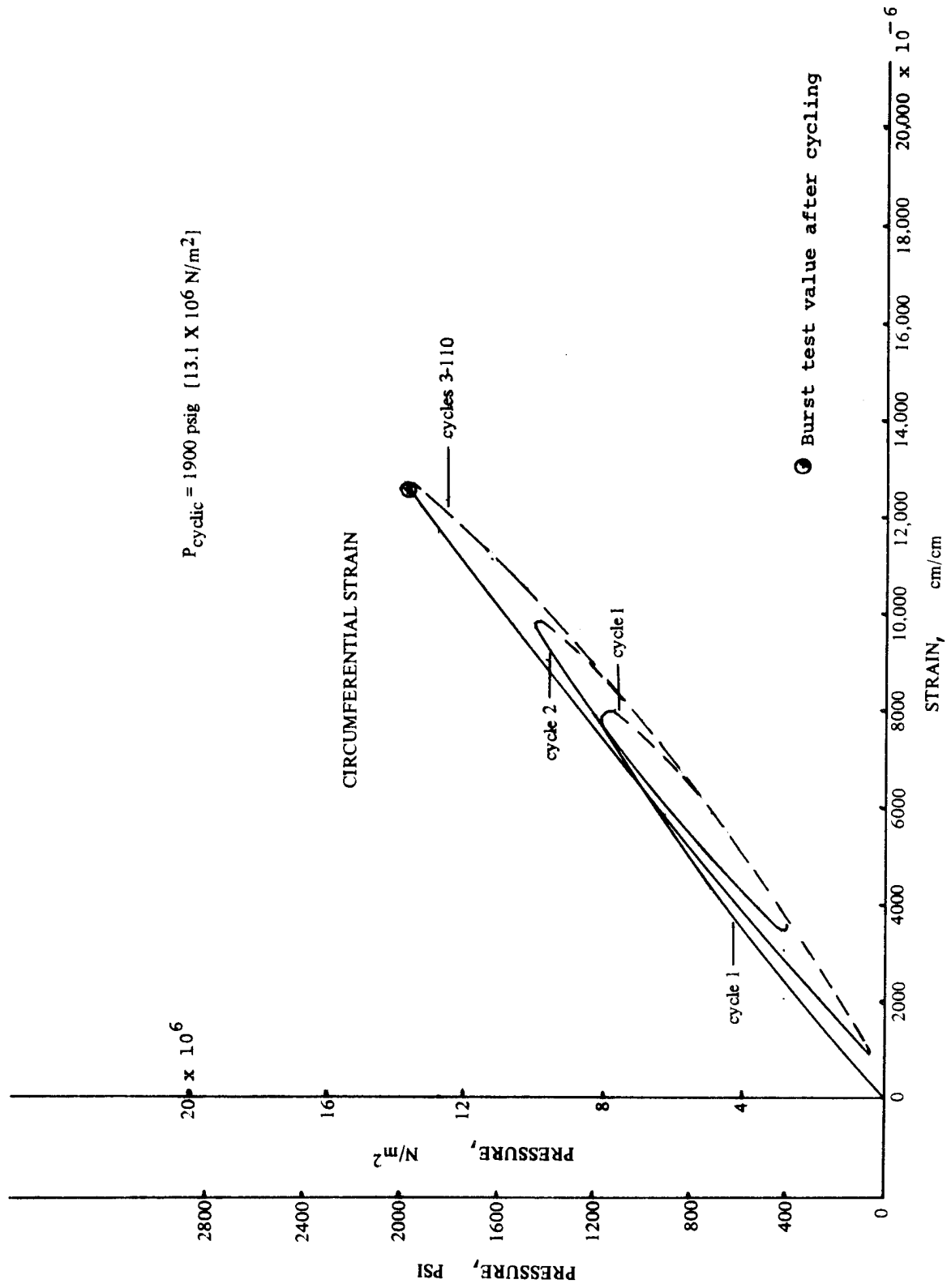


FIGURE 37 PRESSURE VS. STRAIN RELATIONSHIP OF VESSEL NO.10 IN CYCLIC FATIGUE

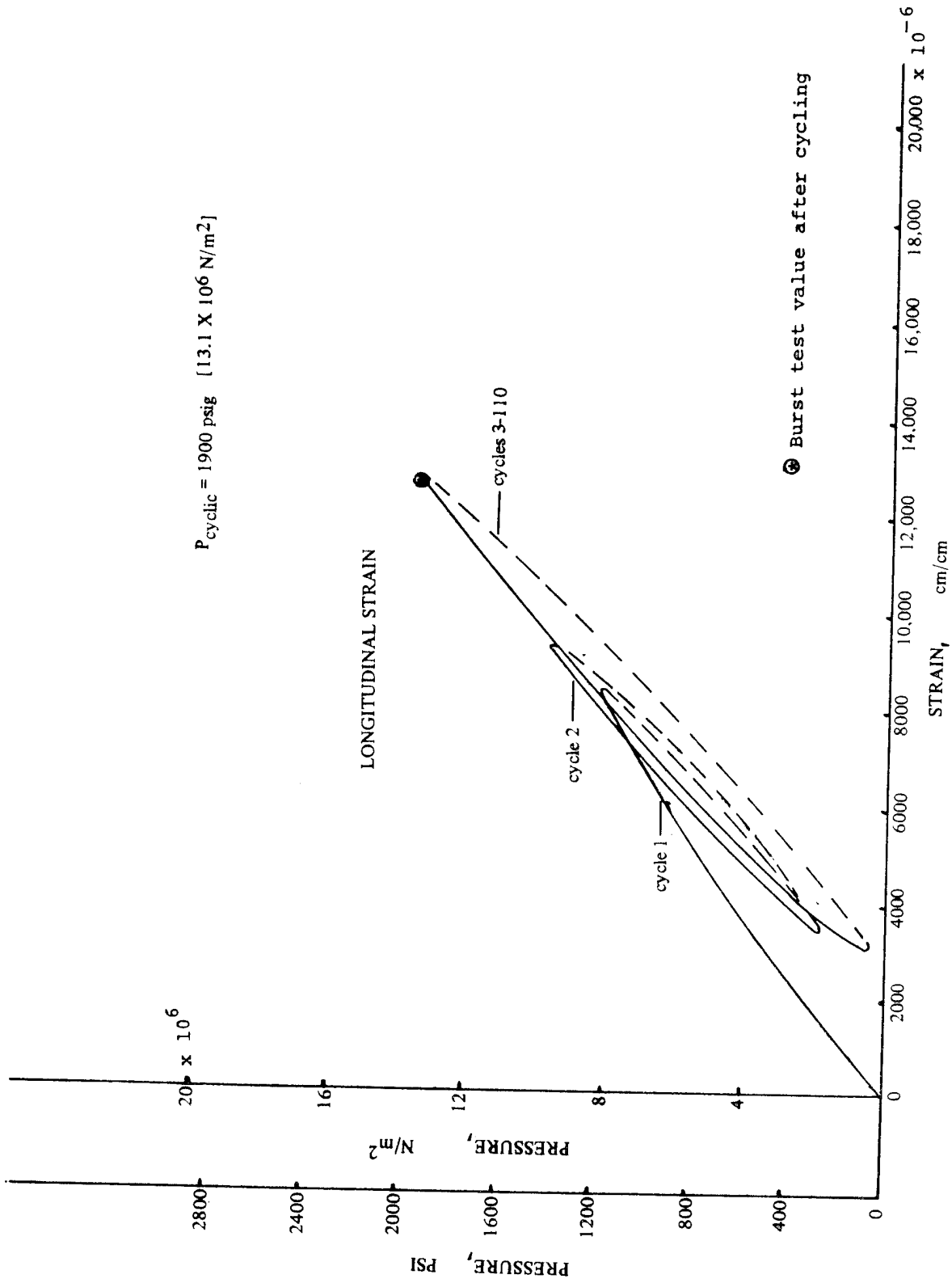


FIGURE 38 PRESSURE VS. STRAIN RELATIONSHIP OF VESSEL NO.10 IN CYCLIC FATIGUE

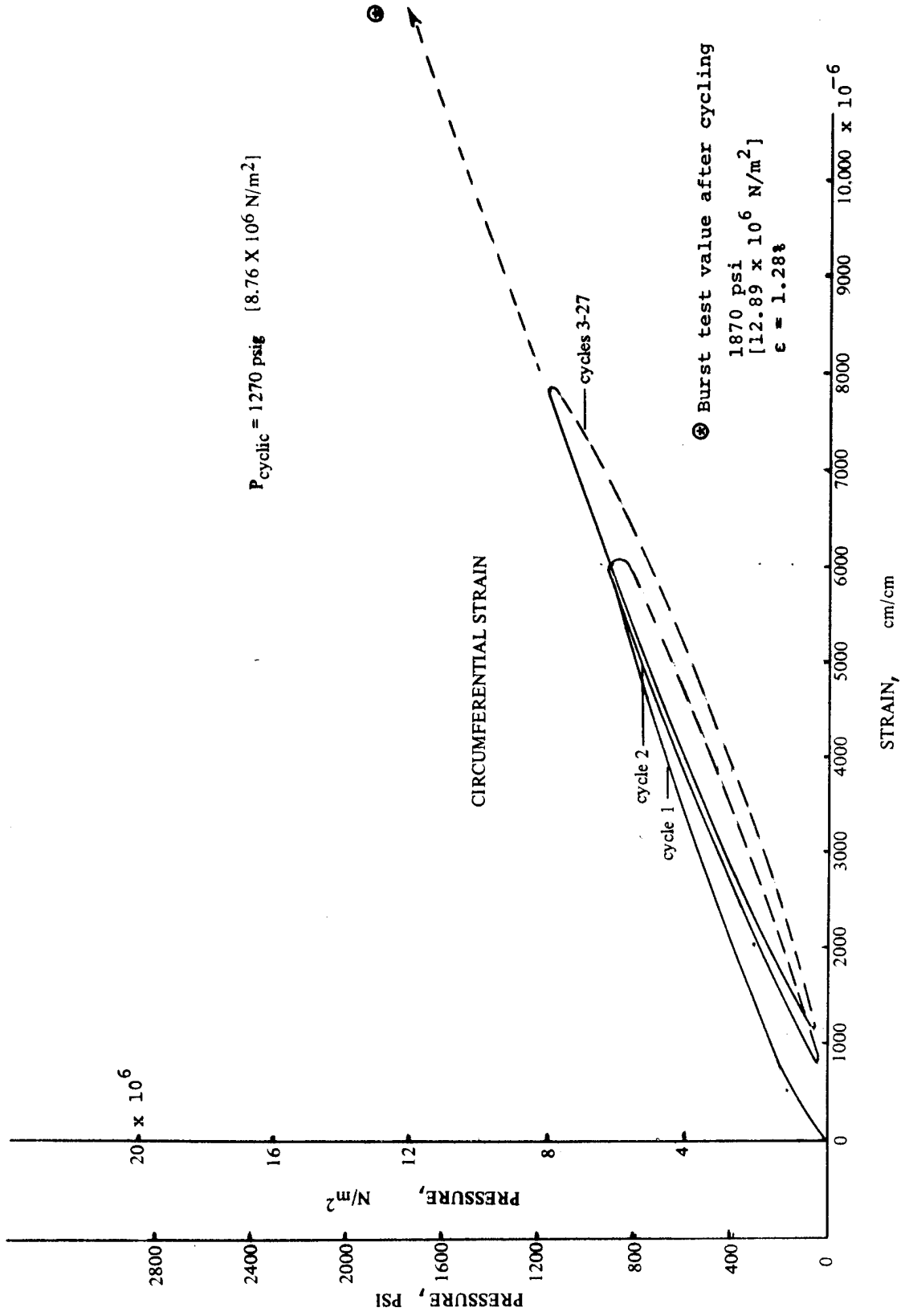


FIGURE 39 PRESSURE VS. STRAIN RELATIONSHIP OF VESSEL NO. 11 IN CYCLIC FATIGUE

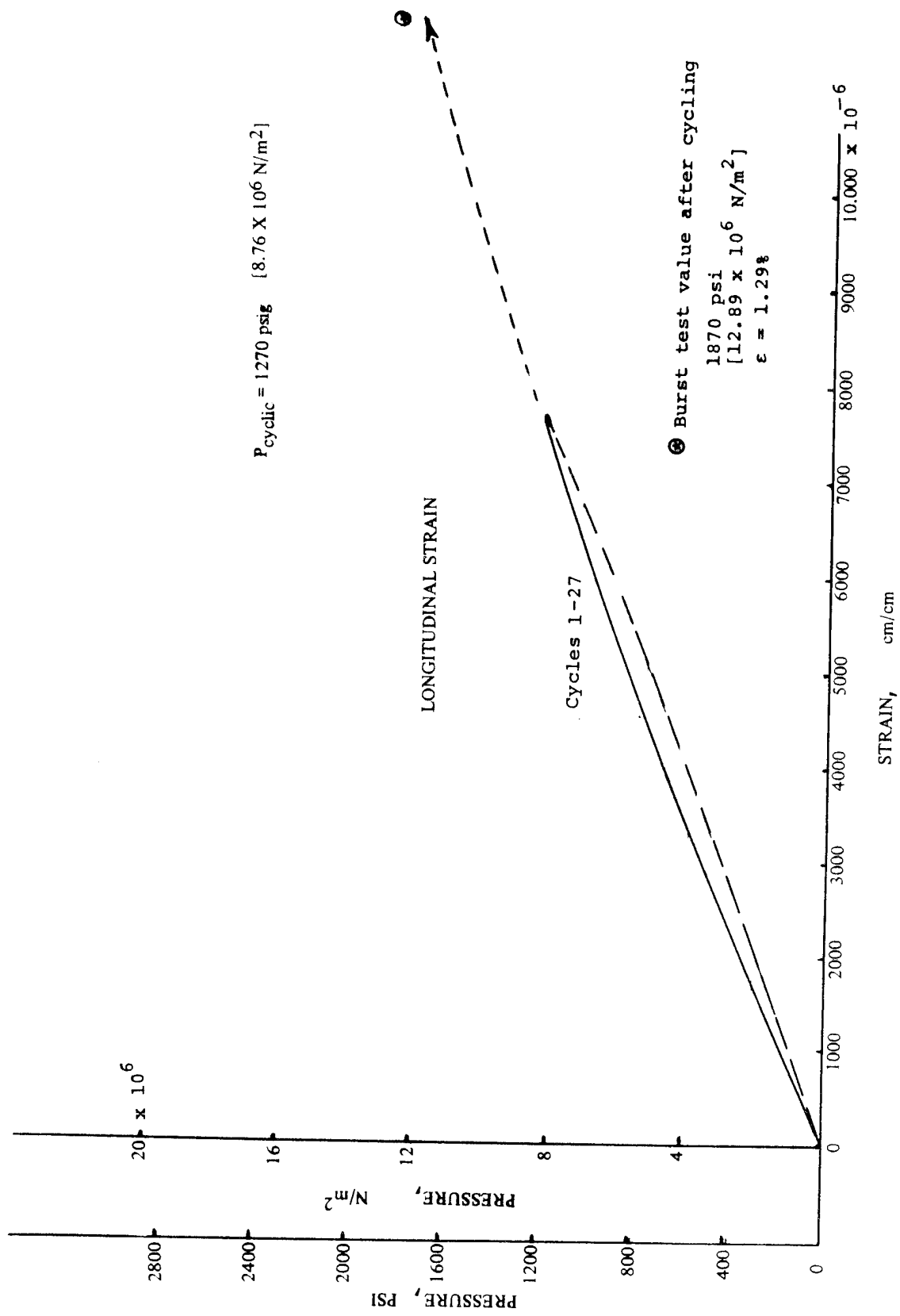


FIGURE 40 PRESSURE VS. STRAIN RELATIONSHIP OF VESSEL NO. 11 IN CYCLIC FATIGUE

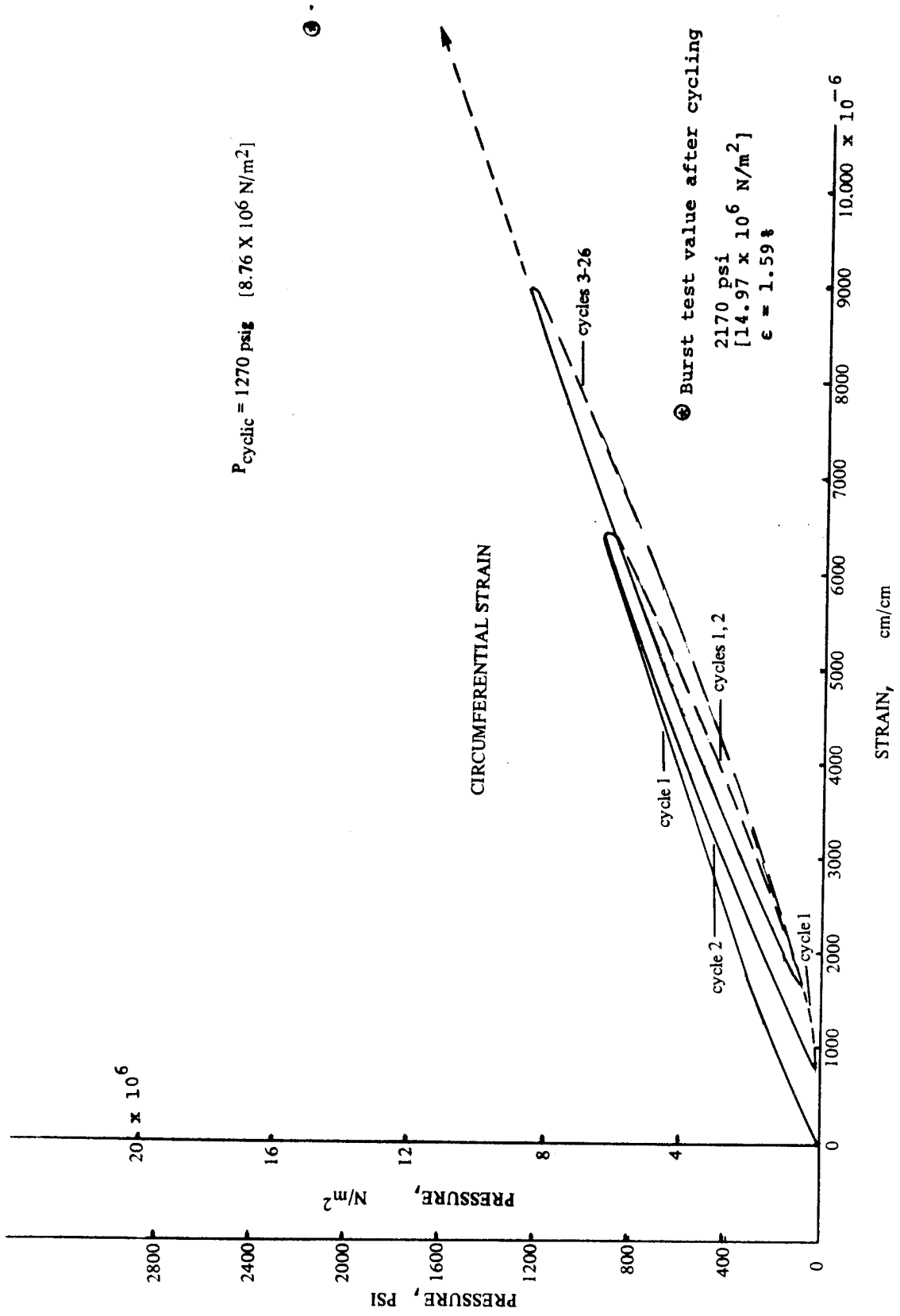


FIGURE 41 PRESSURE VS. STRAIN RELATIONSHIP OF VESSEL NO. 12 IN CYCLIC FATIGUE

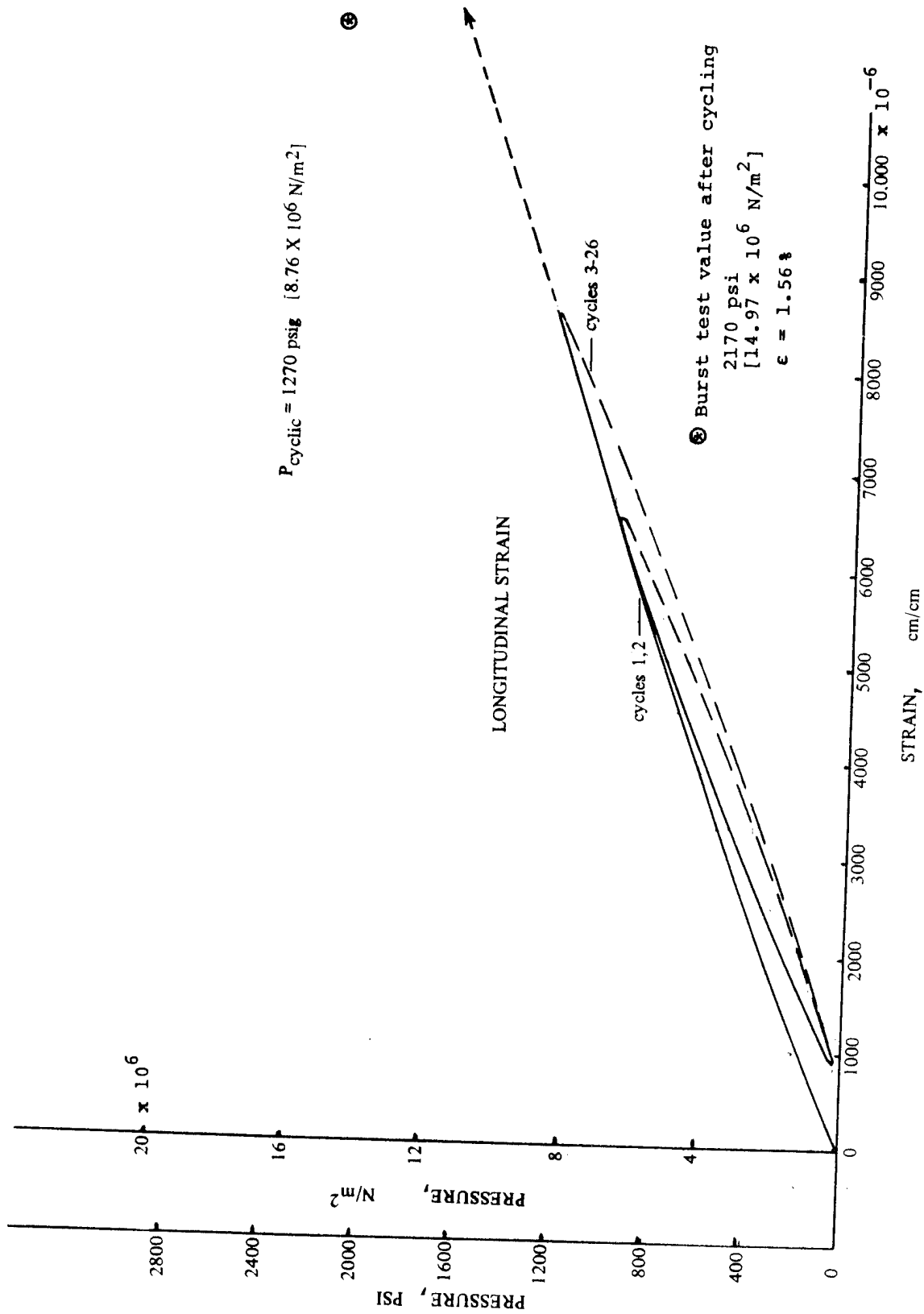
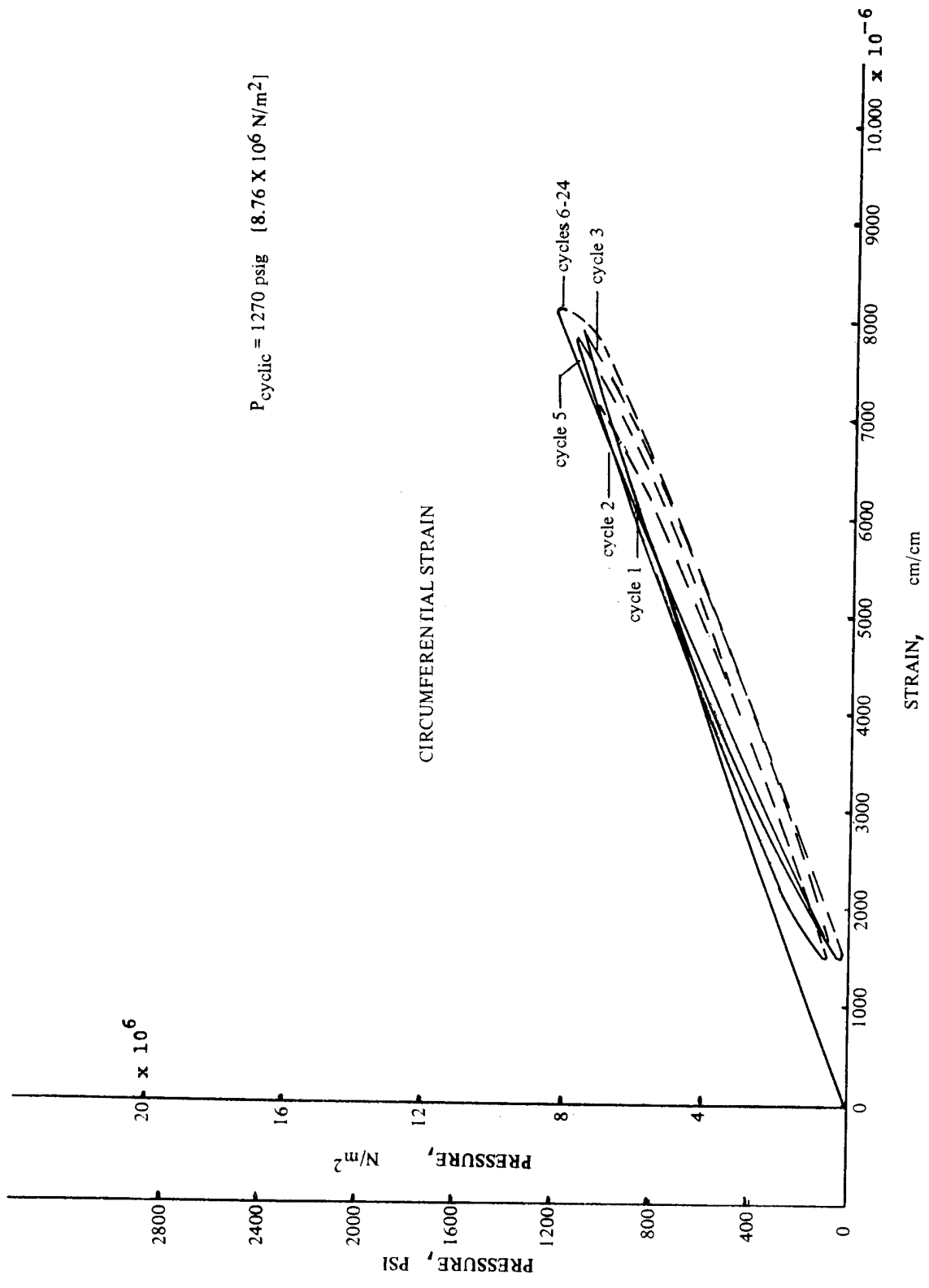


FIGURE 42 PRESSURE VS. STRAIN RELATIONSHIP OF VESSEL NO. 12 IN CYCLIC FATIGUE



$P_{cyclic} = 1270 \text{ psig} \quad [8.76 \times 10^6 \text{ N/m}^2]$

FIGURE 43 PRESSURE VS. STRAIN RELATIONSHIP OF VESSEL NO. 13 IN CYCLIC FATIGUE

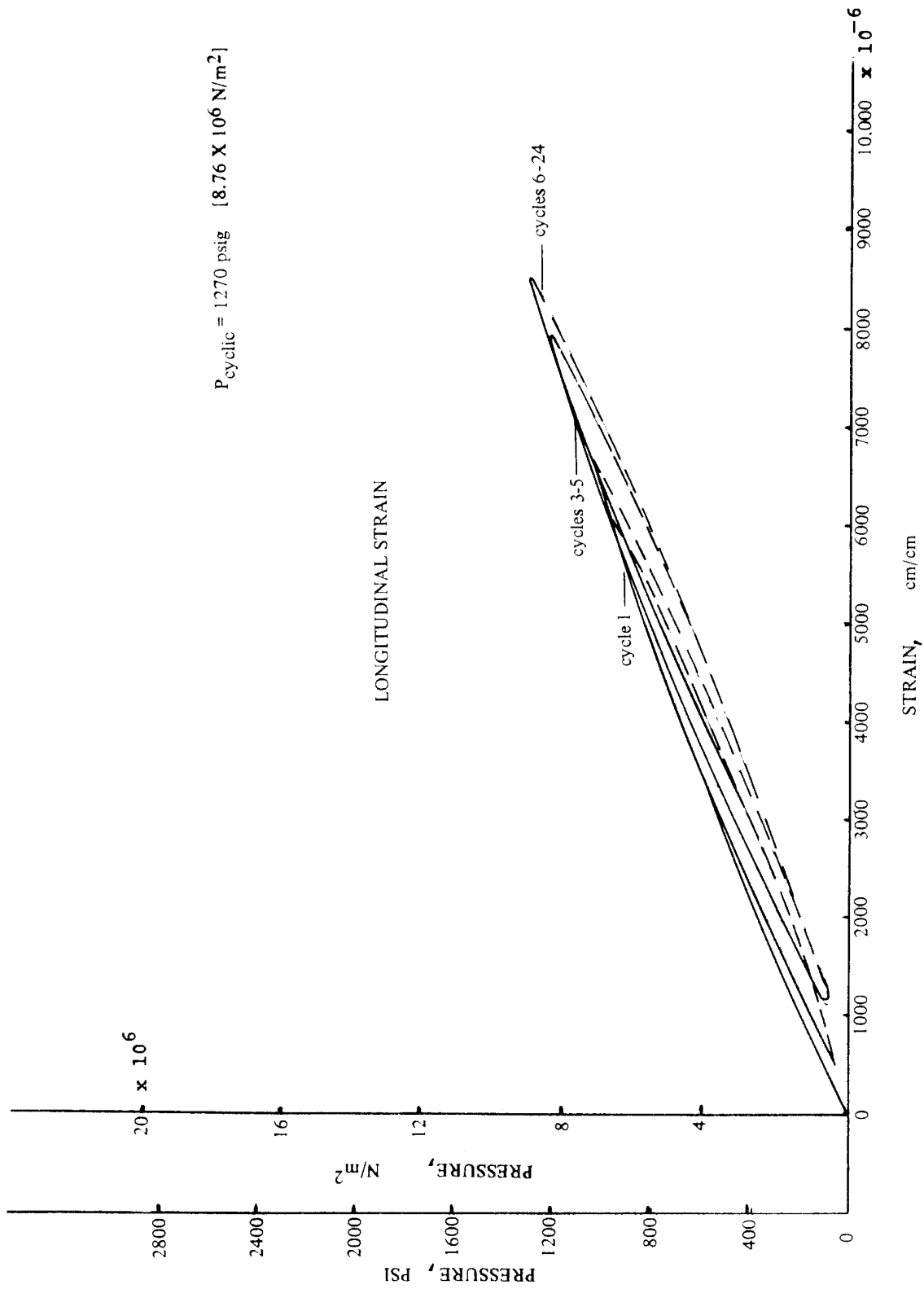
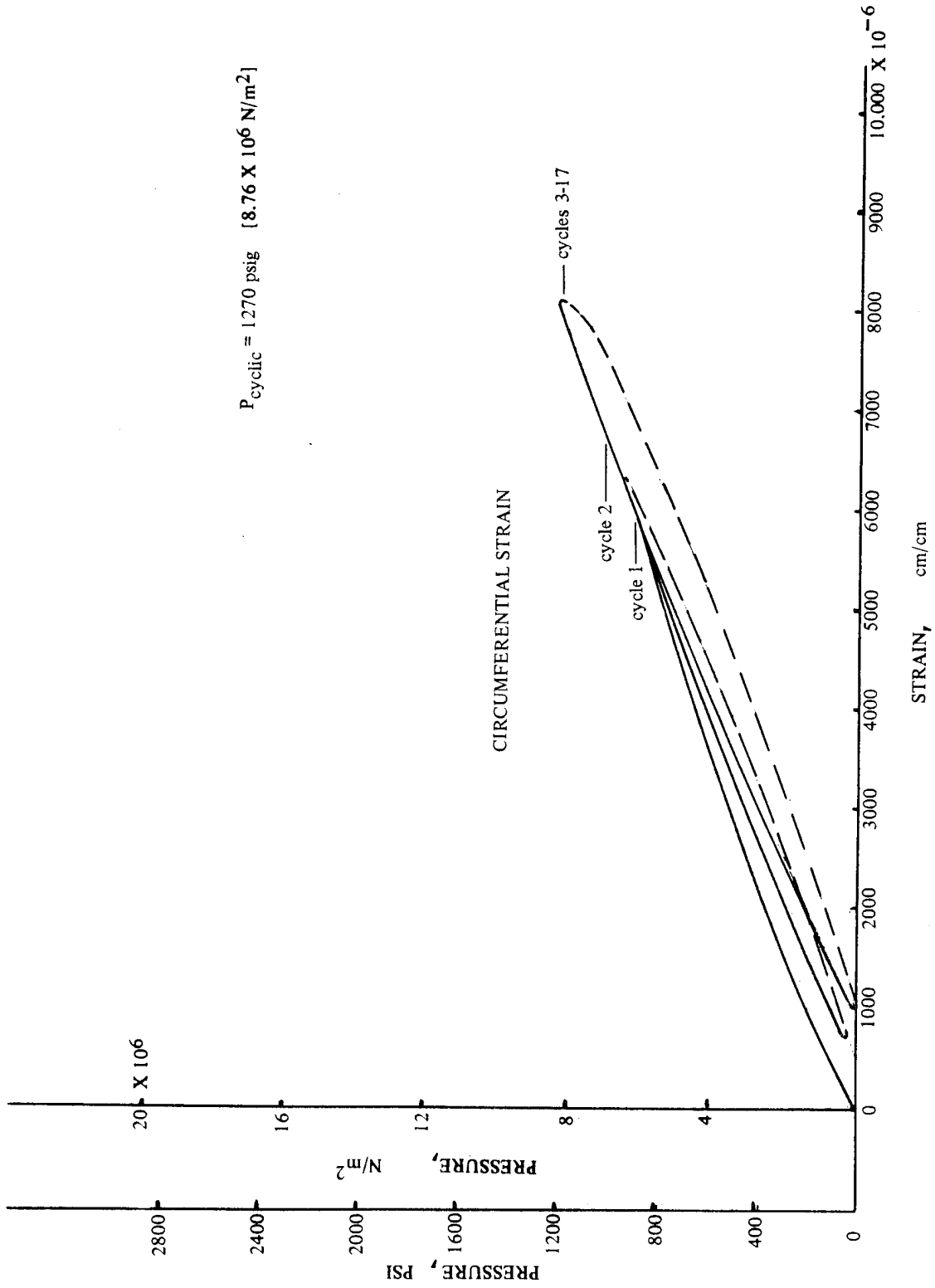


FIGURE 44 PRESSURE VS. STRAIN RELATIONSHIP OF VESSEL NO.13 IN CYCLIC FATIGUE



$P_{cyclic} = 1270 \text{ psig} \quad [8.76 \times 10^6 \text{ N/m}^2]$

FIGURE 45 PRESSURE VS. STRAIN RELATIONSHIP OF VESSEL NO.14 IN CYCLIC FATIGUE

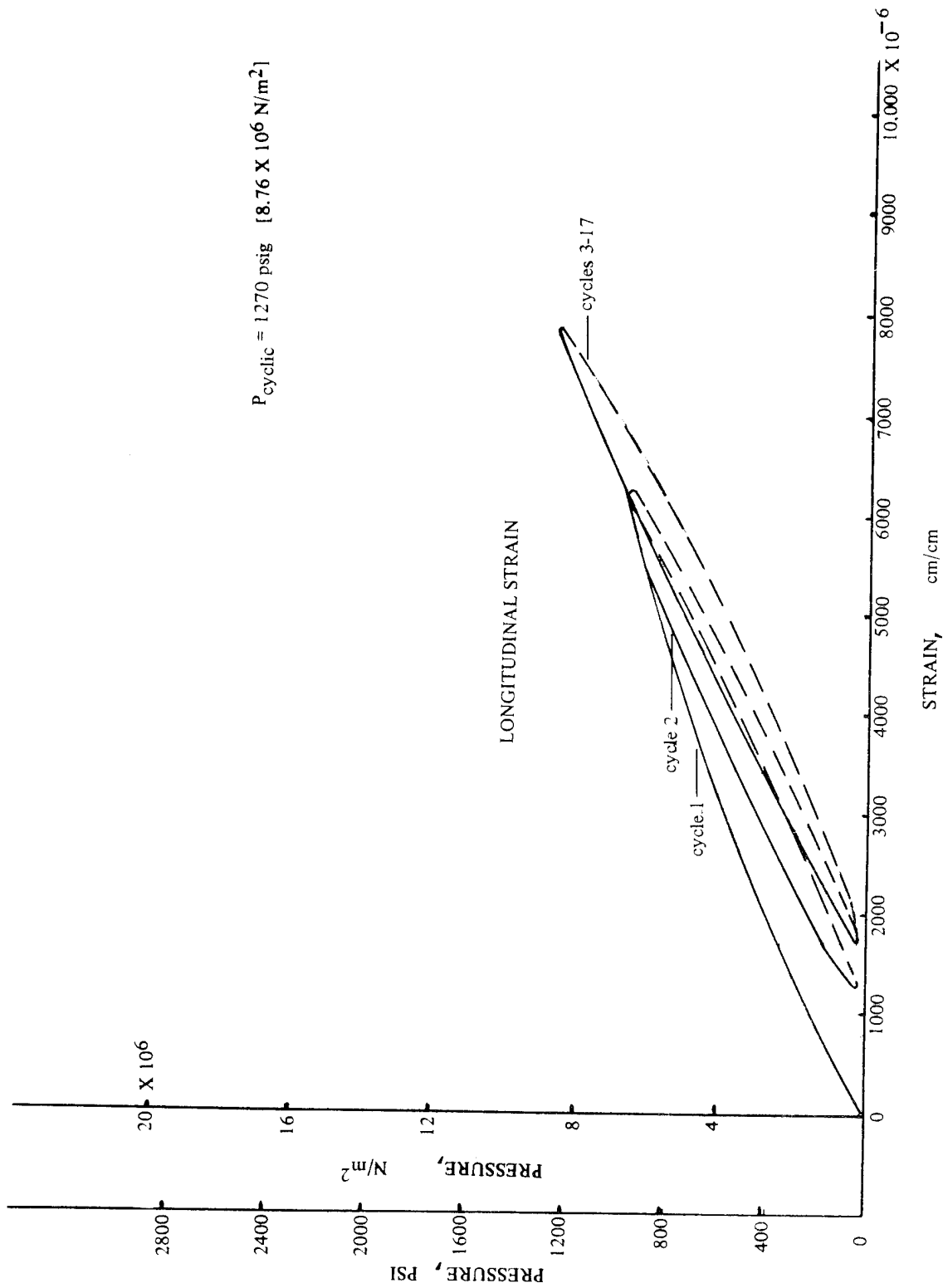


FIGURE 46 PRESSURE VS. STRAIN RELATIONSHIP OF VESSEL NO.14 IN CYCLIC FATIGUE

$P_{cyclic} = 1900 \text{ psig} \quad [13.1 \times 10^6 \text{ N/m}^2]$

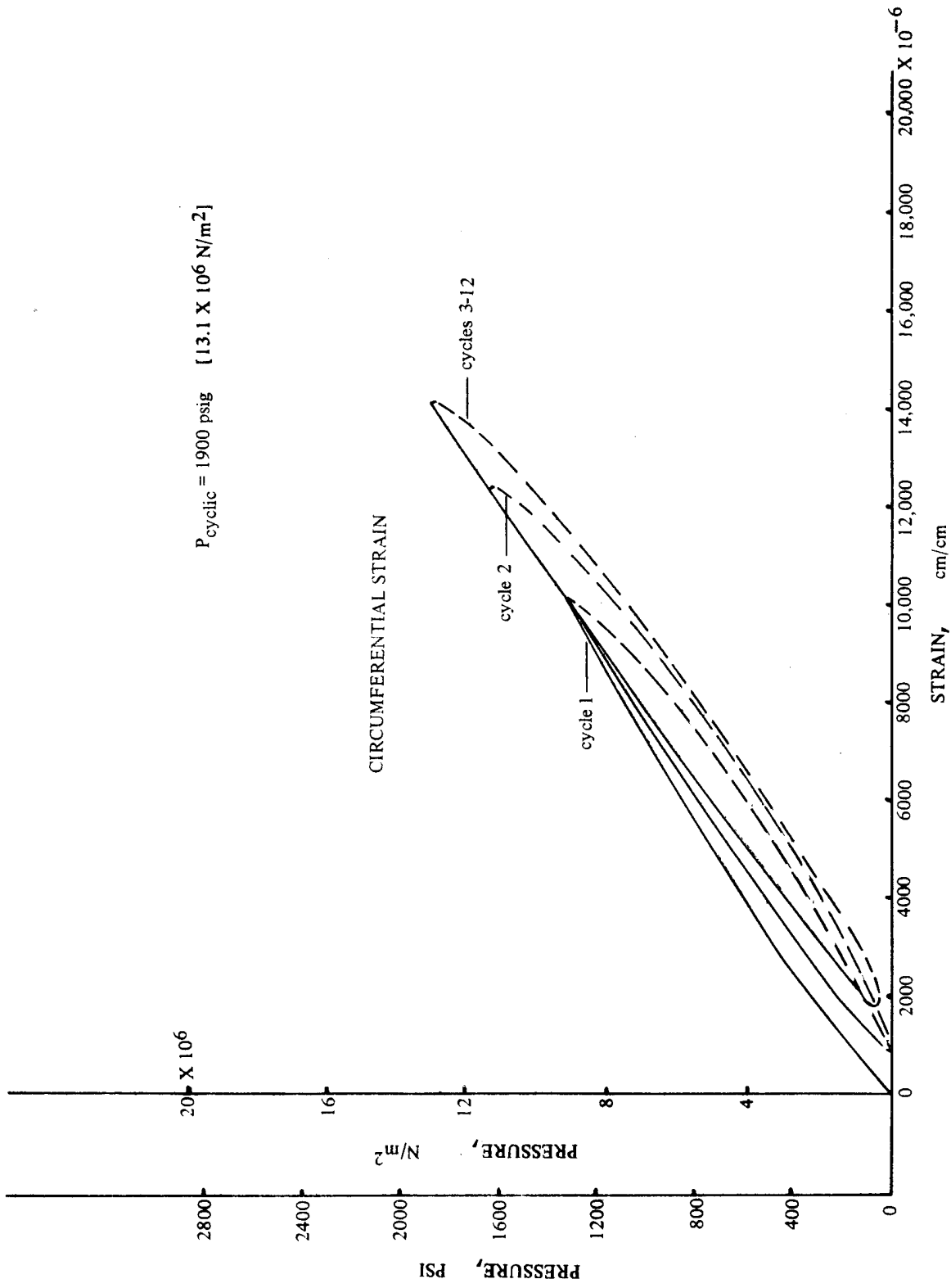


FIGURE 47 PRESSURE VS. STRAIN RELATIONSHIP OF VESSEL NO.15 IN CYCLIC FATIGUE

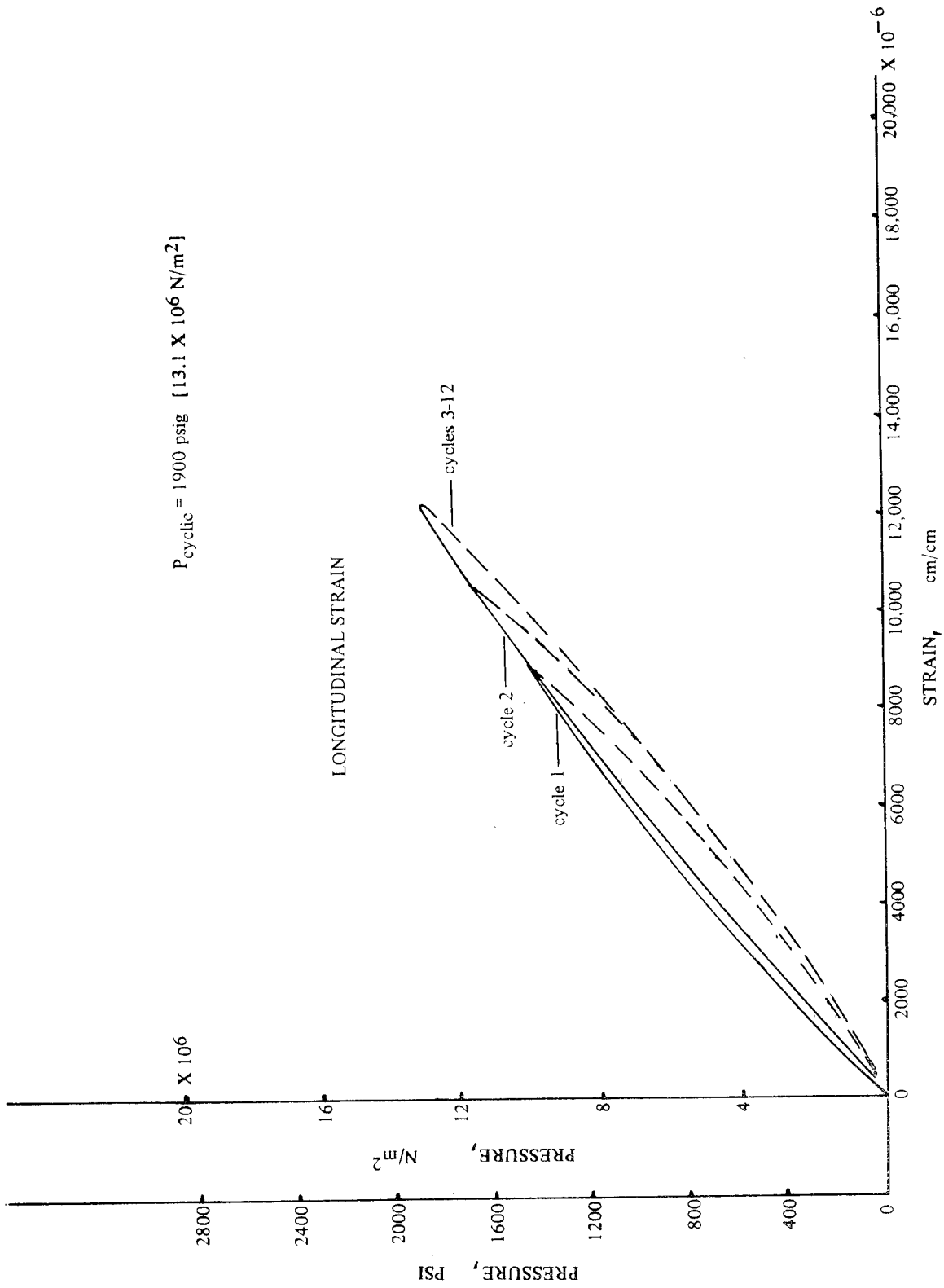


FIGURE 48 PRESSURE VS. STRAIN RELATIONSHIP OF VESSEL NO.15 IN CYCLIC FATIGUE

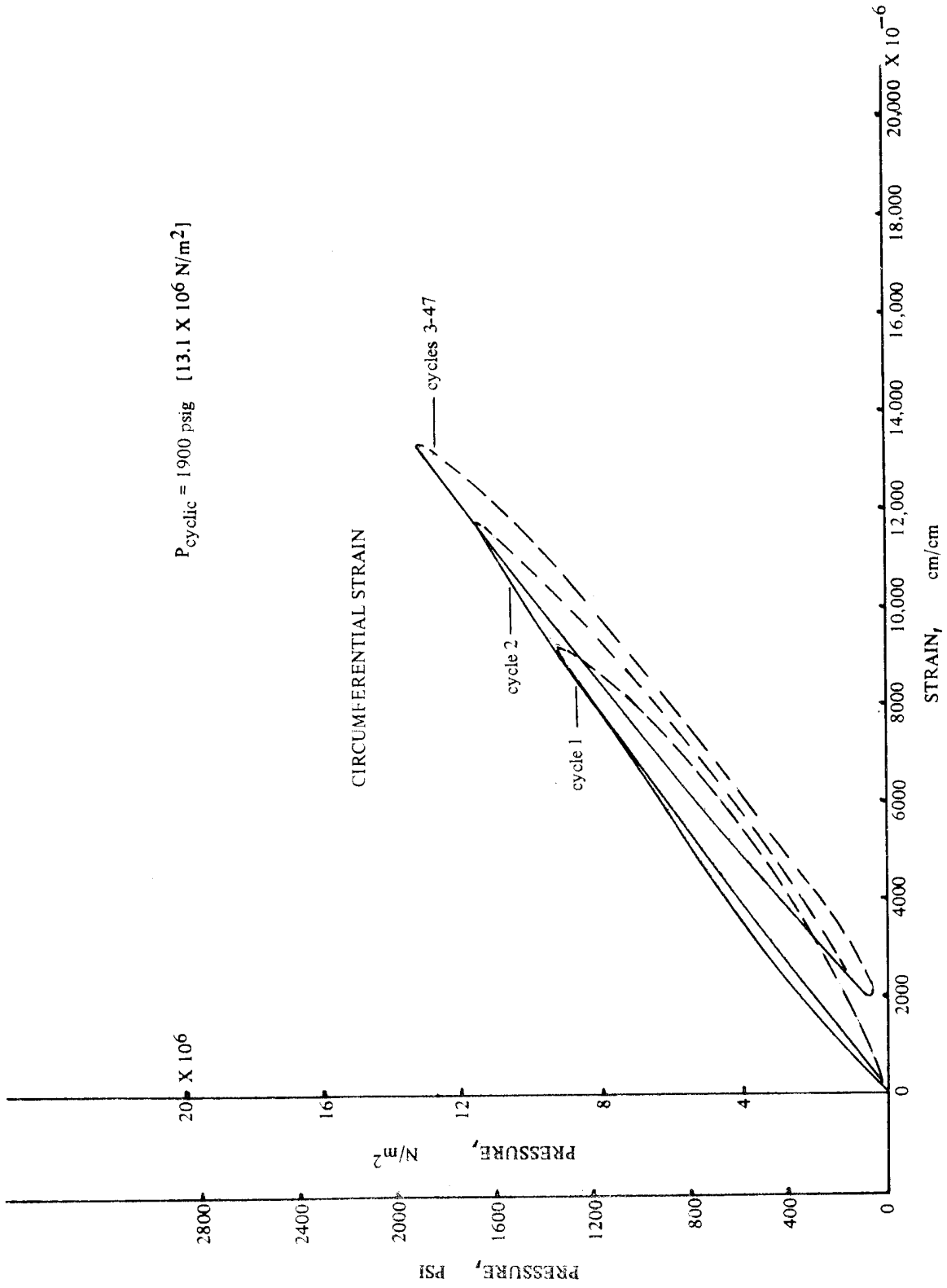


FIGURE 49 PRESSURE VS. STRAIN RELATIONSHIP OF VESSEL NO.16 IN CYCLIC FATIGUE

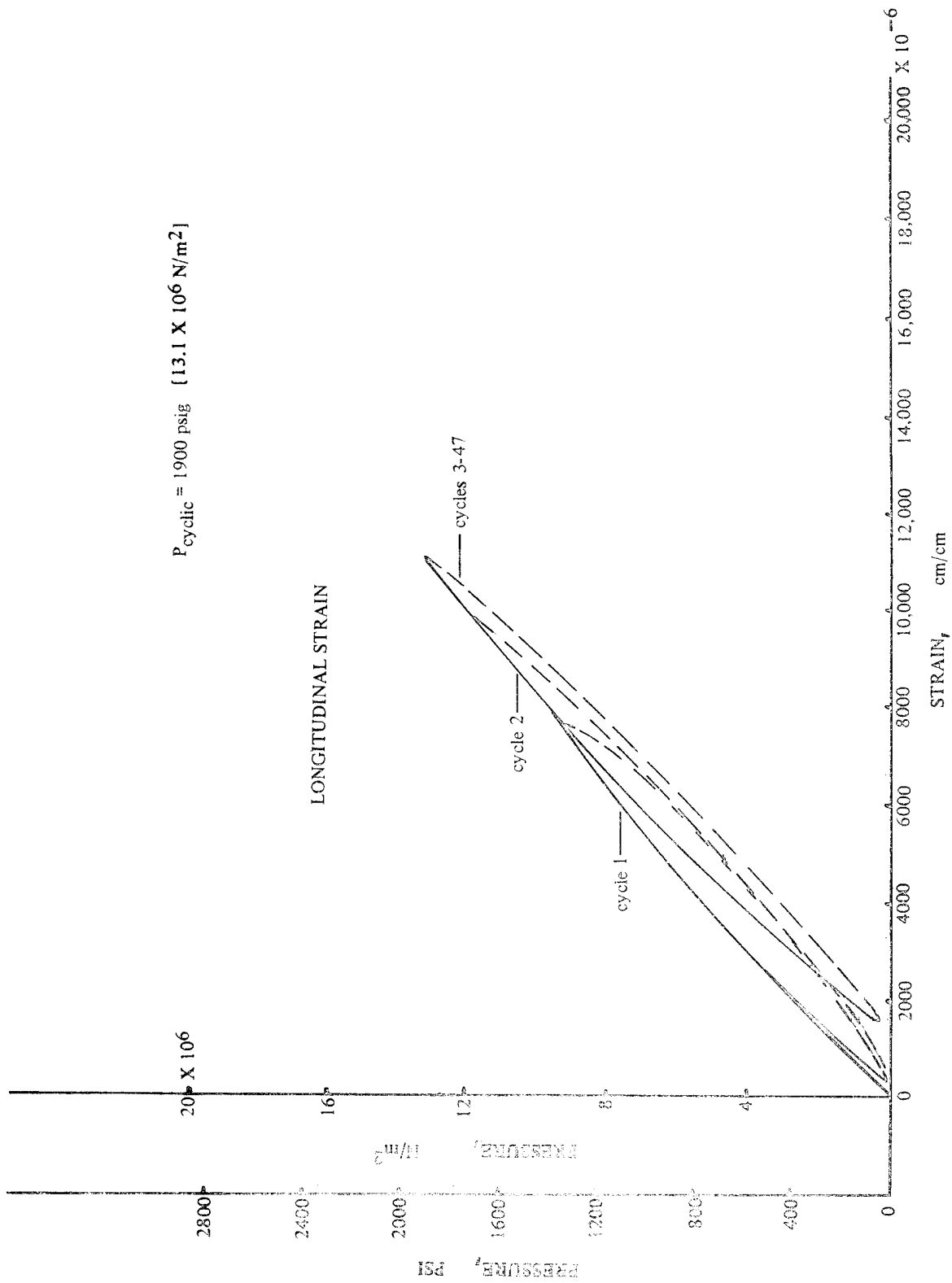


FIGURE 50 PRESSURE VS. STRAIN RELATIONSHIP OF VESSEL NO. 16 IN CYCLIC FATIGUE

$P_{cyclic} = 1270 \text{ psig} \quad [8.76 \times 10^6 \text{ N/m}^2]$

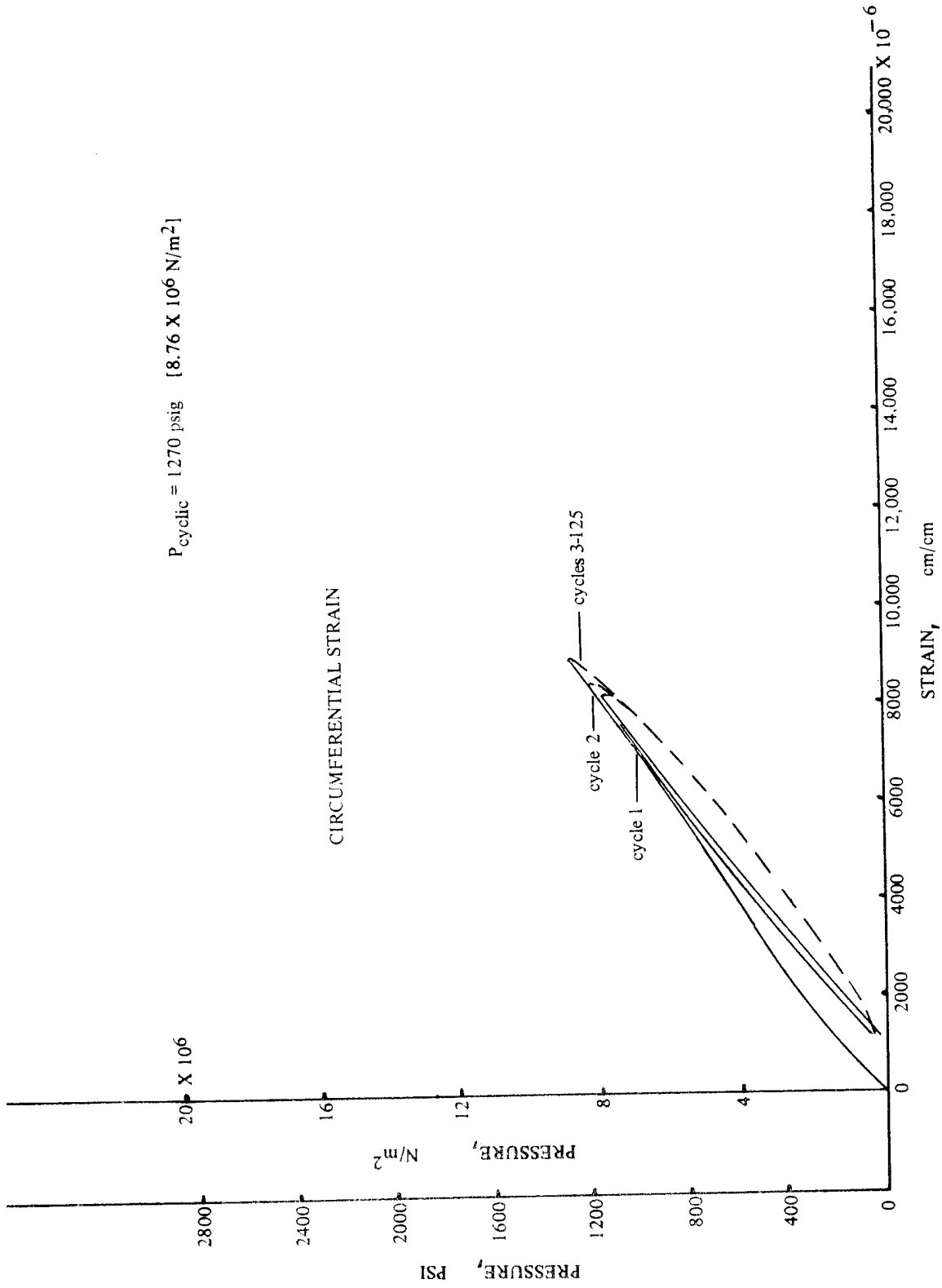


FIGURE 51 PRESSURE VS. STRAIN RELATIONSHIP OF VESSEL NO. 17 IN CYCLIC FATIGUE

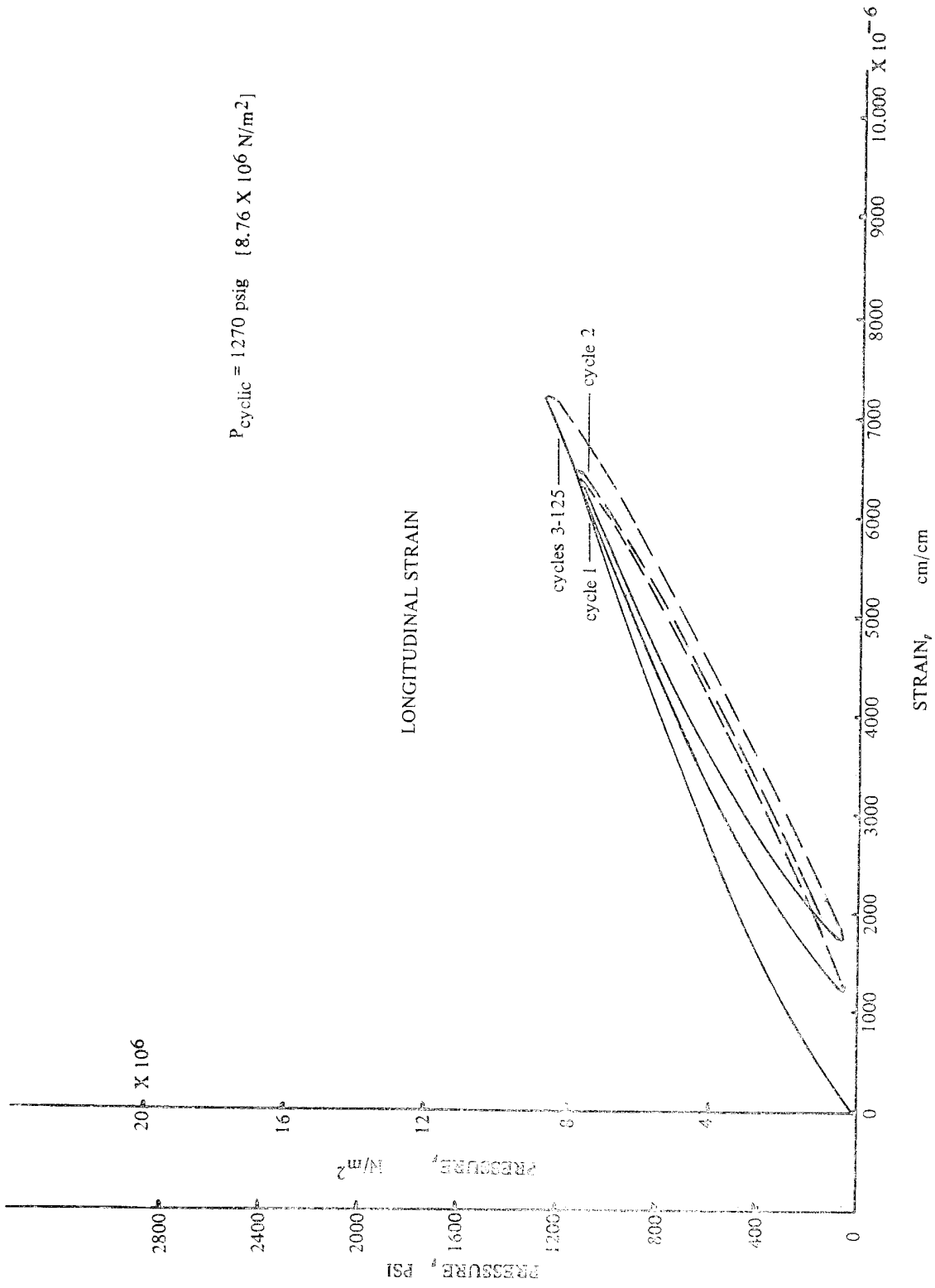


FIGURE 52 PRESSURE VS. STRAIN RELATIONSHIP OF VESSEL NO. 17 IN CYCLIC FATIGUE

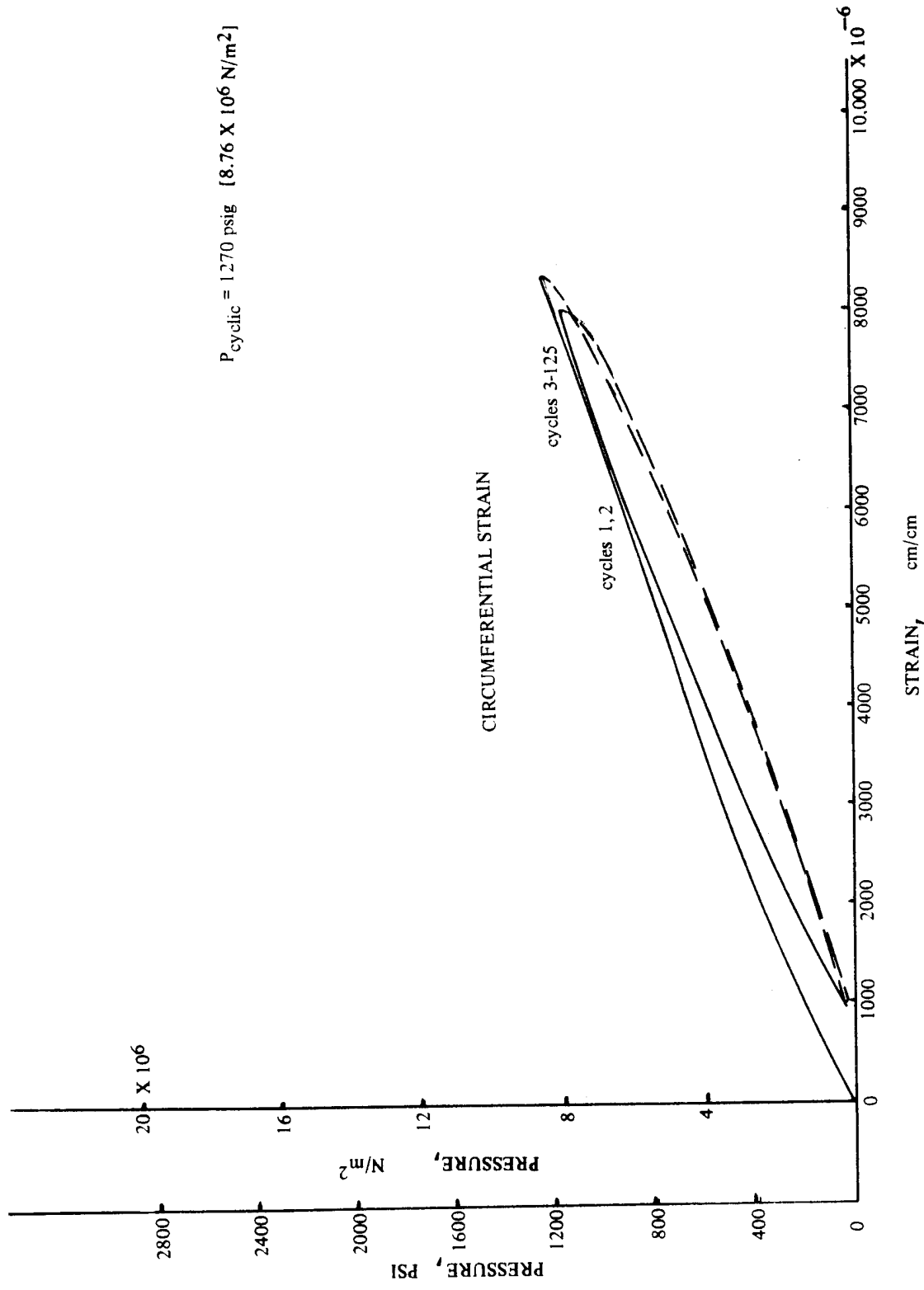


FIGURE 53 PRESSURE VS. STRAIN RELATIONSHIP OF VESSEL NO. 18 IN CYCLIC FATIGUE

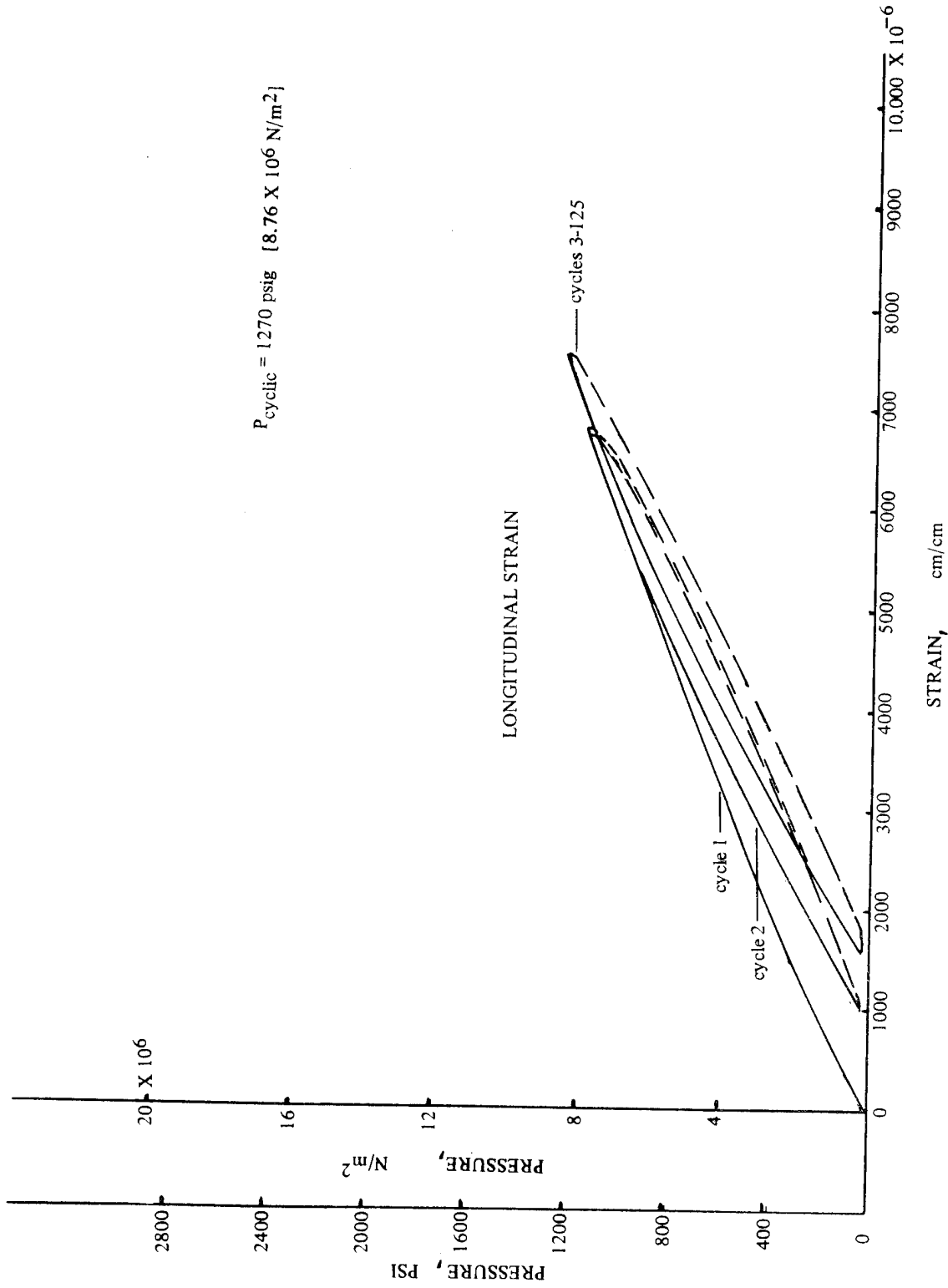


FIGURE 54 PRESSURE VS. STRAIN RELATIONSHIP OF VESSEL NO.18 IN CYCLIC FATIGUE

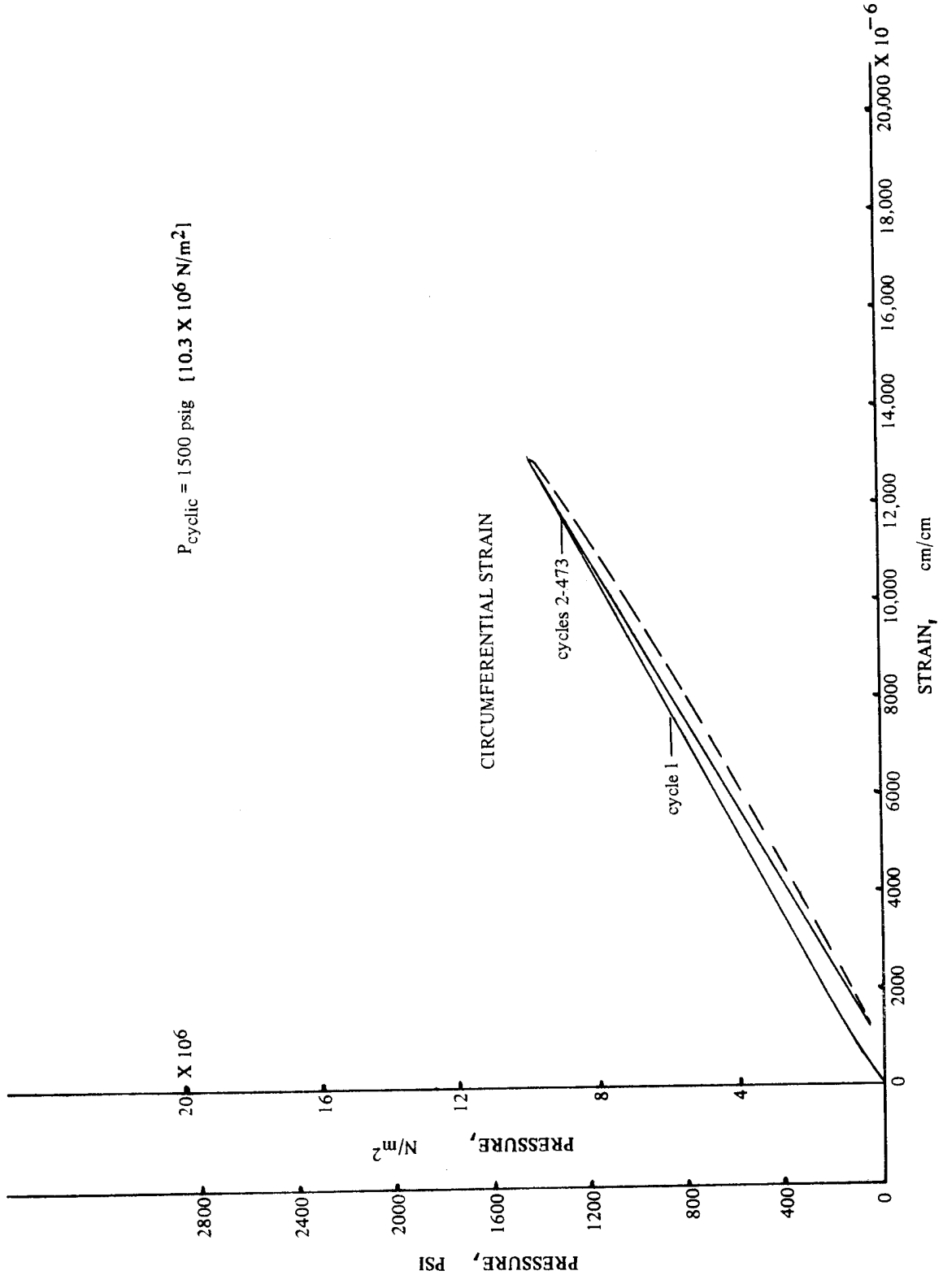


FIGURE 55 PRESSURE VS. STRAIN RELATIONSHIP OF VESSEL NO.19 IN CYCLIC FATIGUE

$P_{cyclic} = 1500 \text{ psig} \quad [10.3 \times 10^6 \text{ N/m}^2]$

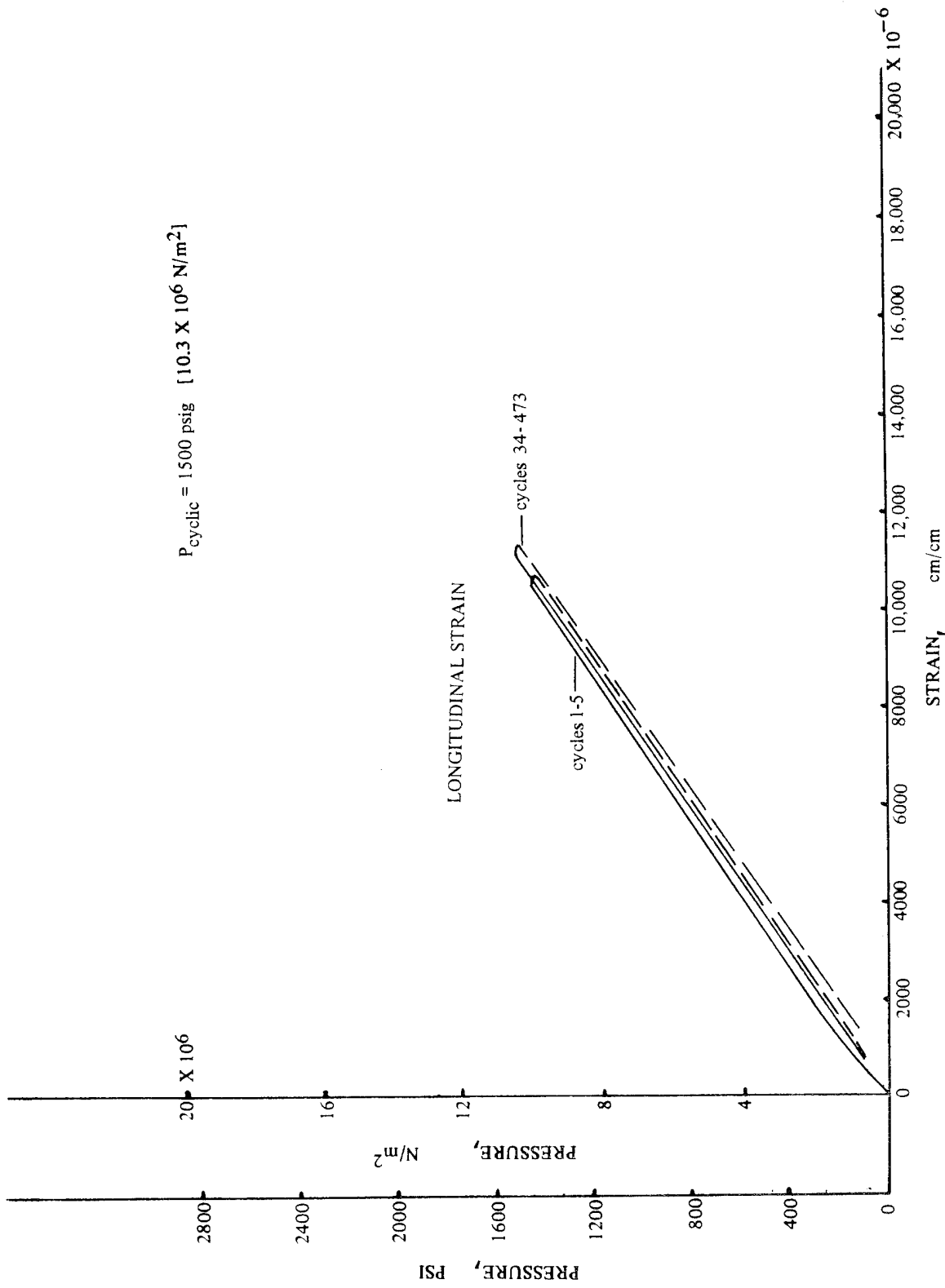


FIGURE 56 PRESSURE VS. STRAIN RELATIONSHIP OF VESSEL NO. 19 IN CYCLIC FATIGUE

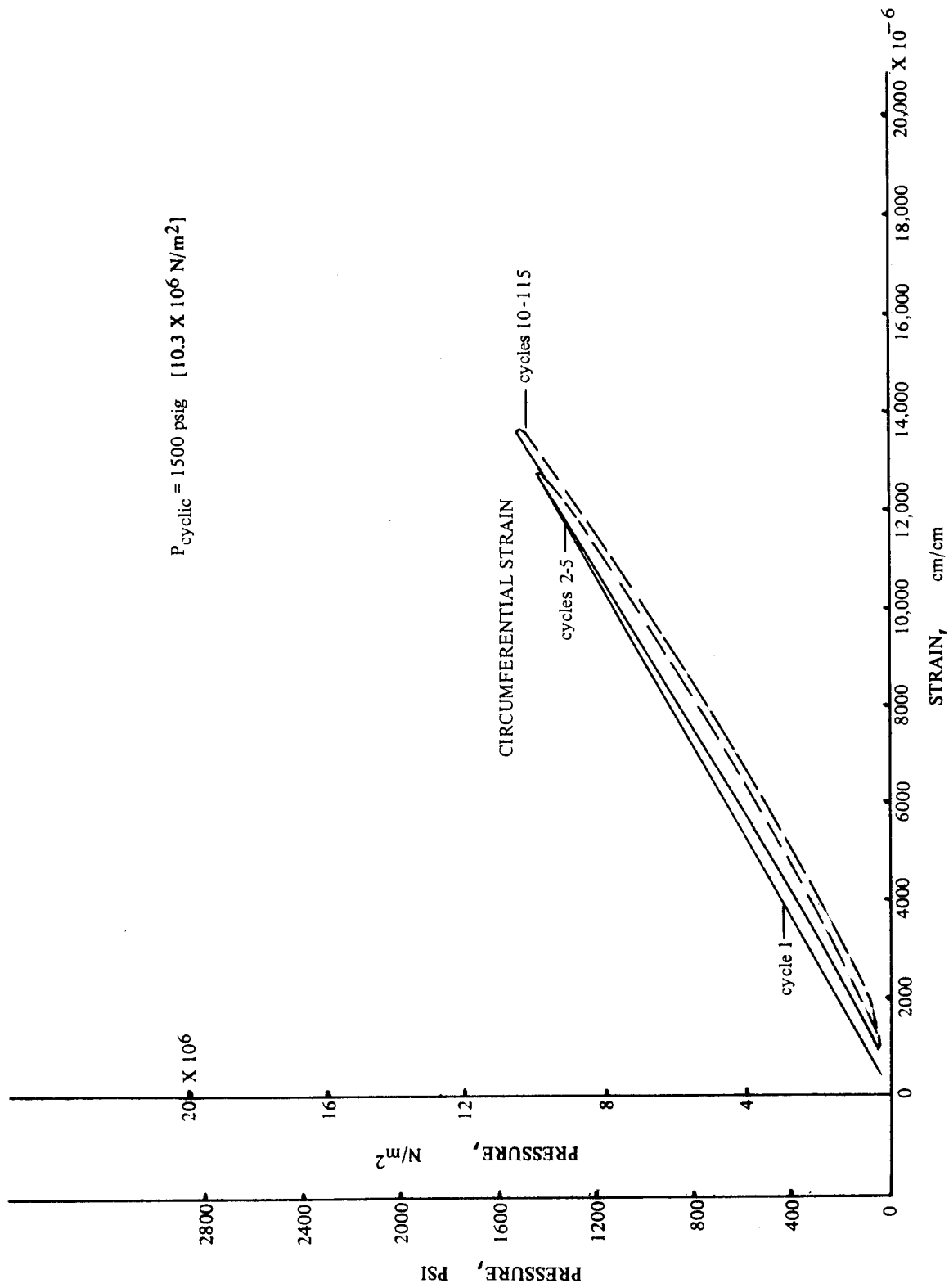


FIGURE 57 PRESSURE VS. STRAIN RELATIONSHIP OF VESSEL NO. 20 IN CYCLIC FATIGUE

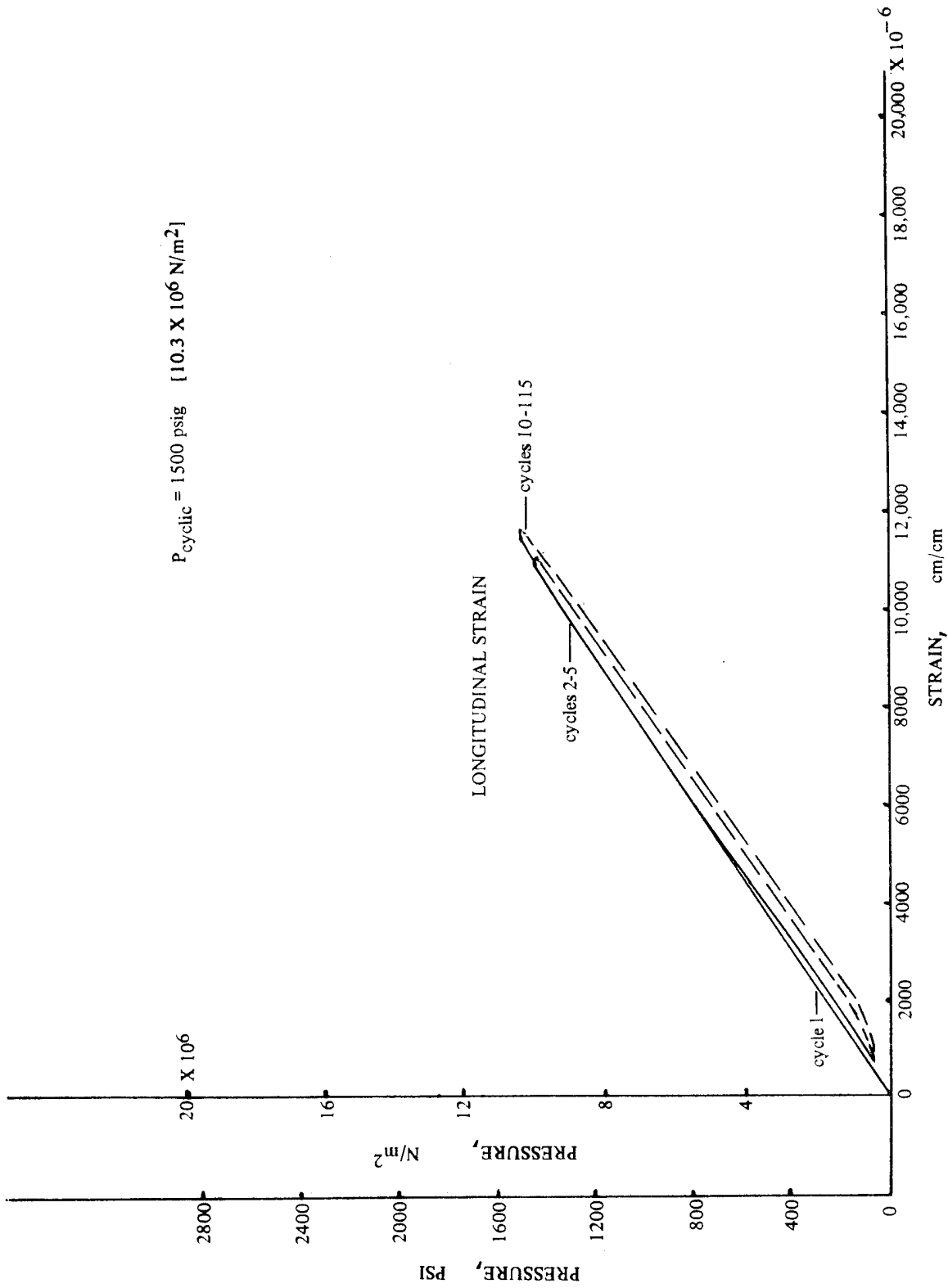


FIGURE 58 PRESSURE VS. STRAIN RELATIONSHIP OF VESSEL NO. 20 IN CYCLIC FATIGUE

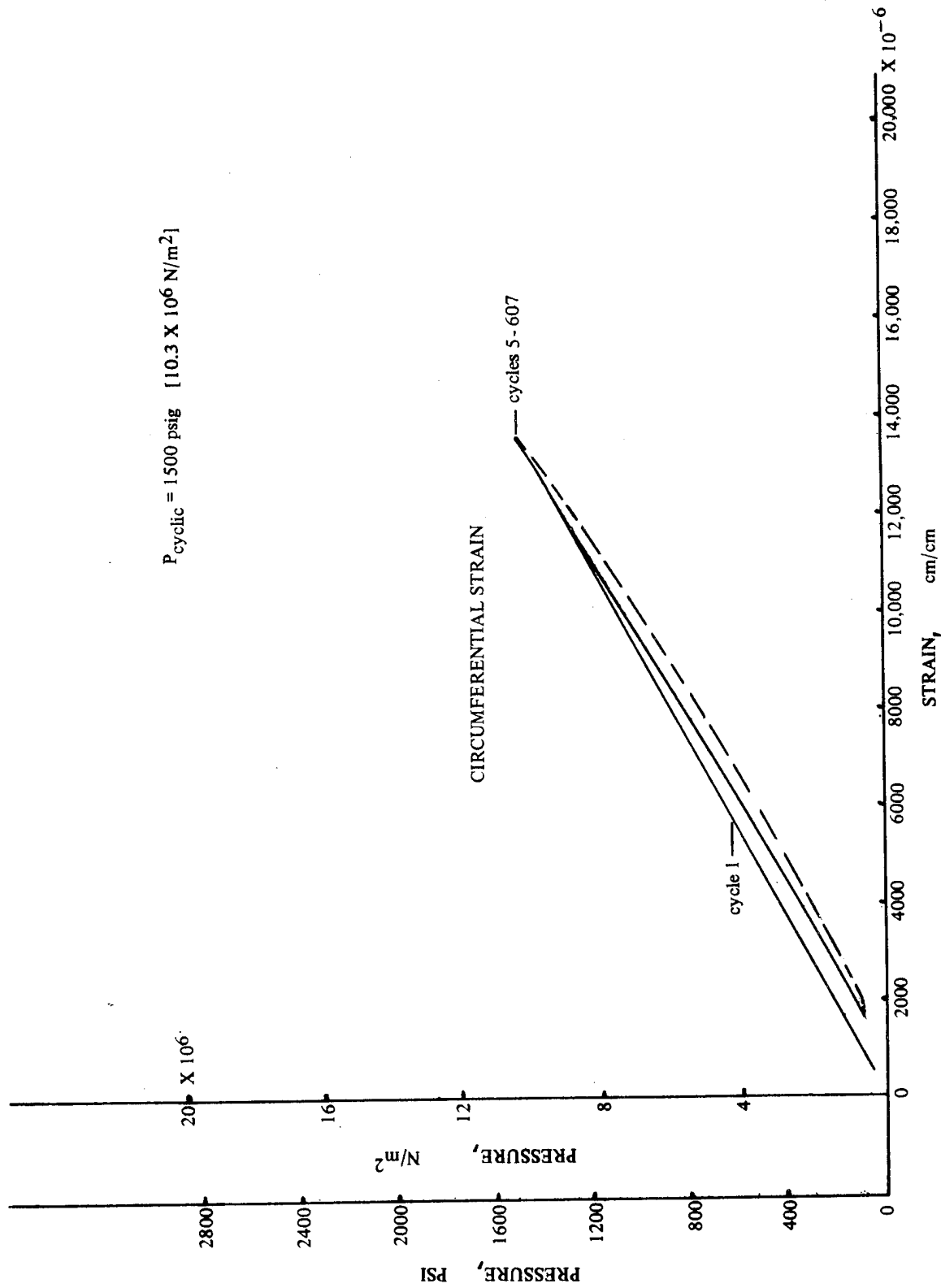


FIGURE 59 PRESSURE VS. STRAIN RELATIONSHIP OF VESSEL NO. 21 IN CYCLIC FATIGUE

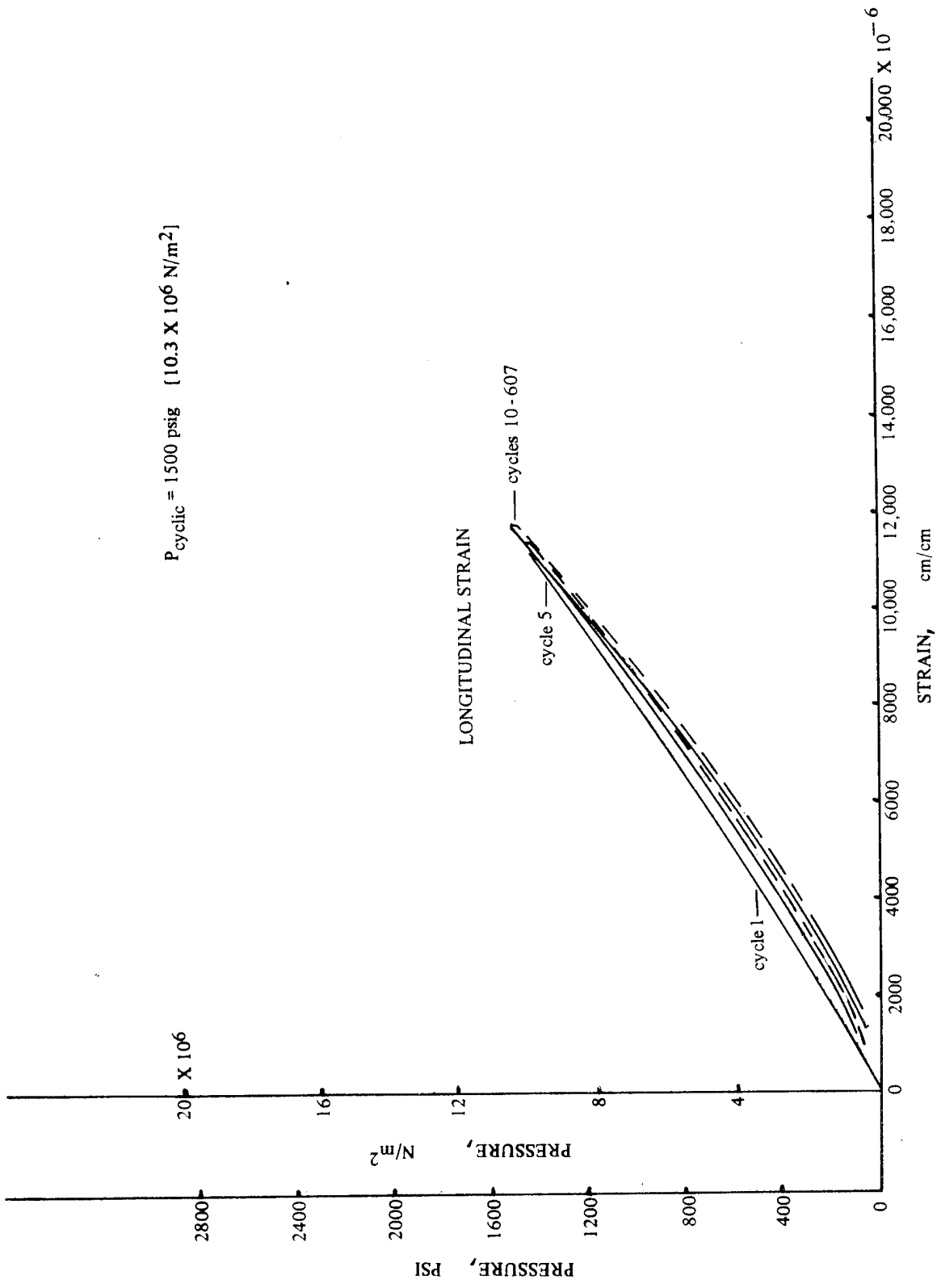


FIGURE 60 PRESSURE VS. STRAIN RELATIONSHIP OF VESSEL NO. 21 IN CYCLIC FATIGUE

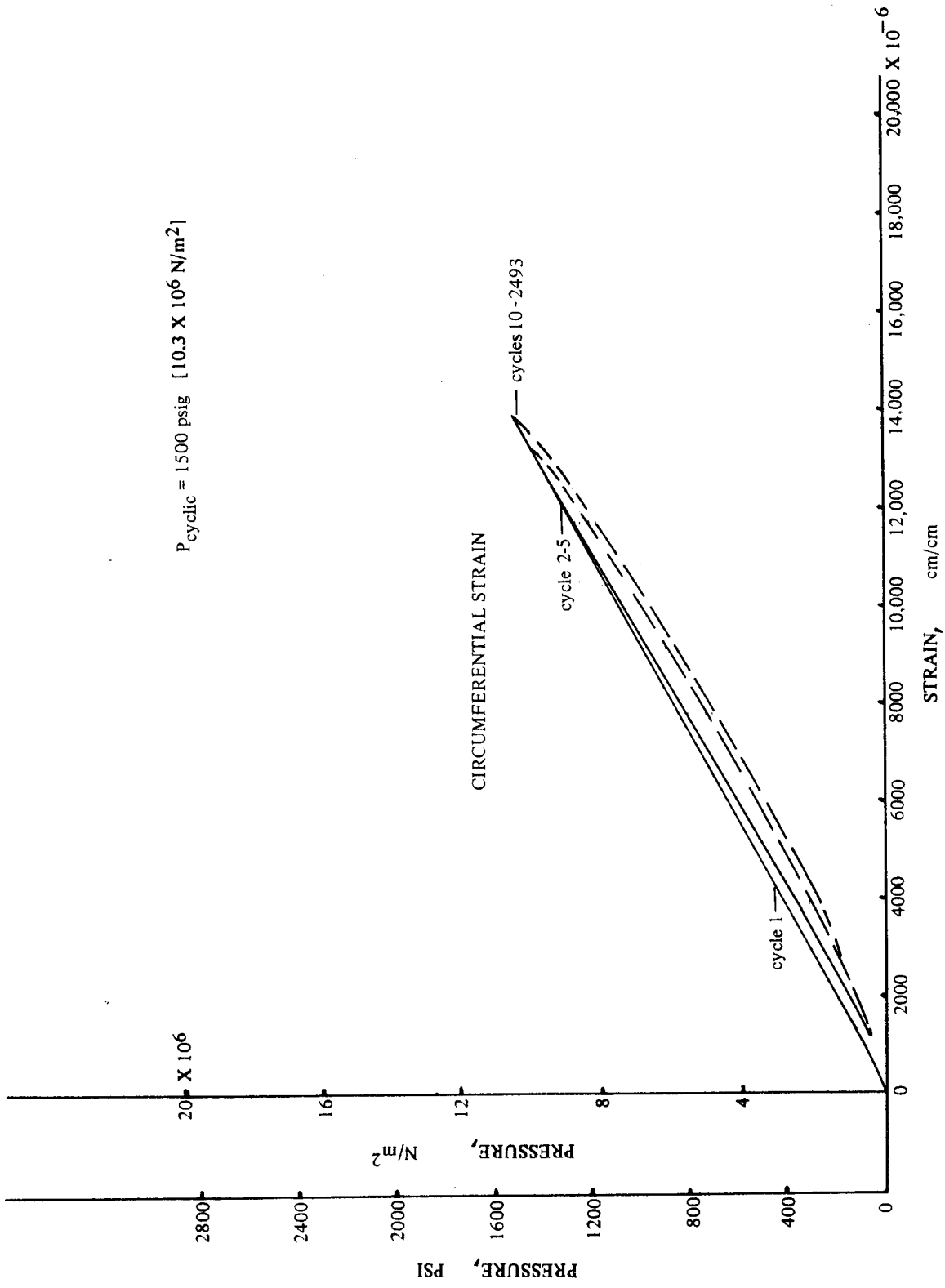


FIGURE 61 PRESSURE VS. STRAIN RELATIONSHIP OF VESSEL NO.22 IN CYCLIC FATIGUE

$P_{cyclic} = 1500 \text{ psig} \quad [10.3 \times 10^6 \text{ N/m}^2]$

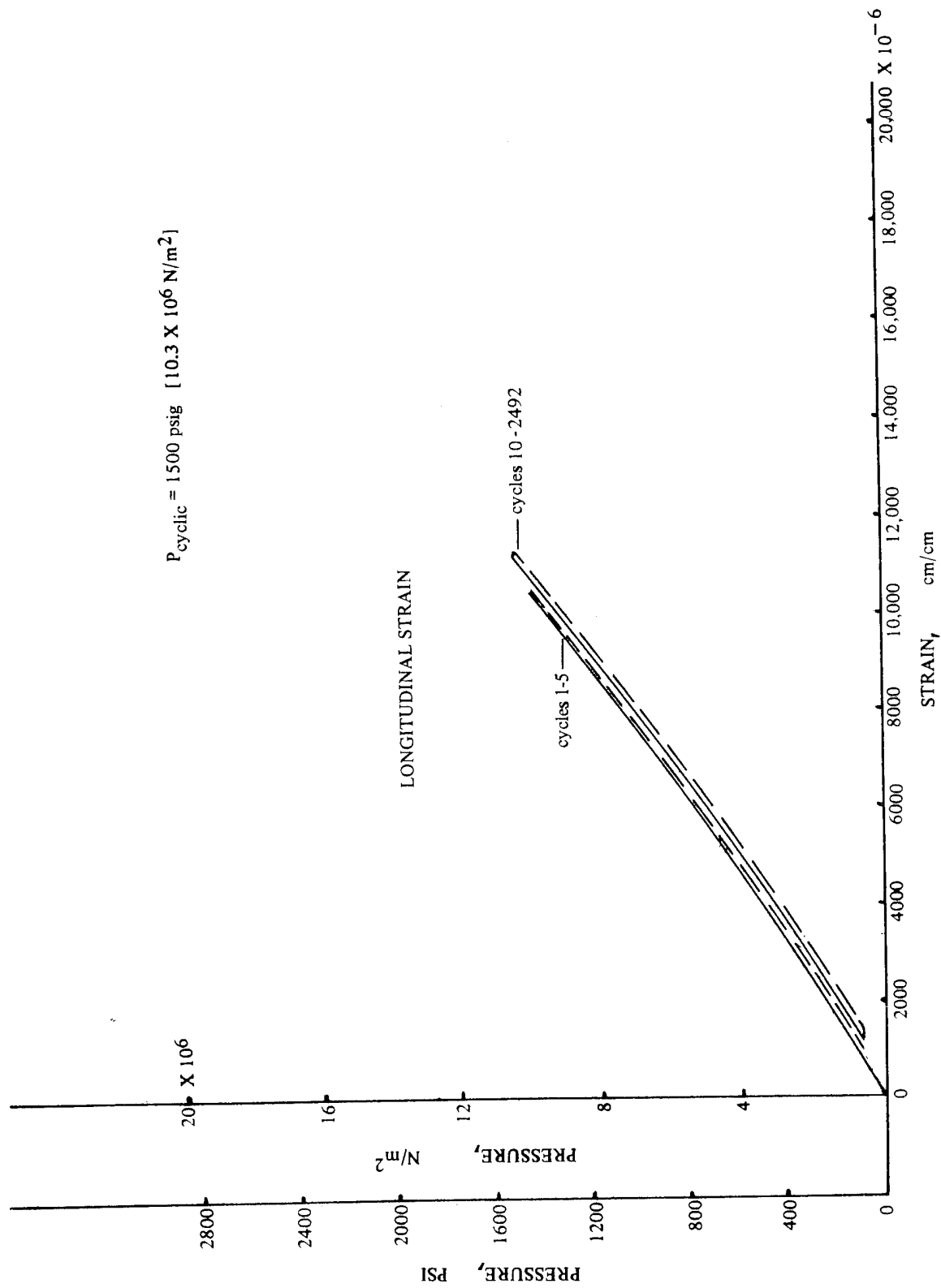


FIGURE 62 PRESSURE VS. STRAIN RELATIONSHIP OF VESSEL NO. 22 IN CYCLIC FATIGUE

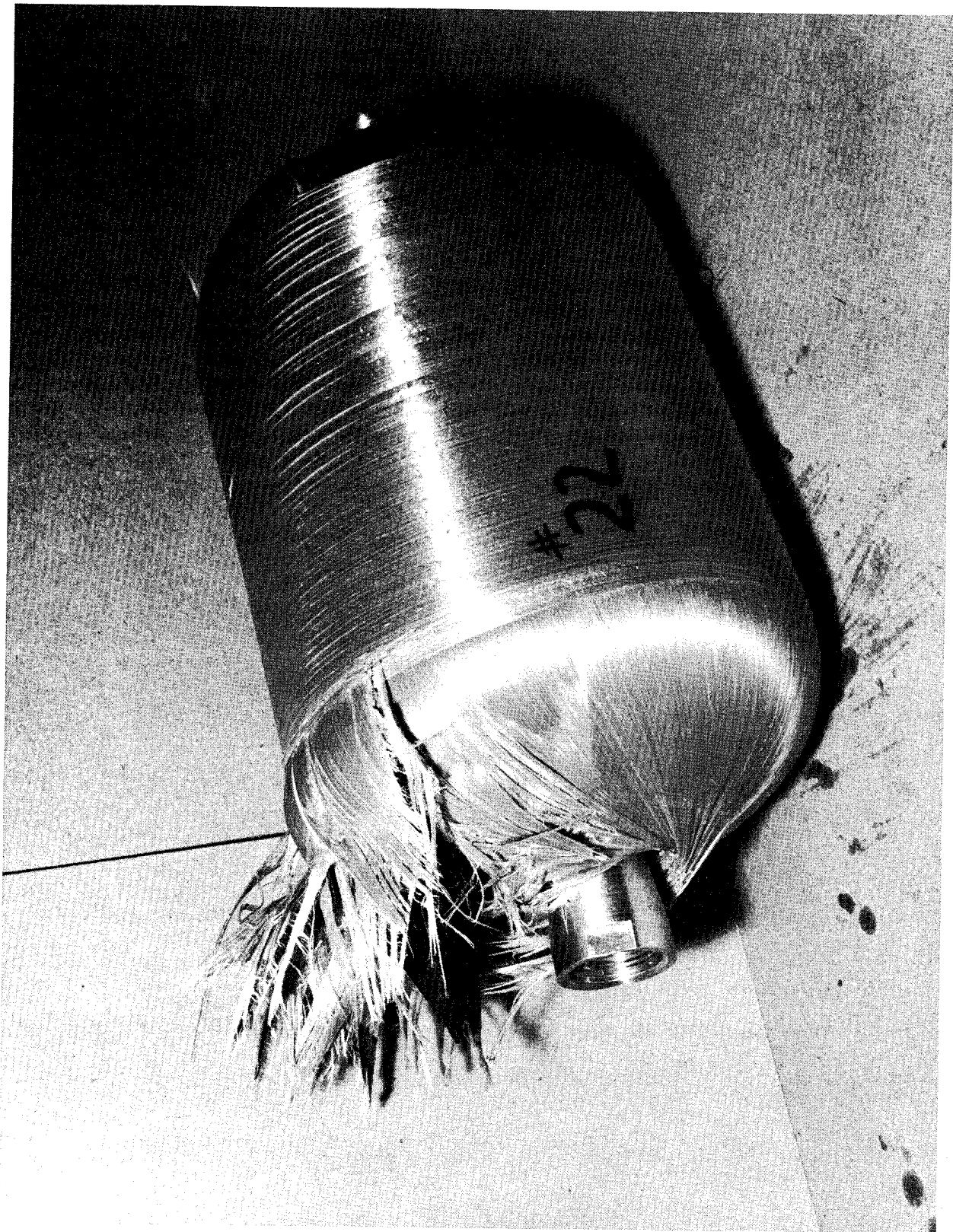


FIGURE 63— VESSEL NO. 22 AFTER CYCLIC TESTING

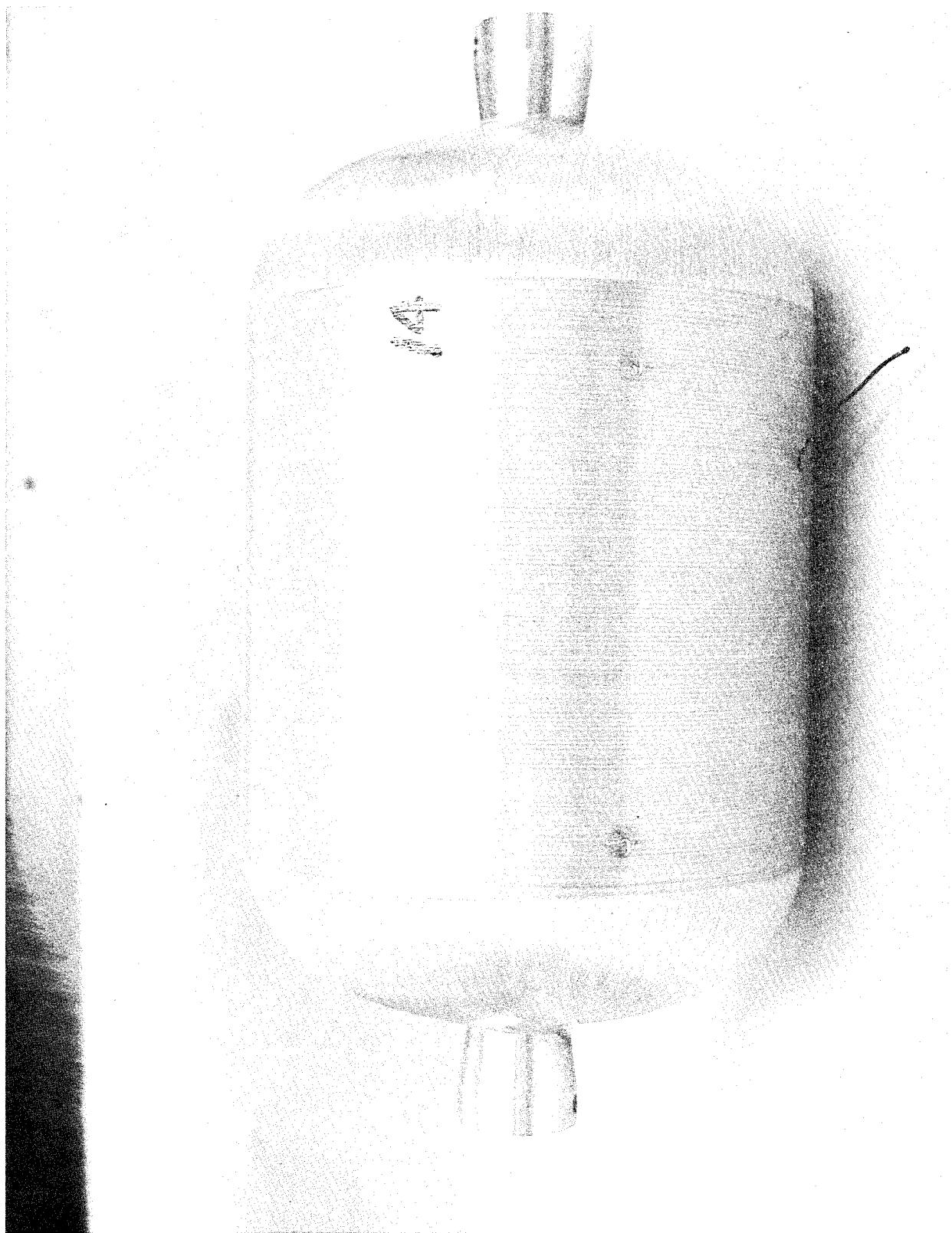


FIGURE 64—VESSEL NO. 14 AFTER CYCLIC TESTING

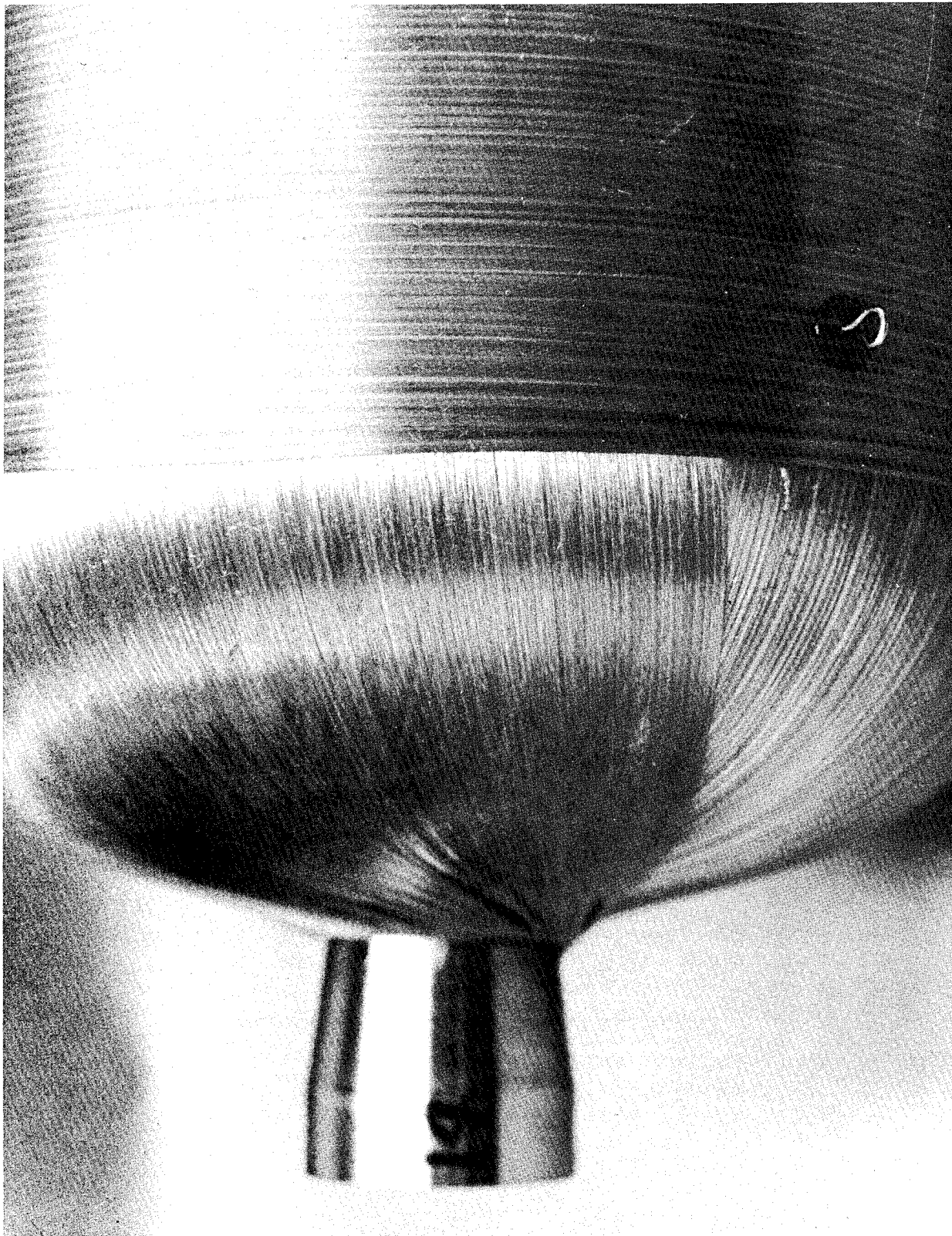


FIGURE 65 - VESSEL NO. 14 AFTER CYCLIC TESTING

P_{ULT} = 1940 psi [13.37 X 10⁶ N/m²]

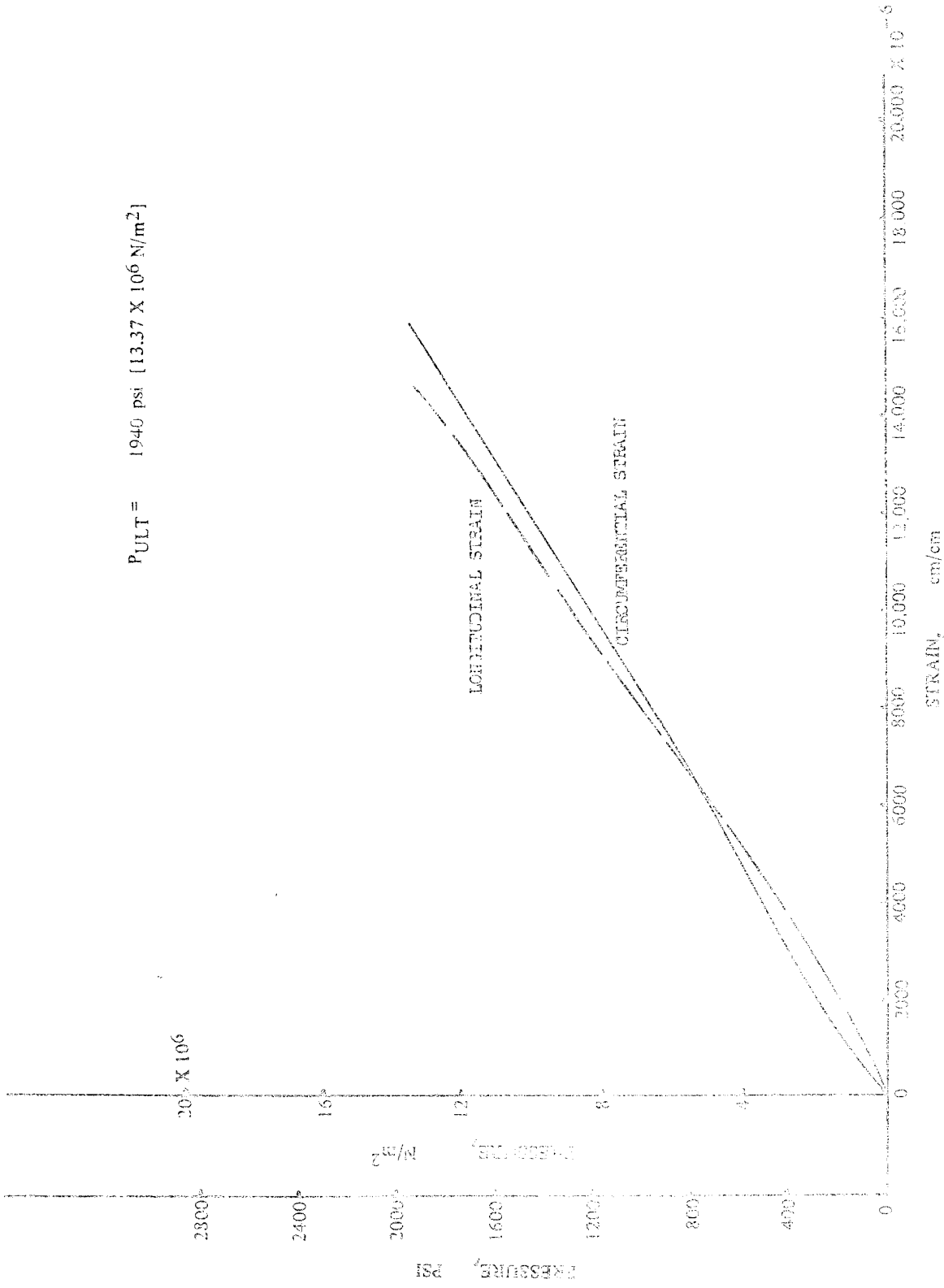


FIGURE 66 PRESSURE VS. STRAIN RELATIONSHIP - VESSEL NO. 19

$P_{ULT} = 2240 \text{ psi} \quad [15.54 \times 10^6 \text{ N/m}^2]$

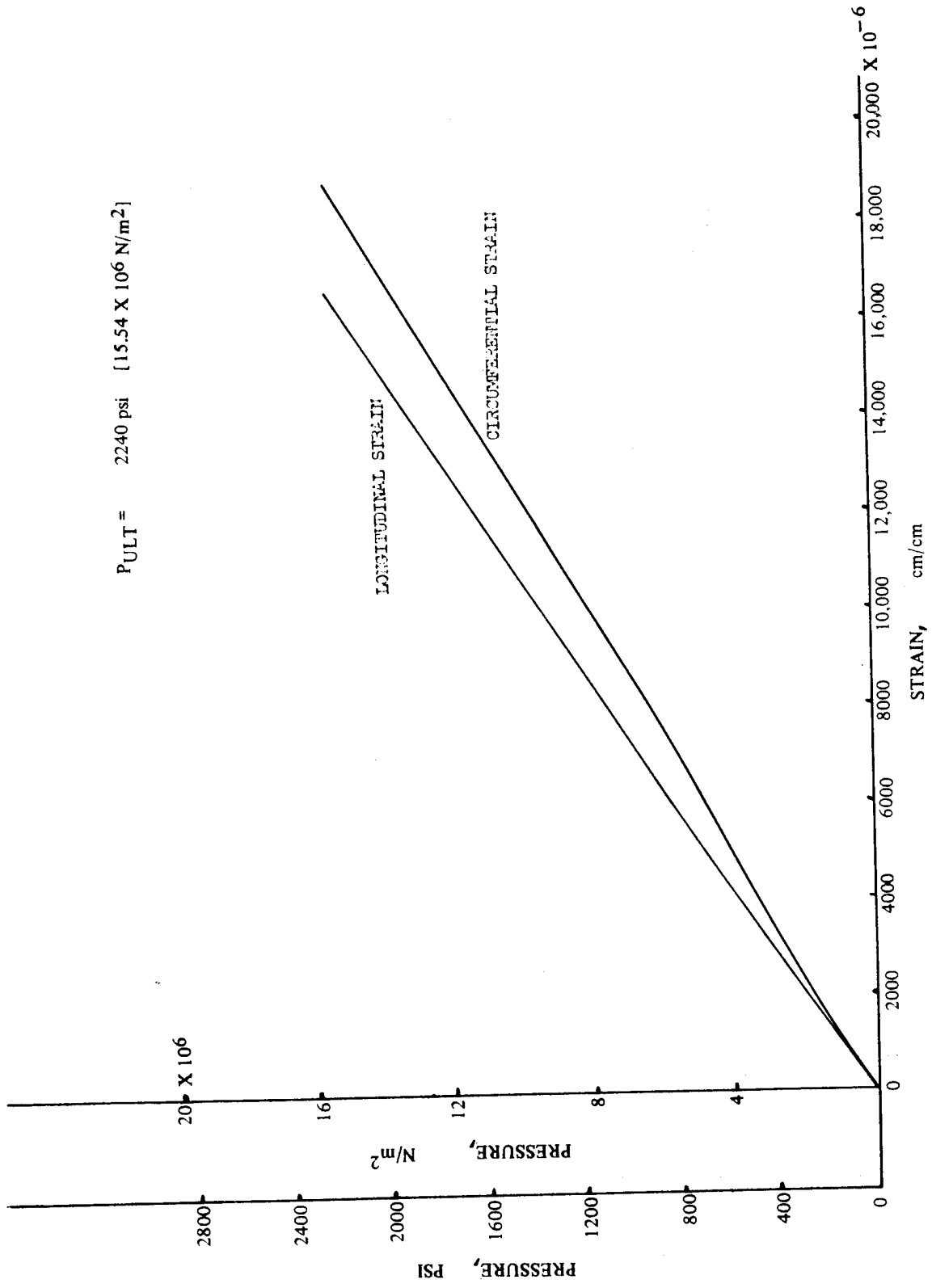


FIGURE 67 PRESSURE VS. STRAIN RELATIONSHIP - VESSEL NO. 20

$P_{ULT} = 2130 \text{ psi} \quad [14.69 \times 10^6 \text{ N/m}^2]$

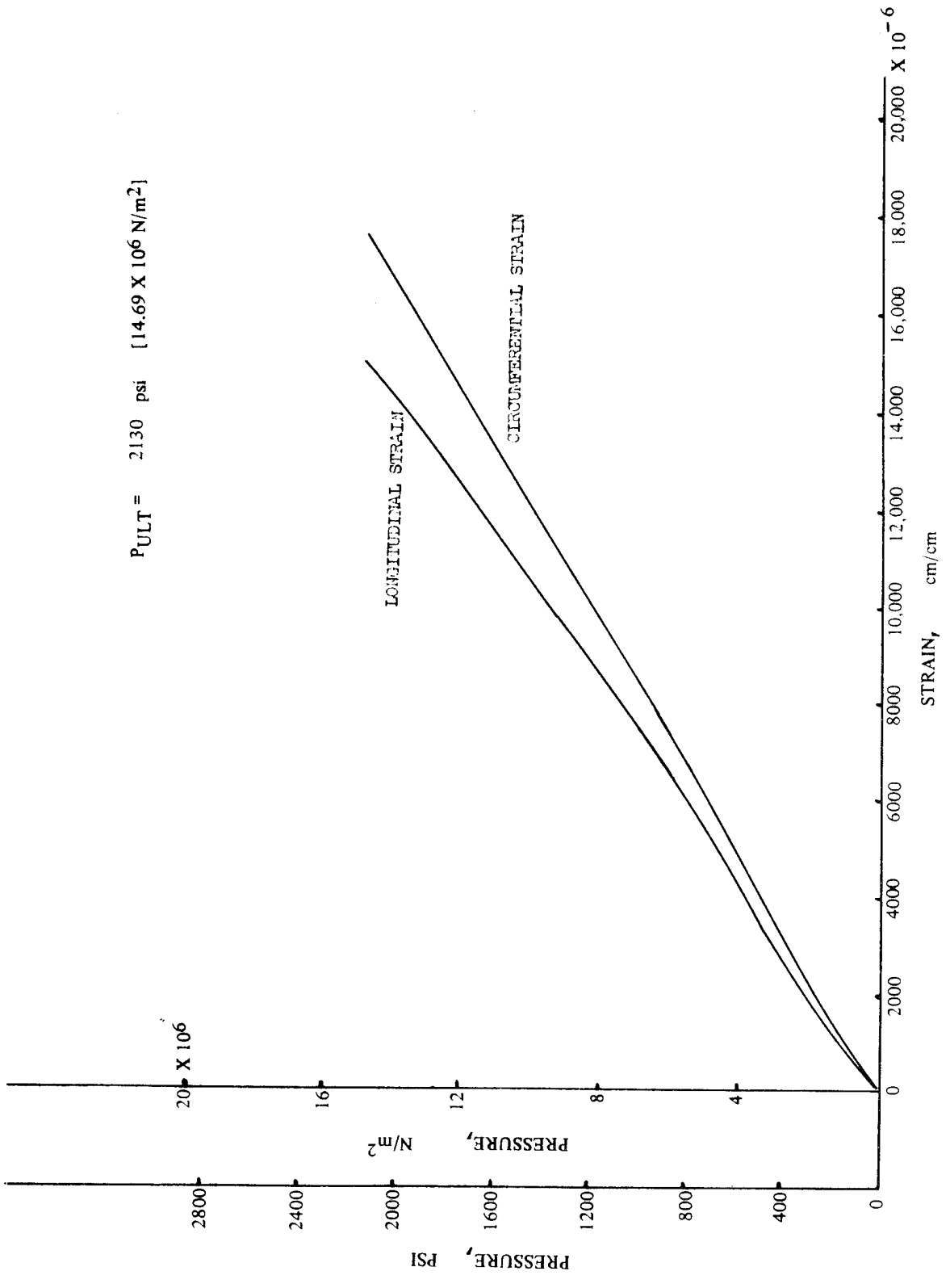


FIGURE 68 PRESSURE VS. STRAIN RELATIONSHIP - VESSEL NO. 21



FIGURE 69—VESSEL NO. 7 AFTER BURST TEST



FIGURE 70—VESSEL NO. 8 AFTER BURST TEST



FIGURE 71 - VESSEL NO. 9 AFTER BURST TEST

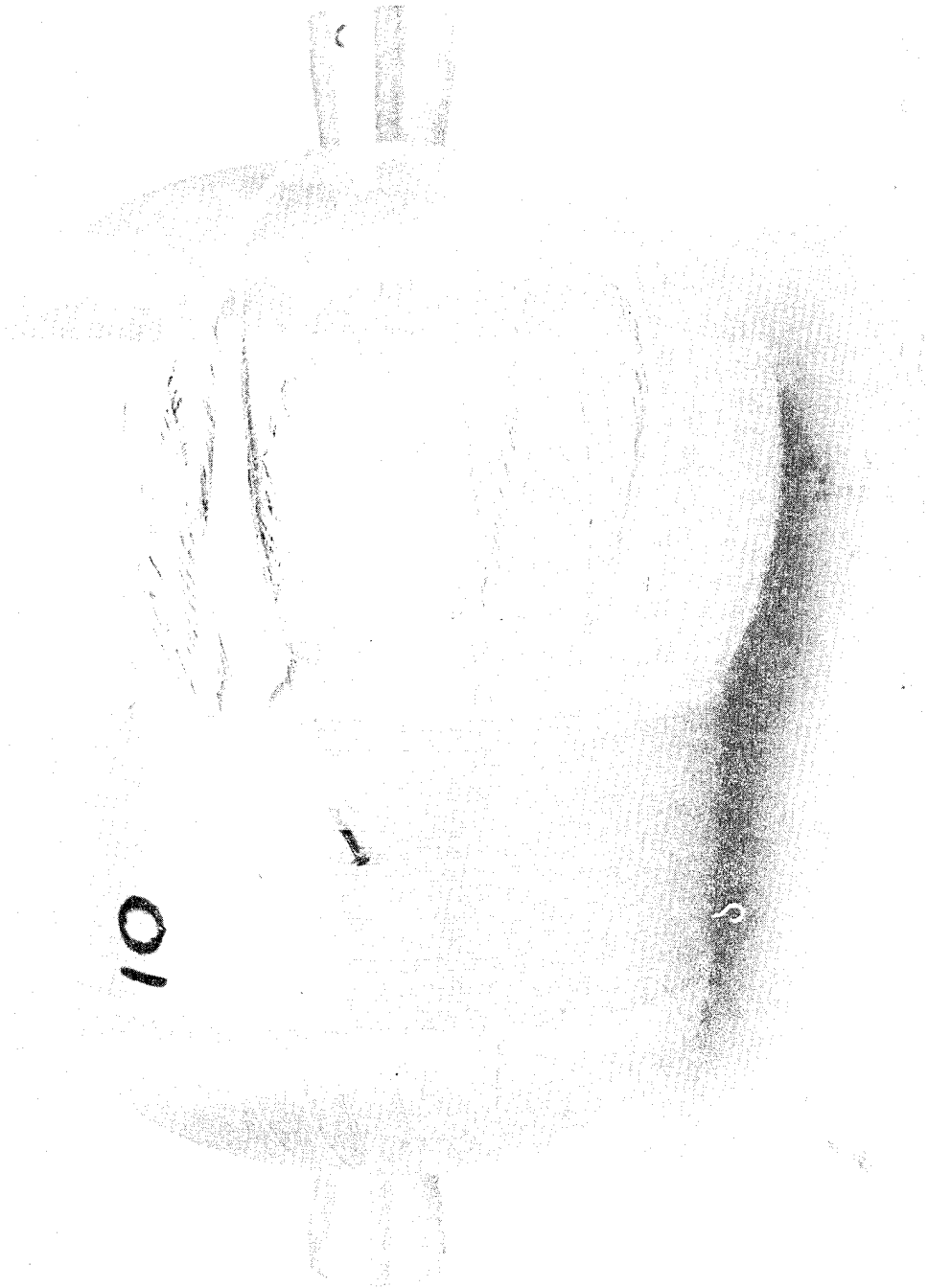


FIGURE 72--VESSEL NO. 10 AFTER BURST TEST



FIGURE 73— VESSEL NO. 11 AFTER BURST TEST



FIGURE 74—VESSEL NO.12 AFTER BURST TEST



FIGURE 75--VESSEL NO. 19 AFTER BURST TEST

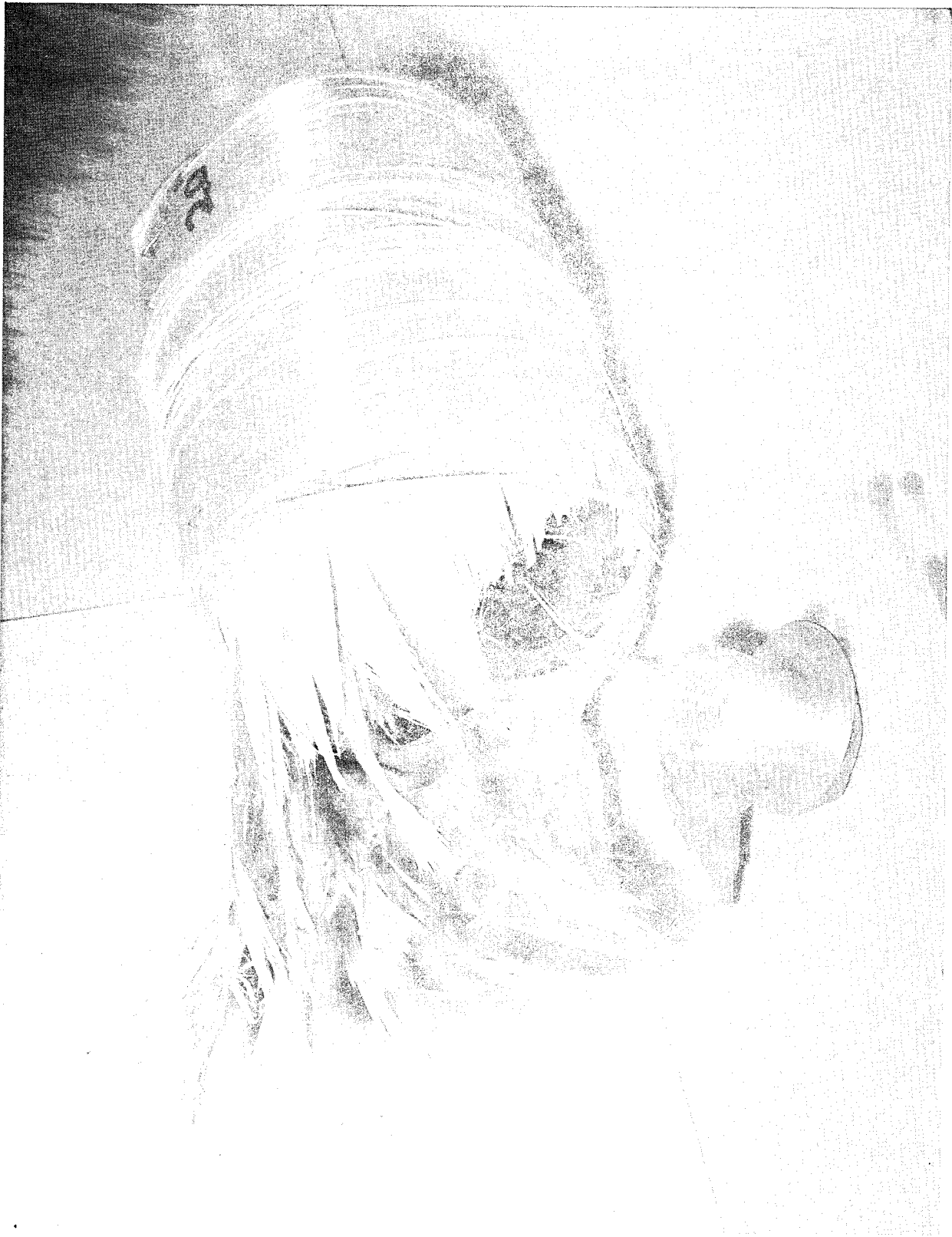


FIGURE 76—VESSEL NO. 20 AFTER BURST TEST

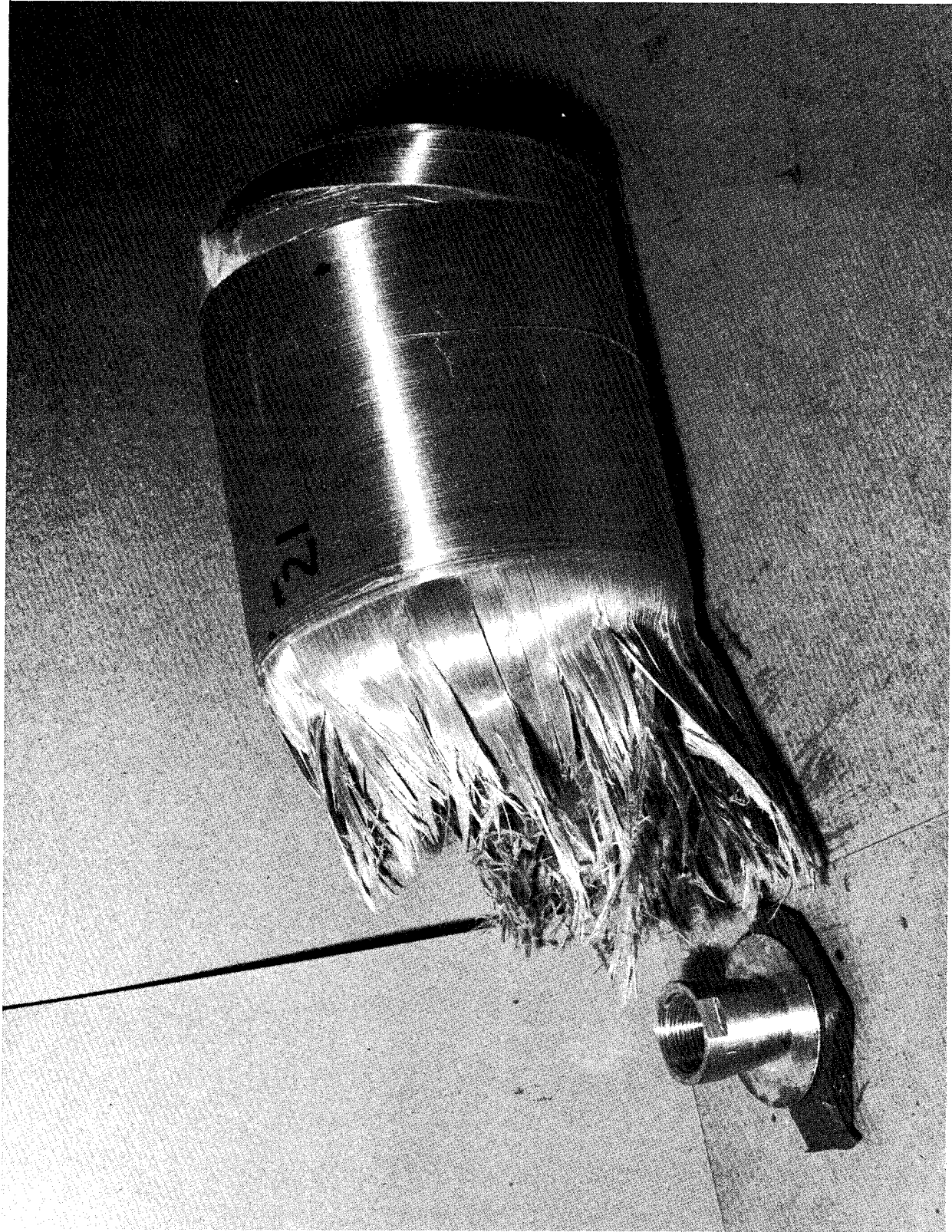


FIGURE 77—VESSEL NO. 21 AFTER BURST TEST

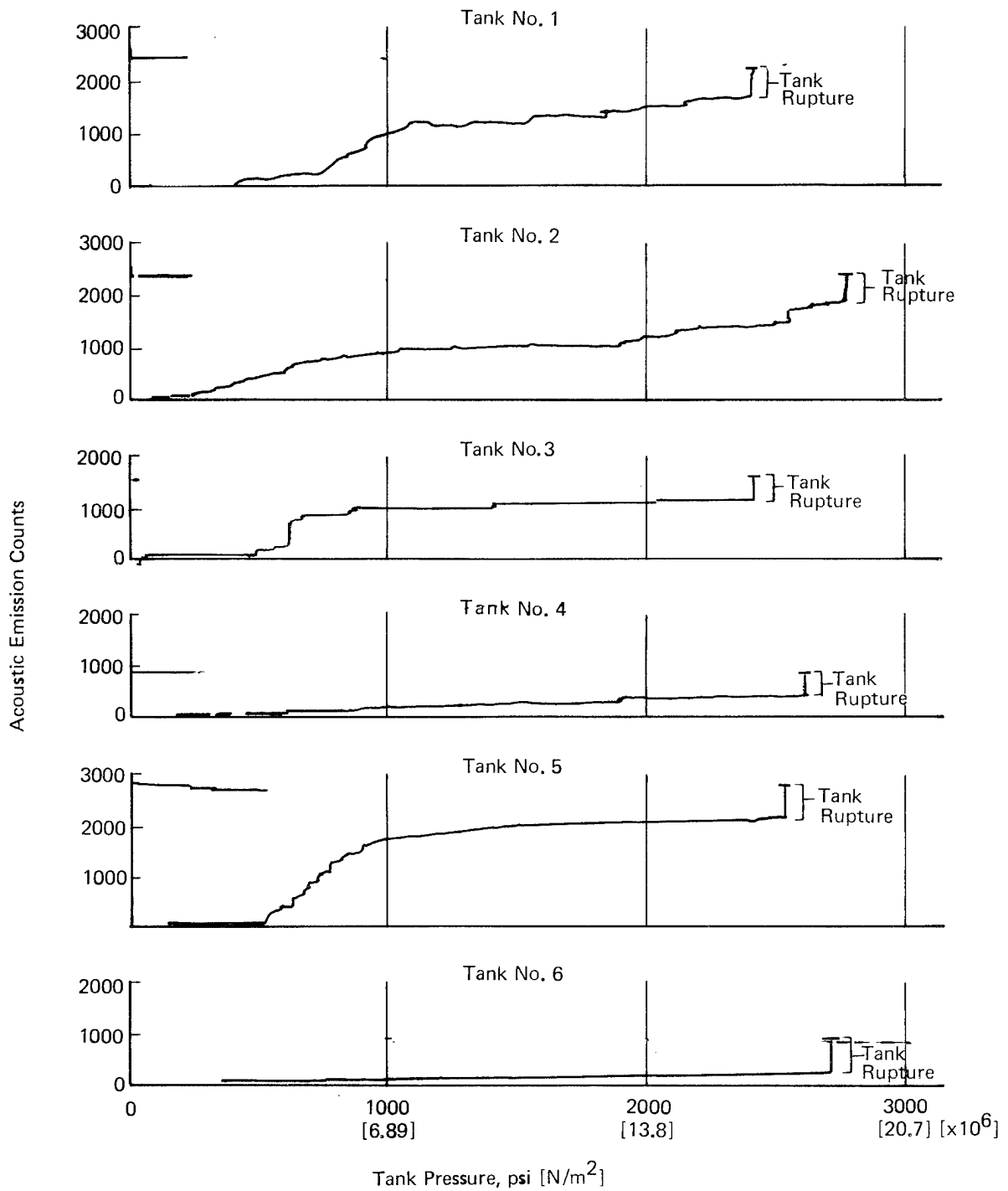


Figure 78: Acoustic Emission Data from Vessel Burst Tests

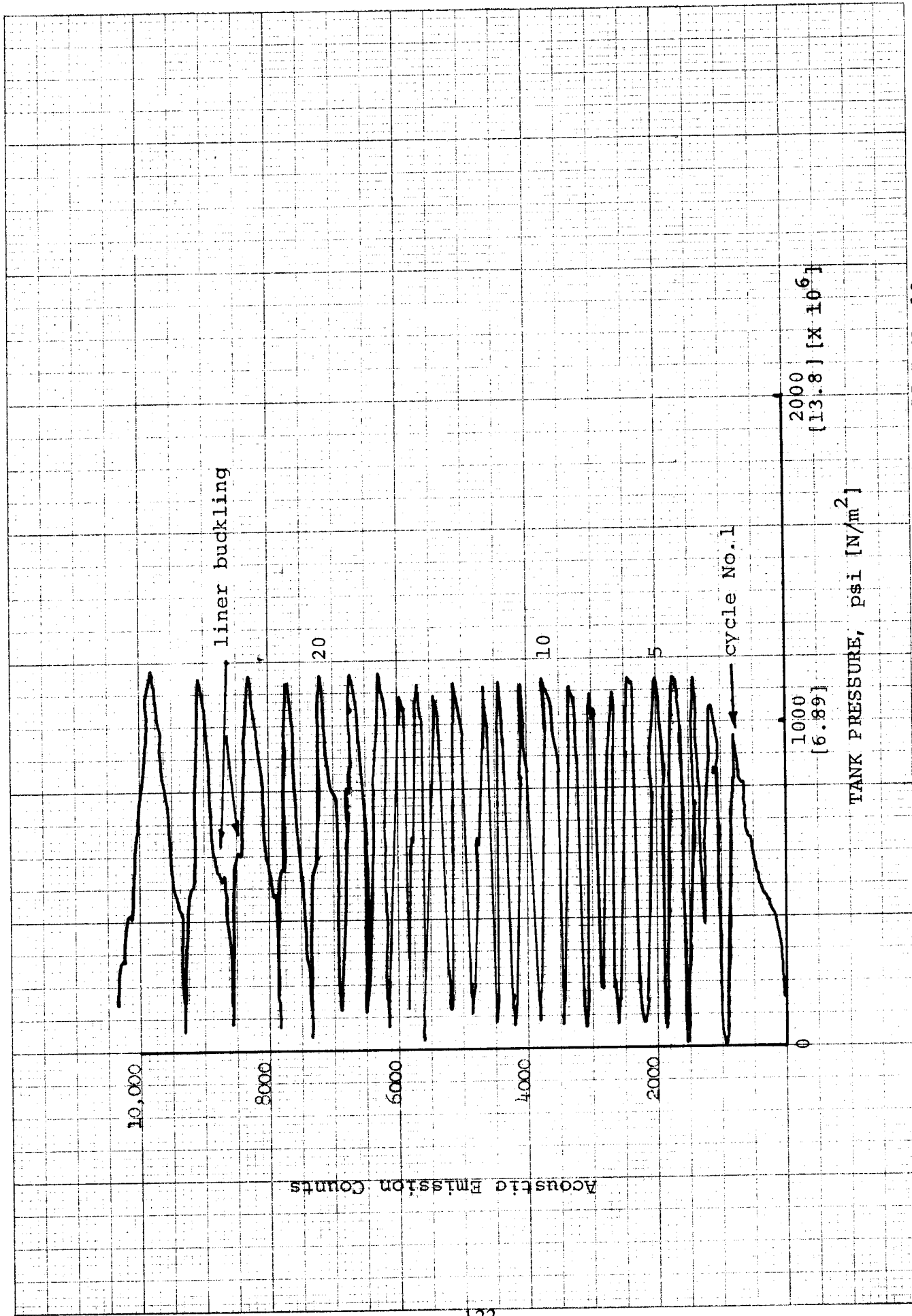


FIGURE 79 ACOUSTIC EMISSION COUNTS DATA FROM VESSEL NO.13

6.0 APPENDIX

APPENDIX A

Filament stresses, modulus values, and performance factors shown in this report were calculated in the following manner:

A. Fiber Stress

Hoop Direction $\sigma_{fh} = P_b R (1-K) / t_{fh}$

Axial Direction $\sigma_{fl} = P_b R (1-K) / 2 t_{fl} \cos^2 \alpha$

B. Composite Modulus

Total Wall, Hoop $E_{ch} = \frac{R}{t_t} \left(\frac{P}{\Delta L/L} \right)_h$

Total Wall, Axial $E_{cl} = \frac{R}{2t_t} \left(\frac{P}{\Delta L/L} \right)_l$

Hoop Windings Only $E_h = \frac{R}{t_{ch}} \left(\frac{P}{\Delta L/L} \right)_h$

Axial Windings Only $E_l = \frac{R}{2t_{cl}} \left(\frac{P}{\Delta L/L} \right)_l$

C. Performance Factor

Composite Only $(P.F.)_c = P_b V / W_c$

Total Wall $(P.F.)_w = P_b V / W_w$

Total Vessel $(P.F.)_v = P_b V / W_t$

where:

σ_{fh} = circumferential fiber stress, psi

σ_{fl} = longitudinal fiber stress, psi

E_{ch} = Modulus of vessel wall in the circumferential direction, psi

E_{cl} = Modulus of vessel wall in the longitudinal direction, psi

E_h = Modulus of circumferential composite windings only, psi

Appendix A (Continued)

- E_1 = Modulus of longitudinal composite windings only, psi
 P_b = Vessel burst pressure, psi
 R = mean radius of vessel in cylindrical section, in.
 t_{fh} = thickness of circumferential filaments, in.
 (No. of yarns per inch x area of yarn)
 t_{fl} = thickness of longitudinal filaments, in.
 (No. of yarns per inch x area of yarn \div $\cos \alpha$)
 α = angle of polar wrap, degrees
 t_t = Total vessel wall thickness, inch
 t_{ch} = Thickness of composite hoop windings, inch
 t_{cl} = Thickness of composite longitudinal windings, inch
 W_C = weight of composite portion of vessel only, lbs.
 W_W = Total weight of vessel, less the weight of end bosses, lbs.
 W_t = Total weight of vessel, lbs.
 V = Total internal volume of vessel, in³
 $\left(\frac{P}{\Delta L/L}\right)_h$ = Slope of pressure-strain curve in circumferential direction, psi
 $\left(\frac{P}{\Delta L/L}\right)_l$ = Slope of pressure-strain curve in longitudinal direction, psi

7.0

FINAL REPORT DISTRIBUTION LIST FOR
NASA CR-134555
THIN-METAL LINED PRD 49-III COMPOSITE VESSELS
CONTRACT NAS3-15840

Copies

NASA-Lewis Research Center	
21000 Brookpark Rd.	
Cleveland, OH 44135	
Attn: Contracting Officer, MS 500-313	1
Technical Report Control Office, MS 5-5	1
Technical Utilization Office, MS 3-19	1
AFSC Liaison Office, MS 501-3	1
Library, MS 60-3	2
Reliability and Quality Assurance Office, MS 500-211	1
R. H. Kemp, MS 49-3	1
R. H. Johns, MS 49-3	1
R. F. Lark, Project Manager, MS 49-3	10
J. R. Faddoul, MS 49-3	1
G. T. Smith, MS 49-3	1
J. C. Freche, MS 49-1	1
R. W. Hall, MS 105-1	1
G. M. Ault, MS 3-5	1
NASA-Office of Advanced Research and Technology	
Washington, DC 20546	
Attn: G. C. Deutsch/RW	1
J. J. Gangler/RW	1
B. Achhammer/RW	1
N. J. Mayer/RW	1
NASA-Langley Research Center	
Hampton, VA 23365	
Attn: E. E. Mathauser, MS 188A	1
R. A. Pride, MS 188A	1
R. W. Leonard, MS 188	1
Library	1
NASA-George C. Marshall Space Flight Center	
Huntsville, AL 35812	
Attn: Library	1
J. M. Stuckey, S&E-ASTN-MNM	1
H. M. Walker, S&E-PP-MXS	1

NASA-Manned Spacecraft Center Houston, TX 77001 Attn: Library	1
L. G. St. Leger, ES	1
R. E. Johnson, SMD-ES-5	1
S. Glorioso, SMD-ES-52	1
J. Smith, SMD-ES-52	1
 NASA-Office of Technical Utilization Washington, DC 20546	 1
 NASA-Ames Research Center Moffett Field, CA 94035 Attn: Library	 1
 NASA-Flight Research Center P. O. Box 273 Edwards, CA 93523 Attn: Library	 1
 NASA-Goddard Space Flight Center Greenbelt, MD 20771 Attn: Library	 1
 NASA-Scientific and Technical Information Facility Box 33 College Park, MD 20740 Attn: NASA Representative	 10
 National Technical Information Service Springfield, VA 22151	 6
 Jet Propulsion Laboratory 4800 Oak Grove Dr. Pasadena, CA 91103 Attn: Library	 1
Warren Jensen	1
 Air Force Materials Laboratory Wright-Patterson Air Force Base, OH 45433 Attn: J. D. Ray/LNC	 1
H. S. Schwartz/LN	1
G. E. Husman/LNC	1
G. P. Peterson/LC	1
E. Jaffe/LC	1
E. J. Morrisey/LAE	1
S. Litvak/LTF	1
A. Olevitch/LAE	1
T. Reinhart/LAE	1

Air Force Flight Dynamics Laboratory Wright-Patterson Air Force Base, OH 45433 Attn: G. P. Sendekyj, AFFDL, FBC	1
Air Force Office of Scientific Research 1400 Wilson Blvd. Arlington, VA 22209 Attn: SIGL	1
Air Force Rocket Propulsion Laboratory Edwards, CA 93523 Attn: J. Branigan	1
Air Force Office of Scientific Research Washington, DC 20333 Attn: J. F. Masi (Dr.), SREP	1
Space and Missile Systems Organization Air Force Unit Post Office Los Angeles, CA 90045 Attn: Technical Data Center	1
U. S. Air Force Washington, DC Attn: Library	1
C. K. Stambaugh (Col.), AFRST	1
Defense Metals Information Center Battelle Memorial Institute Columbus Laboratories 505 King Ave. Columbus, OH 43201	1
Advanced Research Projects Agency Washington, DC 20525 Attn: Library	1
Department of the Army U. S. Army Material Command Washington, DC 20315 Attn: AMCRD-RC	1
Department of the Army U. S. Army Aviation Materials Laboratory Fort Eustis, VA 23604 Attn: A. J. Gustafson	1
Department of the Army U. S. Army Aviation Systems Command P. O. Box 209 St. Louis, MO 63166 Attn: R. Vollmer, AMSAV-A-UE	1

Department of the Army
 Army Materials and Mechanics Research Center
 Watertown, MA 02172
 Attn: B. M. Halpin, Jr. 1

Department of the Army
 Watervliet Arsenal
 Watervliet, NY 12189
 Attn: F. W. Schmiedershoff 1

Department of the Army
 Plastics Technical Evaluation Center
 Picatinny Arsenal
 Dover, NJ 07801
 Attn: H. E. Pebly, Jr. 1

U. S. Army Missile Command
 Redstone Arsenal
 Redstone Arsenal, AL 35809
 Attn: W. S. Crownover, AMSMI-RKP 1

U. S. Army Materials and Mechanics Research Center
 Watertown Arsenal
 Watertown, MA 02192
 Attn: S. Arnold 1

Commander
 Naval Air Systems Command
 U. S. Navy Department
 Washington, DC 20360
 Attn: P. Goodwin, AIR-5203 1
 C. Bersch, AIR-52032A 1
 M. Stander, AIR-52032D 1

Commander
 Naval Ordnance Systems Command
 U. S. Navy Department
 Washington, DC 20360
 Attn: B. Drimmer, ORD-033 1
 M. Kinna, ORD-0333A 1

Director
 Deep Submergence Systems Project
 6900 Wisconsin Ave.
 Washington, DC 20015
 Attn: H. Bernstein, DSSP-221 1

Director
 Naval Research Laboratory
 Washington, DC 20390
 Attn: I. Wolock/8433 1

Department of the Navy
 Office of Naval Research
 Washington, DC 20360
 Attn: J. H. Shenk 1

Director
 Strategic Systems Projects Office
 Department of the Navy
 Washington, DC 20360 1

Department of the Navy
 Naval Ordnance Laboratory
 White Oak
 Silver Spring, MD 20910
 Attn: F. R. Barnet 1
 R. Simon 1

Department of the Navy
 U. S. Naval Ship R&D Laboratory-Annapolis
 Annapolis, MD 21402
 Attn: C. Hershner/2724 1

Aeronutronic Division of Philco Ford Corp.
 Ford Rd.
 Newport Beach, CA 92663
 Attn: Technical Information Department 1

ARDE, Inc.
 19 Industrial Ave.
 Mahwah, NJ 04730
 Attn: A. Cozewith 1

Bell Aerospace Company
 Box 1
 Buffalo, NY 14205
 Attn: S. Cross 1

Bell Helicopter Company
 P. O. Box 482
 Ft. Worth, TX 76101
 Attn: H. Zinberg 1

Brunswick Corporation Defense Products Division P. O. Box 4594 43000 Industrial Avenue Lincoln, NB	1 1
Attn: R. Morse C. G. Zlomke	
Chemical Propulsion Information Agency Applied Physics Laboratory 8621 Georgia Ave. Silver Spring, MD 20910	1
Low Chemical Company Rocky Flats Division P. O. Box 888 Golden, CO 80401 Attn: T. F. Drouillard	1
E. I. DuPont deNemours and Company Textile Fibers Department Wilmington, DE 19898 Attn: C. Zweben, E262 L. Miner J. W. Moore	1 1 1
Esso Research and Engineering Company P. O. Box 45 Linden, NJ 07036 Attn: D. J. Angier	1
Fairchild Hiller Corporation Republic Aviation Division Farmingdale, NY 11735 Attn: J. Clark F. Damasco	1 1
The Fiberite Corporation 512 W. Fourth St. Winona, MN 55987 Attn: S. P. Prosen	1
Fiber Science, Inc. 245 East 157th St. Gardena, CA 90247 Attn: Larry Ashton	1

FMC Corporation Chemical Research and Development Center P. O. Box 8 Princeton, NJ 08540 Attn: Security Officer	1
General Dynamics/Convair P. O. Box 1128 San Diego, CA 92112 Attn: J. L. Christian	1
General Electric Company Valley Forge Space Technology Center P. O. Box 8555 Philadelphia, PA 19101 Attn: J. Anthony	1
Grumman Aerospace Corporation Bethpage, Long Island, NY 11714 Attn: B. Aleck	1
Goodyear Aerospace Corporation 1210 Massilon Rd. Akron, OH 44315 Attn: L. W. Toth	1
General Dynamics P. O. Box 748 Fort Worth, TX 76100 Attn: W. S. Hay T. P. Airhart	1 1
Hercules Corporation Allegheny Ballistics Laboratory P. O. Box 210 Cumberland, MD 21052 Attn: W. T. Freeman	1
Hercules, Incorporated Wilmington, DE 19899 Attn: G. Kuebeler	1
IIT Research Institute Technology Center Chicago, IL 60616 Attn: Library	1

Ling-Temco-Vought Corporation
P. O. Box 5003
Dallas, TX 75222
Attn: M. Pollos 1

Lockheed Missiles and Space Company
P. O. Box 504
Sunnyvale, CA 94087
Attn: R. W. Fenn 1

Lockheed/California Corporation
Burbank, CA 91503
Attn: M. G. Childers 1

Lawrence Radiation Laboratory
P. O. Box 808
Livermore, CA 94550
Attn: Library 1
T. T. Chiao 1

Lockheed-Georgia Company
Advanced Composites Information Center
Department 72-14, Zone 402
Marietta, GA 30060 1

Martin-Marietta Corporation
P. O. Box 179
Denver, CO 80201
Attn: A. Feldman 1

Marquardt Corporation
16555 Saticoy St.
Van Nuys, CA 91406
Attn: J. F. Dolowy 1

Massachusetts Institute of Technology
Cambridge, MA
Attn: F. J. McGarry (Prof.) 1

McDonnell Douglas Aircraft Corporation
3855 Lakewood Blvd.
Long Beach, CA 90810
Attn: H. C. Schjelderup 1

McDonnell Douglas Aircraft Corporation
P. O. Box 516
Lambert Field, MS 63166
Attn: J. C. Watson 1

North American Rockwell, Incorporated
 4300 East Fifth St.
 Columbus, OH 43219
 Attn: R. L. Foye 1

Northrop Space Laboratories
 3401 West Broadway
 Hawthorne, CA 90250
 Attn: D. Stanbarger 1

North American Rockwell Corporation
 Space Division
 12214 Lakewood Blvd.
 Downey, CA 90241
 Attn: Max Nabler 1
 L. Korb 1

North American Rockwell Corporation
 Tulsa Division
 Tulsa, OK 51308
 Attn: J. H. Powell 1

Structural Composites Industries, Inc.
 6344 North Irwindale Ave.
 Azusa, CA 91702
 Attn: E. E. Morris 1

TRW Equipment Group
 23555 Euclid Ave.
 Euclid, OH 44111
 Attn: W. E. Winters 1

United Aircraft Corporation
 Research Laboratories
 East Hartford, CT 06108
 Attn: K. Kreider 1

United Aircraft Corporation
 United Technology Center Division
 P. O. Box 358
 Sunnyvale, CA 94088
 Attn: S. M. Jacobs 1

Whittaker Corporation
 3640 Aero Court
 San Diego, CA 92123
 Attn: V. Chase 1